ISSN 2073-3771 (online)
ISSN 2222-5617 (printed)

МІНІСТЕРСТВО ОСВІТИ І НАУКИ УКРАЇНИ

Вісник Харківського Національного Університету імені В. Н. Каразіна

Серія “Фізика”

Випуск 28

Серія започаткована 1998 р.

Харків 2018

УДК 530.1/539.8

Вісник містить статті, присвячені сучасному стану теоретичних та експериментальних досліджень у галузі фізики Видання призначене для науковців, викладачів, аспірантів та студентів фізичних спеціальностей вищих навчальних закладів та наукових установ.
Видання є фаховим виданням у галузі фіз.-мат. наук (фізика) наказ МОН України №1328 від 21.12.2015.

Затверджено до друку рішенням Вченої ради Харківського національного університету імені В.Н. Каразіна (протокол №7 від 25 червня 2018 р.)

Адреса редакції:
Україна, 61022, Харків, майдан Свободи, 4, Харківський національний університет імені В.Н. Каразіна, фізичний факультет, 057-707-53-83, ruslan.v.vovk@univer.kharkov.ua
Статті пройшли внутрішнє та зовнішнє рецензування.

Свідоцтво про державну реєстрацію КВ №21573-11473Р від 20.08.2015

UDC 530.1/539.8

Bulletin contains articles on the current state of theoretical and experimental research in the field of physics. The publication is intended for researchers, teachers and students of physical specialties of higher education and research institutions.
The publication is a professional Edition in the field of physics and mathematics science (Physics) ordered MES of Ukraine #1328 from 12.21.2015.

Approved for publication by the decision of the Academic Council of Kharkiv Karazin National University. (Minutes №7 dated June 25, 2018 p.)

Editorial address:

Svobody Sq. 4, 61022, Kharkiv, Ukraine, V.N. Karazin Kharkiv National University, Department of Physics, 057-707-53-83, ruslan.v.vovk@univer.kharkov.ua

All articles reviewed.

Certificate of registration KB number 21573-11473P on 20.08.2015

Content

Зміст

Яков Овсійович Гегузін

(1918 – 1987)

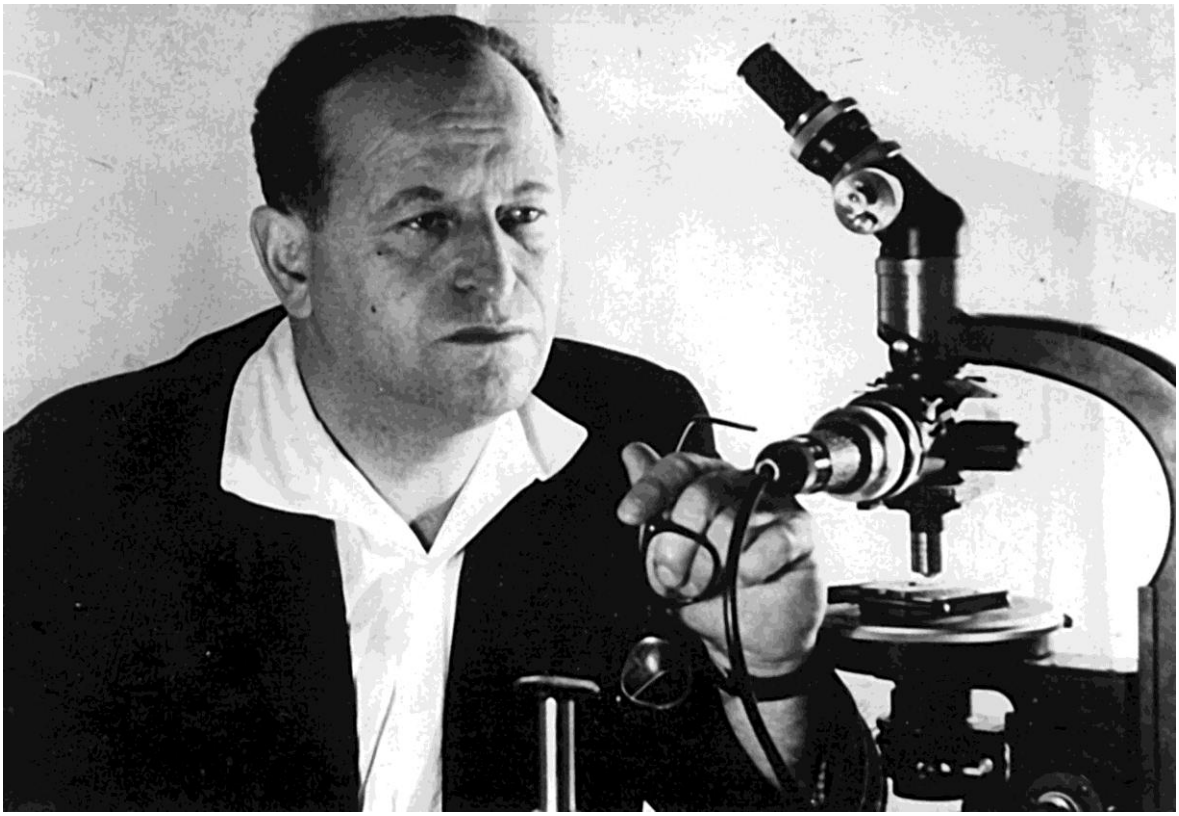

«Наука обязана озарениям тех естествоиспытателей, которые, подобно поэтам и художникам, одарены талантом видеть»

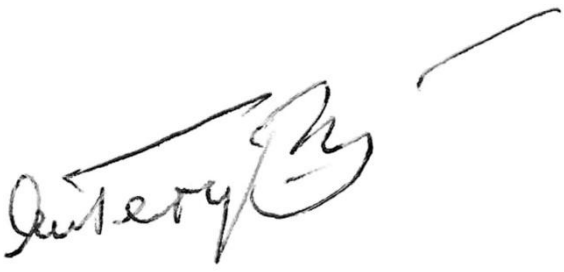

Yakov Evseevich Geguzin
Doktor of physics-mathematical sciences, professor

At the 1-st of august is 100 years from birthday of Ya.E. Geguzin – a scientist of mark, brilliant lecturer and teacher, bright popularizator of science, founder of department of crystal physics, where he create of well known scientific school in our country and abroad.

A number of new directions of investigations at the field of physics of real crystals are connected with Ya. E. Geguzin's name. He is one of founders of physics of sintering-huge sphere of fundamental and applied physics of solid bodies. At his pioneering works researched mechanisms and kinetic behavior of sintering processes in porous bodies which lead a foundation for technology of powder metallurgy. A considerable scientific contribution Ya.E. at physics of sintering was marked by international prize by Ya.I. Frenkel and by honorary diploma of international institute of sintering, where he was elected as a Honorary member. He was a member of editorial stuff of international journal "Powder metallurgy". His monograph "Physics of sintering" was two times editions at the USSR and was translated into German language.

Ya. E. Geguzin discovered and was the first one who investigated a number of physical affects and phenomenon's. They connected with:

1. Directional streams of disbalanced vacancies in metallic and ionic crystals. Results of these investigations were generalized at monographs "Macroscopic defect in crystals" and 'Diffusion zone".
2. Mass transfer on surface and nearsurface layers of crystals. A number of fundamental overviews of this theme, book "Surface diffusion and spreading" under editorship of Ya.E. Geguzin and monograph "Processes of diffusion on crystal surface" (written with Yu.S. Kaganovsky) became the result of these investigations.
3. Processes forming of macroscopic inclusions in crystals and their behavior under action of external force field. Results of these investigations were generalized at monograph "Movement of macroscopic inclusions in solids" (written with M. Krivoglaz), the monograph has international acknowledgment and was published at USA.

Scientific concepts of Ya.E. Geguzin spread far from boundaries university and Kharkov and nourished a number of scientific groups not only at Ukraine but abroad. Scientific seminars devoted present-day problems of physics of real crystals furthered such spreading. These seminars on physics of sintering, radiation physics, processes of mass transfer on the surface of solids, processes in diffusion zone were very popular and collected the best specialists from many countries of the world.

Ya.E. Geguzin was excellent narrator and remarkable popularizator of science, he could narrate about complicated phenomenon so simple that literally everybody could understand. That is why his popular science books "Drop", Why and how void disappears", "Sketches about diffusion in crystals", "Living crystal", Bubbles" and his articles in journals

“Quant”, “Nature”, “Science and life” where famous in our country and abroad, they were published by many issues and translated into the English, German and Spain languages. Their weight and actuality are not lost up today. It is not accidentally that new popular science series “Masterpieces of natural scientific literature” based at 2014 began its publication from Ya.E. books. The series is opened by book “Drop”. Academician V.L. Ginzburg – laureate of Nobel prize - called this book “poem”. Moreover “Drop” such books already have been reissued: “Living crystal”, “Bubbles” and “Sketches about diffusion in crystals”. All books Ya.E. are inherit age of the most bright and nonstandard knowledge’s that unite educational and popularization intention.

Ya.E. was Teacher. He brought up 8 doctors of sciences, more than 40 candidate and more than 500 experts in physics. To teach and to teach up is possible only by setting own example – such was his principle. He was be able to be glad success of his pupils and colleagues. He also was able to admire by handsome poetic stanza and beautiful experiment. He endowed all of those who associated with him by skill to book at the world by king eyes of scientist and artist. Kharkov university was his native home. He was proud of the university and the department of crystals physics created by him and always increased their glory.

This issue of “Vestnik” is devoted to memory of Ya.E. Geguzin. All articles was written by his pupils or the persons who knew him and collaborated with him. All of them remember Ya.E. with gratitude and respect and his important role at their growing up and attitude to scientific researches. It is very pleasant that gwite young scientists sent their articles to that issue. One of them - A. Shkurmanov - graduated from chair created by Ya.E. only at 2014. But he already has defended candidate thesis, has PhD degree, he interests in properties of ultrathin nanowires. The second – O. Zaiceva - now only finishes the second year of physical department. She is fascinated by physics and she is co-author of the article about interesting peculiarities of interaction of two kinds of liquids with different density at low temperatures.

Яков Овсійович Гегузін
доктор фізико-математичних наук, професор

1 серпня виповнилося 100 років з дня народження Якова Овсійовича Гегузіна – видатного вченого, блискучого лектора і педагога, яскравого популяризатора науки, засновника кафедри фізики кристалів, де він створив відому в нашій країні і за кордоном наукову школу.

З ім'ям Я. О. Гегузіна пов'язана ціла низка напрямків досліджень в області фізики реального кристала. Він один із основоположників фізики спікання – величезної області фундаментальної та прикладної фізики твердого тіла. У піонерських роботах Я. О. Гегузіна вивчені механізми і кінетичні закономірності процесів спікання пористих тіл та закладені фізичні основи технології порошкової металургії. Значний науковий внесок Я. О. Гегузіна у фізику спікання був відзначений Міжнародною премією ім. Я. І. Френкеля та почесним дипломом Міжнародного інституту спікання, обранням його Почесним членом цього інституту. Він був членом редколегії міжнародного наукового журналу "Science of Sintering" та радянського журналу "Порошковая металлургия". Його монографія "Физика спекания" двічі перевидавалась у СРСР та перекладена німецькою мовою.

Я. О. Гегузін вніс вагомий внесок у дослідження фізичних ефектів та явищ, пов'язаних з направленими потоками нерівноважних вакансій у металічних та іонних кристалах. Результати цих досліджень узагальнені в монографіях "Макроскопические дефекты в кристаллах" (ця монографія удостоєна премії АН УССР ім. П. Г. Соболевського) та "Дифузионная зона".

Я. О. Гегузіну належать перші дослідження в області масопереносу на поверхні та у приповерхневих шарах кристалів. Результатом таких досліджень стали фундаментальні огляди з цієї проблеми, книга "Поверхностная диффузия и растекание" під його редакцією та монографія "Диффузионные процессы на поверхности кристалла" (написана разом з Ю. С. Кагановським).

Я. О. Гегузін один із перших почав фундаментальні дослідження процесів формування в кристалах макроскопічних включень та їх поведінки у зовнішніх силових полях. Результати досліджень з цієї проблеми узагальнені у монографії «Движение макроскопических включений в твердых телах» (написана разом з М.Кривоглазом), яка має міжнародне визнання і була видана у США.

Наукові ідеї Я. О. Гегузіна розповсюджувалися далеко за межі університету та Харкова і живили наукові колективи не тільки в Україні, а і за її межами. Цьому значно сприяли наукові семінари з актуальних проблем фізики реального кристала, які він організовував на базі кафедри фізики кристалів: з фізики спікання, радіаційної фізики, процесів переносу маси на поверхні твердих тіл та у дифузійній зоні. Вони були дуже популярними і збирали кращих фахівців з багатьох країн світу.

Ми згадуємо Я. О.Гегузіна як прекрасного оповідача та відданного популяризатора науки, який умів розповісти про складні явища так просто, що його міг зрозуміти буквально кожний. Ось чому його науково-популярні книжки "Капля",

“Почему и как исчезает пустота”, “Очерки о диффузии в кристаллах”, “Живой кристал”, “Пузыри” та статті в журналах “Квант”, “Природа”, “Наука и жизнь” широко відомі і в нашій країні, і за її межами, вийшли багатьма виданнями, перекладені на англійську, німецьку та іспанську мови. Їхні вагомість та актуальність не втрачені і зараз. Не випадково нова науково-популярна серія “Шедевры естественно-научной литературы”, яка заснована у 2014 році, почала свої видання публікацією книжок Я. О. Гегузіна з метою долучити сучасного читача до кращих зразків науково-педагогічної літератури. Серію відкриває книга “Крапля”, яку академік В. Л. Гінзбург, нобелівський лауреат з фізики, назвав поемою! Він пише: “Ця книга є уроком радісного знання, “соковитої” фізики і сходить до класичних зразків науково-популярного жанру, таких як знаменита “Історія свічки” Майкла Фарадея”. Окрім книги “Крапля”, вже перевидані також книги Я.О. Гегузіна “Живой кристалл”, “Пузыри”, “Очерки о диффузии в кристалах”. Про значимість цих науково-популярних книг прекрасно написав професор Б.С. Бокштейн – відомий вчений – матеріалознавець: “Яков Овсійович – один з кращих популяризаторів науки. Писати популярні книги дуже важко, для цього потрібен особливий талант. Наукова книга спирається на каркас із формул, у популярній книзі їх дуже мало. Кожна формула зменшує число читачів вдвічі. Якщо не формули, то що? Відповідь – це образи. Популярна книга тримається на образах. І в цьому Яков Овсійович був неперевершений майстер”. Усі книги Я. О. Гегузіна є спадком найяскравіших та нестандартних знань, що з’єднують у собі навчальне та популяризаторське призначення.

Яков Овсійович був Учителем! Він виховав 8 докторів наук, більше як 40 кандидатів та більше 500 фахівців-фізиків. Вчити та навчити можна лише власним прикладом – таким був його принцип. Він умів радіти успіхам своїх учнів та колег. Він також умів захоплюватися красивою поетичною строфою та красивим експериментом, обдаровував усіх, хто з ним спілкувався, умінням дивитися на світ добрими очима вченого та художника. Харківський університет був його рідною домівкою. Він пишався університетом та створеною кафедрою фізики кристалів і завжди примножував їхню славу.

Цей випуск “Вісника” присвячений пам’яті Якова Овсійовича. Усі статті написані або його учнями, або колегами, що його знали та співпрацювали з ним. Усі вони з вдячністю та шаною згадують Якова Овсійовича і його важливу роль у становленні їхнього відношення до наукових досліджень і фізики взагалі. Особливо приємно, що в цей номер Вісника свої статті надіслали зовсім молоді фізики. Один з них – О. Шкурманов закінчив кафедру, створену Я. О. Гегузіним, лише у 2014 році, вже захистив кандидатську дисертацію, має ступінь PhD і займається вивченням властивостей надтонких наноструктур. А ще один – О. Зайцева - зараз закінчує лише другий курс фізичного факультету, але захоплена фізикою і є співавтором статті, у якій описані цікаві особливості взаємодії двох типів рідини з різною густиною при низьких температурах.

Нові нариси Якова Овсійовича Гегузіна

Про Якова Овсійовича Гегузіна - чудового вченого, талановитого фізика, блискучого лектора і просто розумну, добру і чуйну людину - написано чимало спогадів. Його величезний внесок у розвиток фізики, залишений у вигляді статей, монографій і науково-популярної літератури, оцінений не одним поколінням фізиків і досі не втратив своєї актуальності.

У цьому році виповнюється 100 років від дня його народження. Ця дата стала приводом ще раз згадати про цю видатну людину, про його роль у розвитку фізики і величезний внесок у популяризацію фізики та історію фізичних відкриттів. Виявивши в його архівах ще неопубліковані нариси, я вирішила поділитися з читачами фізичного журналу "Вісник" тією інформацією, яка в них міститься, з тим простим і захоплюючим стилем викладу складних фізичних процесів, які були властиві Я.О., і які робили його науково-популярні книги особливо цінними.

Знайдені нариси мали скласти зміст нової науково-популярної книги, яку Я.О. став писати в останній рік життя. Передбачалося, що книга буде називатися "Атомний вибух у кристалі". Я.О. не хотів використовувати слово "вибух", воно йому не подобалося, як не подобалося все, що пов'язане з руйнуванням. Тому книгу він починав зі вступу, в якому доводив, що атомний вибух може бути і творчим, оскільки дослідження його наслідків дасть відповіді на багато питань, які є важливими не тільки для фізиків, але і для багатьох дослідників з інших областей науки. Цей вступ є закінченим нарисом і прекрасно ілюструє і логіку мислення Я.О., і обгрунтованість того, про що він хоче написати.

Для нової книги Я.О. планував написати 14 нарисів, обговорюючи в них, в основному, результати, отримані на кафедрі, а також основні відкриття і дослідження, які стимулювали розвиток наших експериментів і пояснювали їхні результати. На жаль, велика частина нарисів залишилася у вигляді начерків, що відображають лише канву питань, які планував обговорити Яків Овсійович. Майже повністю було написано всього два нариси. Усі три нариси (включаючи вступ) наводяться нижче. Вони наочно показують особливий стиль, яким користувався Я.Е. при написанні науково-популярних книг. Він веде розмову з читачем, залучаючи його до обговорення всіх сумнівів і труднощів, які доводилося долати, щоб отримати єдино правильну відповідь, яка пояснить досліджуване фізичне явище. Він знаходить переконливі аналогії, засновані на подіях повсякденного життя, щоб кожен міг чітко уявити, як відбувається описуваний процес. Така особливість науково-популярних книг Я.О. робить їх корисними і цікавими для найширшого кола читачів: школярів старших класів, наукових співробітників, студентів, викладачів шкіл і вузів і усіх людей, які цікавляться історією фізичних відкриттів.

І.В.Воробйова

Я.Е. Гегузин
“Атомный взрыв в кристалле“

Введение

“Атомный взрыв” – звучит зловеще, а уточняющие слова “в кристалле” должны смягчить название книги. В этом вводном очерке делается попытка представить читателю замысел книги и прокомментировать обе части её названия. Выдающийся венгерский математик и популяризатор науки Альфред Реньи в послесловии своей великолепной книги “Диалоги о математике” говорил о том, что оптимистически настроенный автор не предворяет свою книгу разговором с читателем, так как уверен, что книга говорит сама за себя. Я должен отказать себе в необходимом оптимизме, предполагаемом Реньи, так как испытываю острую потребность представить читателю свою книгу “Введением”. Мне хочется, чтобы кроме собственно “введения” оно играло ещё и роль приглашения в книгу, с которым я и обращаюсь к читателю.

Теперь о названии. Вначале о первой части названия – “**Атомный взрыв**”.

Истоки всего того, чему книга посвящена, восходят к осенним месяцам 1939 года, когда два молодых сотрудника Ленинградского Физико-технического института Константин Антонович Петржак и Георгий Николаевич Флёров открыли принципиально новый вид радиоактивности, при котором тяжелое ядро излучает не отдельные частицы, а спонтанно делится почти пополам. Происходит взрыв самой миниатюрной из возможных атомных бомб – бомбы, состоящей из одного атома. Этот вид радиоактивности получил название “спонтанное деление”. В те годы эффект спонтанного деления представил огромный интерес для дальнейшего развития теории атомного ядра, для проверки предсказаний формировавшейся “капельной модели” ядра, теории его деления, вынуждаемой бомбардировкой ядра нейтронами. Время, лучшим образом оценивающее значимость научных открытий, показало, что спонтанное деление обнаруживает себя во многих явлениях и процессах природы, что оно также распространено, как распространены, пусть в гомеопатических количествах или в виде локальных скоплений, тяжелые элементы, в частности уран. Оно оказалось важным и для физиков, и для геологов, и для инженеров. Оказалось, что одноатомная атомная бомба может быть полезна при решении многих мирных задач. Именно это, или лучше так: в частности это - оправдывает рассказ об одноатомной атомной бомбе.

Известный специалист по урану профессор Ю.А. Шуколюков в книге, посвященной делению урана в природе, сообщает интересный расчет, характеризующий роль спонтанного деления урана в природе. Вот результаты этого расчета. В земной коре содержится около 10^{14} тонн урана. Это приблизительно десятимиллионная часть всей земной коры. За время её существования спонтанно успело распасться около $3.5\ 10^{7}$ тонн урана. Это эквивалентно взрыву приблизительно 10^9 атомных бомб среднего потенциала. В приближенном пересчете на один год это соответствует взрыву одной бомбы. Счастье в том, что в

действительности взрывается не одна полновесная бомба, а великое множество “одноатомных бомб”. Взрываются они в разное время, в разных местах, либо вовсе не причиняя повреждений, либо создают повреждения, которые нужно еще суметь разыскать, и не просто днем с огнём, а пользуясь специальными методами и приборами.

Обсудим теперь, какая энергия выделяется при взрыве одной одноатомной бомбы, и какие частицы образуются в результате такого взрыва. Обычно избегая формул в научно-популярных книгах, в этом очерке я всё же начну с формулы Эйнштейна, которая поможет рассказать о “взрыве” атомного ядра. Как и все великие формулы, на которых основывается естествознание, она предельно проста:

$$E = m_0 c^2$$

Прочтем её вслух: полная энергия E, заключенная в теле, и его масса m_0 пропорциональны друг другу, при этом коэффициент пропорциональности является универсальной мировой константой, численно равной квадрату скорости света (c) в вакууме. Остановитесь здесь, задумайтесь и придите в восторг от простоты и необозримой общности утверждения $E = m_0 c^2$!

Путь от исходных постулатов специальной теории относительности Эйнштейна до интересующей нас формулы не прост. Но преодолевшие его, приобщаются к изумительной красоте. В научно-популярной книге мы лишим себя этой радости. Сделаем нечто иное, прочтем эту формулу чуть-чуть не так, как только что мы читали её вслух. Прочтем вот как: если энергия тела изменяется на величину ΔE, то изменится и его масса на величину $\Delta m = \dfrac{\Delta E}{c^2}$. Это очень важно, т.к. оказывается, что деление ядра атома на две части (осколки!) сопровождается потерей массы. Речь идёт о том, что сумма масс m_1 и m_2 осколков оказывается меньше исходной массы m_0 распавшегося ядра и, следовательно

$$\Delta m = m_0 - (m_1 + m_2) > 0$$

Это означает, что процесс распада должен сопровождаться выделением энергии

$$\Delta E = \left[m_0 - (m_1 + m_2)\right] c^2$$

Написанная формула не показывает, в какой форме эта энергия выделится, из неё лишь следует, что обязательно выделится. Именно эту энергию имеют в виду, когда произносят так много говорящее сочетание слов “атомная энергия”.

И теоретические, и экспериментальные исследования согласованно свидетельствуют о том, что, к примеру, деление ядра $_{92}\mathbf{U}^{235}$ спонтанное или вынужденное нейтронной бомбардировкой (взрыв одноатомной бомбы) сопровождается выделением энергии около 200 MeV. В атомных масштабах это огромная энергия, именно её величина даёт основание для употребления зловеще звучащего словосочетания “атомный взрыв”. В каком виде эта энергия выделяется: во

многих видах. Во-первых, и главным образом, в виде кинетической энергии осколков. Кроме осколков, в момент взрыва возникают и иные носители энергии: свободные электроны, которые уносят с собой около 5 MeV, γ – лучи - около 10 MeV, нейтроны – около 6 MeV, радиоактивный распад осколков – около 20 MeV. Общий баланс: кинетическая энергия двух осколков – около 160 MeV, прочее – около 40 MeV. Итого - 200 MeV! Нас далее будут интересовать, главным образом, осколки, так как именно они являются основной причиной взрывных последствий в кристалле.

Отметим ещё одну особенность деления тяжелого ядра: возникающие осколки являются многозарядными ионами. Обсудим, как формируется заряд иона. Превратить атом в ион – это значит удалить из нейтрального атома один или более электронов. Атом превратится в ион, положительный заряд которого определяется числом удаленных электронов. Это мы знаем. И всё же, пожалуй, нужны несколько фраз, поясняющих слово “удалить”. “Удалить“ – это значит вырвать электрон из атома, например, сообщив электрону энергию, достаточную для того, чтобы он преодолел связь с атомом. Можно было бы указать ещё и другие способы убрать электрон из атома при ионизации. Все они, в конечном счете, сводятся к тому, чтобы насильственно порвать связь электрона с ионизующимся атомом, воспользовавшись при этом извне привнесенной энергией. Эта процедура может быть промоделирована процессом удаления пылинок из ковра, скажем, с помощью пылесоса: недвижимый ковёр лежит на полу, а пылесос отрывает от него пылинки. Впрочем, известен и другой способ удаления пылинки из ковра – встряхнуть его, как бы удалить ковёр из-под пылинки так, чтобы она потеряла с ним связь.

Механизм ионизации осколков подробно исследовал Нильс Бор. Так вот, ионизация по Бору – это удаление из атома наиболее слабо связанных с ним внешних электронов, по схеме очень напоминающей процесс встряхивания ковра. Происходит это вот как. В покоящемся атоме электроны, как известно, движутся с различными скоростями, так что электроны более удалённые от ядра, движутся с меньшей скоростью. Если нейтральному атому мы сообщим скорость большую, чем скорость электронов в оболочке атома, эти электроны не успевают за атомом и окажутся отставшими, оторвавшимся от него, подобно пылинкам, не успевающим за ковром. Чем быстрее будет двигаться атом, тем, естественно, большее число электронов “стряхнётся”, тем более ионизованным окажется атом. Бор предположил, а потом и доказал, что от осколка, обладающего огромной энергией и движущегося со скоростью составляющей почти 0.1 от скорости света, отрывается 15-20 электронов (не успевает за ним), летящий осколок становится многозарядным ионом. Итак, взрыв единичного атома сопровождается появлением осколков – тяжелых многозарядных ионов, имеющих огромную энергию, такую, что ионы летят со скоростью, близкой к скорости света. Десять процентов от скорости света – это уже близко от неё. Вот, пожалуй, и всё, что я хотел сообщить читателю, комментируя первую половину названия книги.

Теперь следует прокомментировать слова: **“в кристалле**”.

Пусть произошло спонтанное деление ядра в кристалле. Не в воздухе, а в кристалле, каждый кубический сантиметр которого заполнен $\approx 10^{22}$ атомами, состоящими из положительно заряженных ядер и отрицательно заряженных электронов. Ионы-осколки, летя в кристалле, на своём небольшом пути теряют эту энергию, все 160 МэВ. Для кристалла это событие не должно пройти бесследно. Одним из последствий такого взрыва в кристалле является формирование протяженной дефектной области вдоль траектории полета осколка - так называемый трек. Впервые треки были обнаружены американцами Р. Фляйшером и П. Прайсом с помощью современного электронного микроскопа. Для нас, интересующихся атомным взрывом в кристалле, условия возникновения трека и его структура и представляют основной интерес. Из него можно и нужно извлечь много важной и уникальной информации и об ионе, и о кристалле, и об их взаимодействии. Трек может дать ответы на множество вопросов, относящихся и к взорвавшемуся ядру, и к собственно кристаллу. Вот некоторые из них: Каким механизмом энергия осколка была передана кристаллу? Быть может, существует не один, а несколько таких механизмов? Быть может, трек со временем исчезнет, залечится? Быть может, сопротивляясь осколку, создающему трек, кристалл зазвучит, выражая своё возмущение осколком? А быть может, он нагреется? Чувствует или не чувствует осколок упорядоченное расположение атомов в кристалле? Быть может, кристалл, содержащий давно возникший трек, был деформирован и трек это запомнил? Нельзя ли как-то повлиять на длину трека? Как давно пролетел осколок разделившегося ядра? Какую информацию об окружающей среде можно получить, регистрируя и исследуя треки осколков деления тяжелых ядер? Как можно сделать треки полезными для человека?

Что, интересные вопросы? Кажется, интересные. Им и подобным вопросам и посвящена эта книга. Её автор - кристаллофизик, поэтому, естественно, что основной акцент в изложении смещен на вторую часть названия книги, на события в кристалле, а об атомном взрыве будет говориться лишь в порядке необходимой информации или напоминания о ней.

Мне очень приятно сознавать, что задумав написать “Атомный взрыв в кристалле”, я берусь, по-моему, за доброе дело, за написание книги об атоме, который, взрываясь, всё же служит делу мира, а не войны. Так много ужасов и горя ассоциируется со словом атомный взрыв, такое необозримое количество немирных атомов заключено в летающих ракетах различных конструкций и в атомных бомбах различных потенциалов, что грешно упускать возможность напомнить людям о том, что атом, даже взрываясь, может и должен быть мирным.

История начинается в Римском университете

События, о которых я хочу рассказать, и, кажется, рассказать о них необходимо, происходили в начале тридцатых годов. Их история начинается в небольшой

лаборатории Римского университета, их развитие (всего 10 лет) определило судьбы человечества.

Я часто думаю об этих событиях, дорожу всяким поводом приобщиться к, пусть иллюзорному, чувству сопричастности к этому романтическому времени, к тем событиям, к тем откровениям и надеждам.

История науки, видимо, не знает десятилетий, в которых, подобно тридцатым годам, были бы так плотно спрессованы научные прозрения и ошибки, драматические личные судьбы ученых, переплетающиеся с судьбами человечества, определяя их и от них завися, торжество непредвзятого мышления и следование традициям, счастливые случайности, сохранившие жизнь миллионам, и их строгая планомерность, которой, казалось бы, противопоказаны неожиданности.

Мне, физику, очень импонирует, что достижения тех лет не были связаны с использование громоздкой аппаратуры промышленного типа. В середине тридцатых годов она уже встречалась в залах некоторых лабораторий мира, напоминающих заводские цеха. Эта аппаратура оказалась, однако, в стороне от центральной магистрали, вдоль которой развивались основные исследования тех лет. Таланты и фантазеры обошлись средствами лабораторий, главное богатство которых составляли примитивные счетчики собственного изготовления и на время одолженные ампулы, заполненные радоном и бериллиевым порошком. Стеклянные ампулы заменяли им еще не построенные циклотроны. Впрочем, основным богатством этих лабораторий, которые в те годы еще не очень щедро субсидировались, конечно же, были не счетчики и ампулы, а таланты и фантазеры, мыслящие непредвзято, иной раз курьезно, иной раз, ведомые интуицией, они, вопреки дисциплинированной логике, начинают искать там, где посветлее. Пути талантов и фантазеров неисповедимы, - в тридцатые годы в атомной проблеме они определили многое, если не все.

Как и всякой иной, этой истории, начавшейся в Римском университете, предшествовала предыстория. О ней - коротко, сухими фразами.

В 1930 году немецкий физик Вальтер Боте с сотрудниками бомбардировал α частицами бериллий. Они обнаружили, что облученный бериллий испускает наведенное проникающее излучение. Это «бериллиевое» излучение они сочли жесткими γ – лучами. Объяснение, лишенное революционности, но вполне разумное, непротиворечивое, скажем так: естественное. Эти опыты вскоре продолжили во Франции супруги Ирен и Фредерик Жолио-Кюри. И они наблюдали «бериллиевое» излучение, и они убедились в том, что оно легко проникает сквозь вещество. Толкование природы излучения, предложенное Боте и Беккером, супруги Жолио сочли состоятельным. Они смогли показать, что «бериллиевое» излучение способно выбивать протоны из водосодержащих веществ. Эти наблюдения не поколебали их веры в том, что «бериллиевое» излучение есть γ - лучи.

В 1932 году, немного изменив опыты французов, в Англии в Кавендишевской лаборатории, сотрудник Резерфорда Джеймс Чедвик показал, что «бериллиевое

излучение» - это поток не γ- лучей, а электрически нейтральных тяжелых частиц. Обнаруженные им частицы получили название нейтронов. К сожалению, так случилось, что Боте и Беккер и супруги Жолио экспериментировали с нейтронами, но не распознали их. Очевидно, Чедвику в лаборатории Резерфорда, которые еще в 1920году предсказал принципиальную возможность существования таких частиц, опознать нейтрон было проще. Ему в помощь были и многолетний и уникальный опыт Кавендишеской лаборатории в области ядерной физики, населяющие ее люди, и все то, что невозможно ни учесть, ни взвесить, не перечислить, а можно лишь назвать атмосферой «школы Резерфорда». В этой школе революционность суждений – явление традиционное, если только слова «революция» и «традиция» можно ставит рядом.

Сразу же после того, как нейтрон был открыт, теоретики увидели достаточно оснований, чтобы найти ему место в ядре. Почти одновременно это сделали в России – Дмитрий Иваненко, в Германии – Вернер Гайнзенберг, в Италии – Эторе Майорана. Согласно их модели в атомном ядре нейтронов, имеющих такую же массу, как и протоны, ровно столько, сколько нужно для того, чтобы вместе с протонами, так же входящими в состав ядра, определить атомный вес элемента.

В то время, когда Энрико Ферми со своими молодыми сотрудниками, которые в полном соответствии с реальностью именовались «мальчиками», в лаборатории Римского университета начали планомерное исследование взаимодействия нейронов со многими веществами периодической системы. Уже было ясное понимание. Что нейтроны – это не только удобные снаряды, которые вследствие отсутствия заряда могут беспрепятственно подлетать к заряженному ядру, но в определенной степени и мишень, так как они входят в состав ядра.

Итак, интересующая нас предыстория завершена открытием нейтральной частицы, нейтрона – отличного снаряда для бомбардировки атомного ядра, не чувствующего их заряда. А вот теперь о собственно истории.

Экспериментальная деятельность группы Римских исследователей началась в первых числах марта 1934 года. В распоряжении экспериментаторов были ионизационные счетчики заряженных частиц примитивной конструкции и возможность покупать (в частности, в аптеке) изучаемые вещества для изготовления мишеней. Источники нейтронов, бомбардирующих ядра атомов, изготавливали сами: стеклянные ампулы заполнялись бериллиевым порошком и радоном, который молодым коллегам дарил работавший по соседству профессор Джулио Трабакки, главный физик министерства здравоохранения Италии. Радон рождал α- частицы, α-частицы бомбардировали ядра бериллия, ядра бериллия рождали нейтроны, а нейтроны направлялись на мишени. Для того чтобы излучение источника не регистрировалось счетчиками, мишени облучались в одной комнате, а счетчики располагались в другой, до которой надо было добежать поскорее, чтобы наведенная активность мишени не успела существенно ослабеть. Бег с облученной мишенью из

комнаты в комнату был непременной процедурной деталью очень многих нейтронных исследований тридцатых годов, и в Италии и в России. В Италии бегал Ферми, а в России – Курчатов!

В марте, двадцать пятого числа, в редакцию журнала Национального исследовательского совета было направлено письмо с сообщением о первых успехах: фтор, подвергавшийся облучение, обнаружил наведенную облучением радиоактивность. Потом письма - четкие и лаконичные – будут направляться в журнал еженедельно.

Эти сообщения из Рима привлекли внимание всех заинтересованных проблемой. В конце апреля Ферми получил письмо из Англии от Резерфорда. В письме - благодарность за сообщение результатов опытов по наведению с помощью нейтронов временной радиоактивности в некоторых элементах, слова о том, что в дальнейшем, видимо, удастся получить сведения и о механизме этого процесса, а в конце письма шутка «Поздравляю Вас с успешным побегом из сферы теоретической физики!»

Незадолго перед началом периода летних отпусков Ферми с сотрудниками, опускаясь вниз по Менделеевской таблице, подошли к торию и урану. Облучая уран нейтронами, они рассчитывали, утяжеляя ядро, получить трансурановые элементы. В отпуск ушли с уверенностью, что трансурановые элементы получены, что право на отдых заработано, Здесь напрашивается словосочетание, которое обычно произносится в иной ситуации: «Ушли на заслуженный отдых».

Идея получения трансуранов в те годы носилась в воздухе. Прямолинейная логика естественно приводила к мысли о том, что образование трансурана – единственное и естественное следствие поглощения нейтронов ядром урана – последнего элемента «стабильной» периодической системы. Предполагалось именно так: ядро урана поглотит нейтрон, станет более тяжелым и станет трансурановым ядром. В том же 1934 году немецкий физико-химик Ида Ноддак прислала в Рим оттиск своей статьи, (опубликованной в немецком журнале прикладной химии), в которой обсуждалась возможность трактовать опыты Ферми и сотрудников как свидетельствующие о распаде облученного нейтронами ядра урана на две части. Но прямолинейная логика оказалась непоколебимой: идея поглощения не уступила место идее распада. Теперь, зная обо всех последующих событиях деления ядра, о мировой войне, о зверствах гитлеровского фашизма, об ужасах Хиросимы, мы, не верящие в бога, бога должны благодарить за то, что итальянские физики оказались загипнотизированными идеей возможности получения трансурановых элементов и, ведомые дисциплинированной логикой, не допустили мысль о возможности деления урана. В своей книге Энрико Ферми и его ученик, участник нейтронных исследований, проводившихся в Риме, Эмилио Сегре, вспоминая об оттиске, присланном Идой Ноддак, размышляет о возможной причине «слепоты» Ферми. Он пишет: «много лет спустя Ферми говорил, что в то время были ошибочные данные по дефектам массы, которые не допускали возможности деления». Мы же теперь можем

констатировать, что пренебрежение соображением Иды Ноддак - счастливое обстоятельство, которому человечество в немалой мере обязано тем, что Гитлер в войне не располагал ядерной бомбой. Кроме великих откровений существуют и великие заблуждения. Заблуждения Ферми и его «мальчиков» относятся к разряду великих. Лишь в 1939 году процесс деления был опознан.

После «заслуженного отдыха» опыты по облучению нейтронами различных веществ были в Риме возобновлены. Обнаружилось неожиданное обстоятельство: интенсивность излучения серебра, наведенная нейтронами, оказалась зависящей от того, на каком столе проводились опыты. С целью разгадать обнаружившуюся неожиданность были поставлены специальные опыты, и выяснилось, что стол оказался не просто столом – подставкой под приборами, а действующей деталью экспериментальной установки. Те же головы, которые совсем недавно подчинялись прямолинейной логике, в этих опытах повели себя независимо и революционно: 22 октября утром между источником нейтронов и серебряной мишенью был поставлен парафиновый блок и активность серебра, наведенная нейтронами, резко возросла. А дело было вот в чем: и парафин, и деревянный стол содержит в себе большое количество атомов водорода. Их ядра – протоны, которые имеют массу такую же, как и нейтроны, эффективно нейтроны тормозят, а заторможенные нейтроны взаимодействуют с ядрами серебра эффективнее, чем быстрые. А ведь все, всегда и везде считали – и это кажется очень естественным - что именно быстрым нейтронам доступно проникновение в ядро, а не медленным.

В тот же день 22 октября в научный журнал было послано письмо с сообщением об открытии эффекта замедления нейтронов. Затем Ферми и его сотрудникам потребовалось шесть недель для того, чтобы всесторонне исследовать этот эффект. Громоздкое оборудование и в этом случае не оказалось необходимым: экспериментировали с блоками парафина, опускали мишень и нейтронный источник в небольшой водяной бассейн во дворе Римского университета. По существу, как писал поэт, сочиняли ничем ни на чем: думали, сомневались, проверяли сомнения. Энрико Ферми, на счету которого много выдающихся достижений в области современной физики, открытие эффекта замедления нейтронов считал своей наибольшей удачей.

Здесь необходима передышка для подведения попутного итога. Строго говоря, в своей надежде получить трансурановый элемент, добавляя к урану нейтрон, римские физики не обманулись. В их опытах действительно уран-238, поглотив нейтрон, превращался в первый трансурановый элемент, занимающий девяносто третью клетку таблицы Менделеева и именуемый теперь нептунием. Было и это! Но было и многое другое, не менее, а быть может, более важное, в чем физики группы Ферми поначалу не разобрались. Понять это другое, в данном случае им, видимо, мешала некоторая прямолинейность мышления, преодоленная иными физиками.

Исследованиями в области нейтронной физики, начавшимися в лаборатории Римского университета, стали заниматься во многих лабораториях Европы и Америки. В 1938 году эти исследования приобрели особую остроту. Теперь основные

события происходили не в Римской, а в других лабораториях: в Париже - в лаборатории Ирен Кюри (в институте, созданном Марией Кюри) и в Берлине - в лаборатории Отто Гана, Фрица Штрассмана и Лизы Майтнер (в институте химии Кайзера Вильгельма). История научного соревнования двух этих лабораторий детально, день за днем, прослежена историками науки. Здесь мы ограничимся лишь фразой, заключающей эту историю: в декабре 1938 года Ган и Штрассман убедительно показали, что при облучении урана медленными нейтронами образуются барий, лантан и церий – элементы, расположенные в середине периодической системы Менделеева, а не за ураном. Ядро урана делится!

Ган и Штрассман – химики-аналитики и они не взяли на себя право обсуждать физическую причину такого результата. Но результат - удивительный и чрезвычайно важный, они решили срочно опубликовать. 22 декабря 1938 года в немецкий научный еженедельник поступило их письмо. 6 января 1939 года оно было опубликовано.

Существо открытия, сделанного Ганом и Штрассманом отчетливо поняла их бывшая сотрудница Лиза Майтнер, изгнанная Гитлером из Германии за неарийское происхождение. Письмо Гана она получила в небольшом шведском городке, и именно она первая произнесла слово деление, распад ядра урана, вызванный поглощением нейтрона. Этот распад ей представился подобным делению бактерий.

Итак, исследования, начатые в 1934 году, завершились в 1938 году открытием деления ядер урана под влиянием бомбардировки медленными нейтронами. Это открытие породило множество вопросов. Среди них главный был такой: если энергии, привносимой в ядро медленным (тепловым) нейтроном, оказывается достаточно для того, чтобы, потеряв устойчивость, ядро разделилось на два осколка, то возможно иногда ядро может разделиться и спонтанно, самопроизвольно, случайно приобретя необходимую для этого энергию.

Для нашего дальнейшего повествования ответ на этот вопрос необходим. Описанию поисков ответа на этот вопрос и посвящен следующий очерк.

Спонтанное деление тяжелых ядер

Об открытии спонтанного деления ядер Константином Антоновичем Петржаком и Георгием Николаевичем Флёровым написано много напыщенных фраз, так как некоторые журналисты стремились щедро облагодетельствовать их, сравнивая с детективами. Мне, тоже пишущему об их открытии, очень хотелось бы рассказать об этом открытии попроще, обратив внимание на два аспекта проблемы спонтанного деления: “как было обнаружено” и “как было объяснено”. “Как было обнаружено” – это всегда интересно потому, что отыскивая ответ на этот вопрос, приходится следить за переплетением зрелого мастерства и обычного человеческого упорства со случайностью находок; естественной предопределённости результата с множеством обстоятельств, маскирующих его; желание обнаружить искомое с необходимостью отодвигать этот момент сомнениями, контрольными опытами, мысленной и реальной

дискуссией с оппонентами, которые, как известно, бывают всякими. С ответа на вопрос “как было обнаружено” мы и начнем рассказ о спонтанном делении ядра.

В 1939 году одна из основных задач в области ядерной физики формулировалась так: могут ли нейтроны, возникшие в процессе деления, вызвать деление ядер U^{238}, который составляет основную массу природного урана? Эта задача привлекла к себе интерес многих лабораторий. В Ленинградском физико-техническом институте экспериментально исследовать эту возможность Игорь Васильевич Курчатов поручил двум своим ученикам - Константину Антоновичу Петржаку и Георгию Николаевичу Флёрову. В кратком очерке, посвящённом воспоминаниям о тех днях, Георгий Николаевич пишет: “Как мы потом убедились, это решение Курчатова оказалось правильным. Работе не помешало то, что мы были друзьями. Наоборот, в сумме нас было больше, чем двое”. Добавим: их было двое, оба были очень молоды, оба были преисполнены творческого энтузиазма и неподдельного интереса к науке.

Спонтанное деление урана неожиданно обнаружило себя на самой начальной стадии работы экспериментаторов, готовившихся к поиску ответа на вопрос, заданный им учителем. Экспериментальная задача состояла в том, чтобы создать установку, которая с высокой степенью чувствительности могла бы регистрировать осколки ядер, разделившихся под влиянием бомбардирующих их нейтронов. Слова “высокая чувствительность” надо подчеркнуть, так как ожидавшийся эффект мог быть слабым, то есть число возможных осколков малым и недостаточно чувствительный счетчик мог бы на фоне “фона” не зарегистрировать их. А для этого надо, чтобы “фон“, то есть случайные импульсы, которые счетчик регистрирует и тогда, когда нейтроны извне в камеру не поступают, было поменьше, а число облучаемых ядер урана - побольше. Эту задачу экспериментаторы решили, поместив в ионизационную камеру не одну, а 15 параллельно расположенных пластин, покрытых слоем окиси урана так, что отрицательно и положительно заряженные пластины чередовались. Их общая площадь была 1000 $см^2$.

Сохранились воспоминания о многих трудностях, которые надо было преодолеть, создавая камеру и счетчик. Так, например, очень сложна было процедура нанесения ровного тонкого слоя окиси урана на поверхность пластин. Сделать это не просто: слой должен быть тонким (10 – 20 $мг/см^2$) и однородным по толщине. Эту операцию сумел осуществить Петржак. У него был давнишний опыт художника, работавшего на заводе фарфоровых изделий.

Собранная и отрегулированная установка обнаружила устойчивый “фон” – шесть импульсов в час. Собственно в этом устойчивом “фоне” и заключалось открытие спонтанного деления урана: источника нейтронов нет, а счетчик считает импульсы. Видимо, именно появление осколков спонтанно делящихся ядер и определяет эти импульсы. Предположение разумное, тем более, что принципиальная возможность эффекта, как мы знаем, теоретически была предсказана и Я.И. Френкелем, и Н.Бором. Н. Бор и Дж. Уилер осуществили количественный расчет и показали, что время жизни ядра урана по отношению к спонтанному распаду равно ~

10^{22} лет. Время огромное, но 6 импульсов в час при высокой чувствительности установки этому времени не противоречат.

Не очень бдительный экспериментатор, пожалуй, прошел бы мимо этого малого фона, а не очень придирчивый экспериментатор нашел бы, пожалуй, основания для мгновенной радости по поводу состоявшегося открытия. Тем более, что интенсивность фона не противоречит оценкам теоретиков. В каждом человеке в какой-то степени живёт подспудная готовность принять желаемое , а тем более очень желаемое, за действительное и тем более, если действительное - не пустячок, а открытие нового вида радиоактивности. Необходима строго дисциплинированная логика, обострённое чувство ответственности перед наукой и, главным образом, перед самим собой, чтобы этой готовности противопоставить скрупулёзность, исключающую тень сомнений. К.А. Петржак и Г.Н. Флёров именно это сделали. Рассуждали они так.

Сомнение 1. Быть может, слышимые импульсы обусловлены каким-то внешним источником колебаний. Для того, чтобы это сомнение устранить (или убедиться в его обоснованности), естественно убрать из камеры окись урана. Пластины, разумеется, сохранить, они основная деталь ионизационной камеры, а покрывающую их окись урана убрать. Поставили такой опыт. Оказалось, что камера с пластинами без окиси урана за 5 часов не зарегистрировала ни одного импульса, а должна зарегистрировать 30 импульсов! То есть явно не внешний источник колебаний рождает импульсы.

Сомнение 2. Так как окись урана эмитирует α - частицы, то не исключено, что именно их появление камера и регистрирует. Проверили это в следующих опытах. Камеру заполняли не окисью урана, которая кроме α– частиц, делясь, рождает осколки, а препаратами, не содержащими уран, то есть не рождающими осколки, но эмитирующими α - частицы. Из этих опытов однозначно следовало, что дело не в α – частицах, не они определяют фон.

Сомнение 3. Быть может, за фоновые щелчки счетчика ответственны случайные разряды на поверхности слоёв окиси урана, покрывающих пластины камеры. Для того, чтобы разрешить это сомнение были поставлены два опыта, результаты которых должны были дополнять друг друга. Первый опыт состоял в следующем. Слой окиси урана на пластинках был покрыт микронной металлической, то есть проводящей, фольгой, назначение которой состояло в том, исключить разряды на поверхности слоя окиси урана. Это фольга делала, но кроме того, как выяснилось, она и уменьшала число фоновых щелчков. Это уменьшение могло быть обусловлено поглощением фольгой части осколков, возникающих при спонтанном делении. Чтобы убедиться в состоятельности такого предположения, понадобился второй опыт, в котором экспериментаторы убедились в том, что фольга в равной степени уменьшает число импульсов, создаваемых осколками, рождающимися и при спонтанном делении, и при делении, вынужденном потоком нейтронов от внешнего источника. В качестве такого источника К.А. Петржак и Г.Н. Флёров воспользовались ампулой, заполненной радоном и порошком бериллия. В те годы такие ампулы были

основными источниками нейтронов и в опытах группы римлян, и в опытах ленинградцев, и в опытах харьковчан, и в опытах кавендишевцев. У этих ампул огромная заслуга перед ядерной физикой. Впрочем, эту заслугу можно было бы сформулировать и более торжественно, упомянув при этом не только ядерную физику, но и цивилизацию в целом.

Сомнение 4. Быть может, фоновые импульсы обусловлены осколками, возникающими не при спонтанном делении, а под влиянием космической радиации. Следовательно, от неё надо избавиться. Решили провести опыты глубоко под землёй, под слоем твёрдого грунта, поглощающего космическое излучение. Для размещения подземной лаборатории избрали недавно созданную шахту станции “Динамо” московского метрополитена.

Здесь я пренебрегаю возможностью пофантазировать на заманчивую тему ядерная физика, лаборатория в подземелье строящегося метро, ночные бдения экспериментаторов, стремящихся избежать помех, обусловленных дневной работой метро. Этой возможностью с большой журналистской выдумкой и разным успехом и до меня пользовались многие. Важно здесь лишь вот что: под землёй эффект обнаруживался так же, как он обнаруживался и на поверхности земли. Итак, “фон” не случайность, а свидетельство спонтанного деления ядер урана!

В своей первой статье, посвященной открытому ими явлению, К.А. Петржак и Г.Н. Флёров пишут менее категорично, чем это написано в предыдущей фразе. Пишут они так: “Мы склонны думать, наблюдаемый нами эффект следует приписать осколкам, получающимся в результате спонтанного деления урана”. Они не ошиблись, спонтанное деление ядер – одно из фундаментальных явлений природы было ими открыто. И ещё одно замечание об этой статье. Она завершается благодарностью руководителю работы профессору И.В. Курчатову “ наметившему все основные контрольные эксперименты и принимавшему самое непосредственное участие в обсуждении результатов исследований”. Я полагаю, что читателю, которому интересна не только физика, но и её история, знать об этой благодарности следует. В ней и благородство учеников, и значимость Учителя.

Теперь обратимся ко второму аспекту проблемы: как явление было объяснено? Собственно, теоретики спонтанное деление не объяснили, а предсказали. Я.И. Френкель, создавая электрокапиллярную теорию деления ядра, отчетливо понимал, что спонтанное деление должно происходить, а Н. Бор и А. Уиллер, как уже упоминалось, даже вычислили период полураспада ядра U^{235}. Да и обычная интуиция, воспитанная на явлениях классической физики, подсказывает, что утяжеляющееся ядро должно приблизиться к пределу, когда его существование станет нестабильным, когда случайное искажение формы ядра может завершиться его распадом, спонтанным делением. В действительности, однако, интуиция здесь заведомо недостаточна, так как спонтанное деление – эффект квантовый, а, следовательно, классическая интуиция может лишь создать иллюзию понимания. А речь идет о том, что даже при условии, что деление на две почти равные части энергетически

целесообразно – ядро от деления охраняет потенциальный барьер, означающий необходимость затратить для деления некоторую энергию. Скажем так: шарику, лежащему в ложбине на горе, выгоднее оказаться у подножья горы. Но для того, чтобы получить такую возможность, ему надо затратить энергию, чтобы выбраться из ложбины на вершину горы, а потом скатиться. Это соображение очевидное, ”классическое”. А квантовость эффекта обнаруживается в том, что преодоление барьера происходит не простым перепрыгиванием через него, а проникновением сквозь барьер механизмом “туннелирования”. Оно происходит тем легче, чем меньше высота барьера, который должен быть преодолён.

Я, конечно же, ничего читателю не объяснил, разве лишь сопоставил спонтанное деление тяжелых ядер с иными явлениями, в основе которых лежит эффект квантового “туннелирования”: распад радиоактивных ядер, эмиссия электронов из холодного металла и другие.

Итак, спонтанное деление было открыто, сообщения об этом были направлены и в отечественные, и в американские журналы. Вскоре началась война – до того, как появились реакции научной общественности на очень примечательное событие в науке об атомном ядре.

Вісник ХНУ, серія «Фізика», вип. 28, 2018. с. 25-32

PACS: 46.25-y
UDC: 530.1/539.8

Topological aspects of linear elastisity theory (methodological notes)

V. D. Natsyk[1,2], I. M. Pakhomova[1]

1. V. N. Karazin Kharkiv National University, sq. Svoboda 4, Kharkiv 61077, Ukraine
2. B.Verkin Institute for Low Temperature Physics and Engineering of the National Academy of Sciences of Ukraine, 47 Nauky Ave., Kharkiv, 61103, Ukraine

ORCID: *0000-0001-9107-474x*

DOI:10.26565/2222-5617-2018-28-01

A comparative discussion is given of the deformation properties of three-dimensional (3D) and two-dimensional (2D) solids, which are considered in the approximation of continuum mechanics as elastic continua with three and two spatial dimensions. Attention is drawn to the effectiveness of attracting concepts and methods of geometry to establish the general patterns of deformation of such systems without taking into account the physicochemical properties of atoms and the interatomic forces. In a geometric description, these continua are elastic spaces with different topological properties, which leads to significant differences in the relationships between the characteristics of their elasticity: Young's moduli, shear, bulk moduli, and Poisson's ratio. Deformation characteristics that can be considered as unique topological invariants of 3D and 2D elastic continua are established.

Keywords: topology, Young's moduli, shear, bulk moduli, and Poisson's ratio.

Проведено порівняльне обговорення деформаційних властивостей тривимірних (3D) і двовимірних (2D) твердих тіл, які розглядаються в наближенні механіки суцільного середовища як пружні континуум з трьома і двома просторовими вимірами. Звернуто увагу на ефективність застосування понять і методів геометрії для встановлення загальних закономірностей деформування таких систем без урахування фізико-хімічних властивостей атомів і сил міжатомної взаємодії в них. При геометричному описі ці континууми уявляються як пружні простори з різними топологічними властивостями, що призводить до істотних відмінностей співвідношень, що пов'язують між собою характеристики пружності: модулі Юнга, зсуву, всебічного стискання і коефіцієнти Пуассона. Встановлено деформаційні характеристики, які можна розглядати як своєрідні топологічні інваріанти 3D і 2D пружних континуумів.

Ключові слова: топологія, модуль Юнга, модуль зсуву, коефіцієнт Пуассона, модуль всебічного стиску.

Dedicating present article to memory of Yakov Evseevich Geguzin we recall one of the remarkable personality namely his gift of teacher and popularization of Physics. At his lectures and popular books scientific severity and accuracy are wonderfully and in proportion combined with the original nonstandard and often unexpected point of view about discussion subject. At proposed methodical notes we try as far as possible to follow this stylistic approach at discussion of a certain problem of modern linear elasticity theory.

Introduction

The mechanics of reversible deformation of solid states, regarded as an elastic continuous medium (continuum) draws up the content of the linear elasticity theory. Its basic equations and relations were established by Cauchy and Poisson in the second decade of XIX century [1].

Their research at that time played a very significant role in creating the prerequisites for the development and deepening of several areas and sections of fundamental mathematics, including geometry. The modern historian of mathematics notes that "in the future many outstanding mathematicians were constantly interested in the theory of elasticity with its clearly expressed geometric character" [2].

At present a large number of crystalline and vitreous (glassy) systems where the centers of microscopic structural elements (atoms or molecules) are located in the plane are intensively studied in solid state physics. The most general rules for geometric classification of mathematical and physical objects are developed in one of the sections of geometry - topology [3, 4]. In the frame of topological representations (Appendix), a plane may be considered as a continuously filled space with two dimensions: in it the positions of the centers of elementary structural units of a solid state are determined by specifying two coordinates. Therefore, the above-mentioned physical systems have been called two-dimensional (2D) crystals or glasses: they have different translationally symmetric (crystals) or chaotic (glass) arrangement of elementary structural units. The study of

two-dimensional systems has a rather prolonged history [5-7], but over the last decade interest in this problem has increased significantly due to discover and initiation of an intensive investigation of 2D graphene crystals - a plane translationally ordered system of carbon atoms [8].

Mathematical description and theoretical analysis of the properties of such 2D structures require a significant modification of models and methods which were developed before for 3D solid bodies: in topology, they are associated with a three-dimensional space in which the position of the elementary structural units is determined by specifying three coordinates. In particular at description the mechanical properties of 2D structures in the continuum approximation by methods of linear elasticity theory, it is necessary to formulate statements and equations of 2D elasticity theory [9, 10]: because the theory has specific special features and differences in comparison with the well-known elasticity theory for 3D solids [1]. However, some of these features are not directly related to the physics of interatomic interactions in 3D or 2D systems, but are caused by significant differences in concepts, theorems, equations and analysis methods in those sections of mathematics, in particular at geometry, which are attracted for comparative description of both clearly mathematical and physical objects with a different number of space dimensions.

The main intention of this publication is to attract the attention of teachers and students who specialize in solid-state physics and crystal physics to the effectiveness of attracting concepts and methods of geometry to describe the general laws of deformation of elastic solid-state systems without taking into account the physicochemical properties of atoms and the interatomic forces. It is also important to emphasize the specific topological features and differences resulting in the comparative description of the elastic deformations of three-dimensional and two-dimensional solids. These remarks explain the expediency of using the terms "topological aspects of the linear elasticity theory".

The object of analysis and description in the article will be small deformations of isotropic solids, considered in the continuum approximation (as continuous media). It allows to use the concepts, relationships and equations of the linear elasticity theory of three-dimensional [1] or two-dimensional [9] continua.

Physical space in the linear elasticity theory

A brief description of the algorithm for "geometrization" of physical systems is given in the Appendix. Here we will consider a concrete example of such a system – solids whose atomic structure has a short (chemical) order: they consist of a large (in the limit – infinite) number of basic (chemically identical) atomic groups, and the centers of the groups are located in empirical 3D space (in terms of mathematics this G_3 space with zero curvature). The translationally symmetric or chaotic arrangement of the centers, the distribution of sizes and orientations of these groups when placed in space corresponds to a crystalline or vitreous structure of solids. Neglecting the dimensions but preserving the physical properties of such groups turns them into physical points, and the continuous filling of these points with a 3D space or 2D space (G_2 space with zero curvature) leads to the concepts of 3D or 2D material continua.

Let us note some of the most important physical properties of these continua:

- the presence in them of the force interaction between the points, which in the continuum limit corresponds to the interaction between the atoms of the basic groups, it can be divided into a contact interaction between the nearest groups (short-range interaction) and interaction at distances exceeding the interatomic (long-range) interaction;
- the ability of continuum to deform without disruption of continuity, in which individual elements of the continuum under the action of neighboring elements or external force fields can change their shape and dimensions but the continuity of point distribution is not disrupted;
- 3D volume and 2D plane solids can be detected from an infinitely extended continuum as fragments. They have sharply outlined outer boundaries that are continuously filled with points inside the boundaries and with complete absence of points outside them;
- an infinitely extended continuum, its individual regions or bodies in the initial state (before deformation) are in a state of thermodynamic equilibrium at some given temperature and keep stability with respect to arbitrary deformations.

To avoid misunderstandings it is necessary to note that the physical continuum with the abovementioned properties is the ultimate ideal model of solids, this model is applicable for describing the mechanical properties of real materials at sufficiently low values of relative deformations, until the elasticity or fracture limits are reached [1, 9].

To formulate the foundations of the linear elasticity theory for description the deformation properties of the 3D continuum [1], we first of all consider the simplest forms of deformation – homogeneous tension (or compression) and pure homogeneous shearing in an isotropic continuum. The study of several simple problems of this type makes it possible to introduce the concepts of moduli or coefficients of elasticity which

serve as the physical characteristics of the continuum, establish the relationships between them and find intervals of possible change of their significances, which are compatible with the assumption of the thermodynamic stability of the continuum at the initial (not deformational) state. The same approach has been also realized in the formulation of the foundations of the linear elasticity theory for the 2D continuum [9, 10]. The comparison of the deformation properties and the elasticity characteristics of 3D and 2D continua was carried out at [10] and showed significant differences that are not related to the nature of the force interaction between physical points (between atoms in real bodies) but caused by differences in topological properties of these continua. In the following sections of the article, the differences in the deformation properties of elastic bodies with three-dimensional and two-dimensional geometry will be discussed in more detail.

Homogeneous deformations and elastic moduli of an isotropic 3D continuum [1]

Let us consider a homogeneous isotropic and infinitely extended elastic medium (continuum), which at the initial state is a thermodynamic equilibrium physical system with G_3 (or 3D) geometric properties of the space. The position of every point in such a space is determined by the three-component radius vector $\vec{r} = (x_1, x_2, x_3) = (x_i)$ as regards to Ox_i $(i = 1,2,3)$ rectangular coordinate system with origin at an arbitrary point O. The configuration of the points of medium under deformation can be described by a three-component vector displacement field $\vec{u}(\vec{r}) = (u_i)$, components $u_i(\vec{r})$ and their first derivatives $\nabla_k u_i(\vec{r}) = \frac{\partial}{\partial x_k} u_i(\vec{r})$ are considered as continuous functions of $\vec{r} = (x_i)$. In the linear theory of elasticity, the local deformations of the continuum can also be described by the tensor field of relative deformations $\varepsilon_{ik}(\vec{r}) = \varepsilon_{ki}(\vec{r})$:

$$\varepsilon_{ik} = \frac{1}{2}(\nabla_i u_k + \nabla_k u_i),$$
$$\nabla_i = \frac{\partial}{\partial x_i}, \quad i,k = 1,2,3 \tag{1}$$

This tensor has nine components, six of them are independent $\varepsilon_q(\vec{r})$ ($q = 1,2,...,6$):

$$\varepsilon_1 = \varepsilon_{11}, \quad \varepsilon_2 = \varepsilon_{22}, \quad \varepsilon_3 = \varepsilon_{33},$$
$$\varepsilon_4 = \varepsilon_{23} = \varepsilon_{32}, \quad \varepsilon_5 = \varepsilon_{13} = \varepsilon_{31}, \quad \varepsilon_6 = \varepsilon_{12} = \varepsilon_{21}. \tag{2}$$

The diagonal components of the strain tensor ε_{11}, ε_{22}, ε_{33}, determine the relative change in the length of a small rectilinear segment in a continuum oriented before a deformation along one of the coordinate axes Ox_i (stretching-compression deformation), and the sum

$$\varepsilon_{nn} = \varepsilon_{11} + \varepsilon_{22} + \varepsilon_{33} \tag{3}$$

describes the relative change of the volume of a small element of the continuum (dilatation). The rule of summation over repeated coordinate indexes is used for writing of the vector and tensor relations.

Nondiagonal components of the tensor ε_{ik} at $i \neq k$ determine the change of angle between two mutually perpendicular segments along the axes Ox_i and Ox_k (shear deformation).

Any local deformation of the continuum can be represented by the sum of the dilatation (the spherical component) ε_{nn} and pure shear $\tilde{\varepsilon}_{ik}$, if the identity is used

$$\varepsilon_{ik} \equiv \frac{1}{3}\varepsilon_{nn}\delta_{ik} + \tilde{\varepsilon}_{ik}, \qquad \tilde{\varepsilon}_{ik} = \varepsilon_{ik} - \frac{1}{3}\varepsilon_{nn}\delta_{ik}, \tag{4}$$

where δ_{ik} – Kronecker symbol ($\delta_{11} = \delta_{22} = \delta_{33} = 1$, $\delta_{12} = \delta_{21} = \delta_{13} = \delta_{31} = \delta_{23} = \delta_{32} = 0$), at $\delta_{nn} = 3$. Tensor $\tilde{\varepsilon}_{ik}$ is called the deviator of the strain tensor, of its off-diagonal components $i \neq k$ only three remain independent ε_4, ε_5 and ε_6 but $\tilde{\varepsilon}_{nn} = 0$.

In the linear elasticity theory the bulk density of the free energy of the deformed continuum is considered as a function of temperature T and six independent components of the strain tensor $\varepsilon_{ik} = (\varepsilon_q)$. The deformation component of the free energy of an isotropic continuum can be represented in the form of two equivalent quadratic forms:

$$F(T, \varepsilon_1 \varepsilon_2, ... \varepsilon_6) - F_0(T) = \frac{1}{2}\lambda(T)\varepsilon_{nn}^2 + \mu(T)\varepsilon_{ik}\varepsilon_{ik} = \\ = \frac{1}{2}K(T)\varepsilon_{nn}^2 + \mu(T)\tilde{\varepsilon}_{ik}\tilde{\varepsilon}_{ik} \tag{5}$$

Here $F_0(T)$ – is equilibrium value of the free energy density of an undeformed continuum, and $\lambda(T)$, $\mu(T)$ and $K(T)$ – are equilibrium isothermal parameters that characterize the continuum's ability to accumulate elastic energy under deformations.

In the elasticity theory, the important role is played by the concept of internal mechanical stresses, which characterize the changes in the forces of short-range interaction between neighboring elements of the continuum under its deformations. To describe these forces, we introduce the tensor field of internal stresses $\sigma_{ik}(\vec{r}) = \sigma_{ki}(\vec{r})$, which under isothermal reversible deformations is determined by the relations

$$\sigma_{ik} = \left(\frac{\partial F}{\partial \varepsilon_{ik}}\right)_T \tag{6}$$

A separate component of the stress tensor has a physical dimension $\sigma_{ik}\ \left[\frac{force}{area}\right]$. It means the force that is directed along the axis Ox_i and acts on a unit area with the normal along Ox_k on the interface between adjacent elements of the continuum.

Using (6) and quadratic forms (5) we obtain two types of relations between the components of the stress tensor $\sigma_{ik}(\vec{r})$ and the strain tensor $\varepsilon_{ik}(\vec{r})$:

$$\sigma_{ik} = \lambda\varepsilon_{nn}\delta_{ik} + 2\mu\varepsilon_{ik}, \qquad (7)$$

$$\sigma_{ik} = K\varepsilon_{nn}\delta_{ik} + 2\mu\tilde{\varepsilon}_{ik}. \qquad (8)$$

These are two forms of recording the Hooke's law, which determines the linear relationship of local internal stresses in the continuum with its local deformations, and the parameters λ, μ and *K* have been called isothermal elastic moduli. These moduli are considered as equilibrium characteristics of the deformation properties of the continuum. Since according to (4) any deformation can be represented by the sum of the dilation ε_{nn} and pure shear $\tilde{\varepsilon}_{ik}$, it is sufficient to specify only two parameters for a complete characterization of the deformation properties of an isotropic elastic continuum, for example *K* and μ or λ and μ. Physical dimension of the elasticity moduli of the 3D continuum λ, μ, *K* $\left[\frac{force}{area}\right]$ coincides with the dimension of the components of the tensor σ_{ik}.

Symmetric stress tensor σ_{ik}, and tensor ε_{ik}, can be represented by the sum of the spherical σ_{nn} and deviatoric $\tilde{\sigma}_{ik}$ components according to the identity:

$$\sigma_{ik} \equiv \frac{1}{3}\sigma_{nn}\delta_{ik} + \tilde{\sigma}_{ik}, \qquad \tilde{\sigma}_{ik} = \sigma_{ik} - \frac{1}{3}\sigma_{nn}\delta_{ik}, \qquad (9)$$

Then the following relations hold:

$$\sigma_{nn} = 3K\varepsilon_{nn}, \qquad \tilde{\sigma}_{ik} = 2\mu\tilde{\varepsilon}_{ik}, \quad i \neq k. \qquad (10)$$

The first one determines the change in the relative volume of the small element of the continuum ε_{nn} under the action of the forces of hydrostatic compression σ_{nn}. Therefore the parameter *K* is called the bulk modulus. The second one relates the pure shear strains $\tilde{\varepsilon}_{ik}$ and the shear forces $\tilde{\sigma}_{ik}$, and parameter μ is called shear modulus. These moduli are used when writing Hooke's law in the form of relation (8). If Hooke's law is represented by the relation (7) then the parameters λ and μ are called Lame coefficients. The comparison (7) and (8) gives the relation

$$K = \lambda + \frac{2}{3}\mu. \qquad (11)$$

At the applied parts of the elasticity theory such as engineering and construction mechanics along with the shear modulus and bulk modulus, two other characteristics of the elastic properties of materials are used Young's modulus and Poisson's ratio. They are convenient for description of the elastic bodies deformation of limited dimensions, for example, tension (or compression) of a rod like a fragment of an elastic continuum of cylinder shape. A homogeneous deformation under the action of forces is considered. The force are applied to the ends of the rod and directed along its longitudinal axis with a free lateral surface. In a system of rectangular coordinates with an axis Ox_3 along the longitudinal axis of the rod, the deforming stress in its volume has one component $\sigma_{33}(\vec{r}) = P = const$, created by the stress *P* at the ends. It follows from the relations (7) (8) and (10) that under such a load a uniform deformed state appears in the rod $\varepsilon_{ik}(\vec{r}) = const$ with three non-zero diagonal components of the strain tensor ε_{11}, ε_{22} и ε_{33}. All of them are proportional to the load P, and their relationship to each other can be represented in the form:

$$\sigma_{33} = E\varepsilon_{33}, \qquad \varepsilon_{11} = \varepsilon_{22} = -\nu\varepsilon_{33} \qquad (12)$$

Here the role of the elasticity characteristics of a solid body instead of moduli μ and *K* is played by the parameters *E* – Young's modulus and ν – Poisson's ratio:

$$E = \frac{9K\mu}{2K+\mu}, \qquad \nu = \frac{3K-2\mu}{2(3K+\mu)}. \qquad (13)$$

Thus, the deformation properties of any isotropic 3D continuum can be characterized by a set of five parameters λ, μ, ν, *K* and *E*. But since they are related by (11) and (13), only two of them should be regarded as independent and the choice of such a pair is determined by the specific conditions of the problem under consideration.

Homogeneous deformations and elastic moduli of the 2D continuum [9, 10]

Two-dimensional system of rectangular coordinates $x_1 O x_2$ will be used at the description of deformation of thermodynamical equilibrium homogeneous continuum with the geometrical properties of G_2 space (or 2D). The position of an individual point is defined by a two-dimensional radius vector $\vec{r} = (x_1, x_2) = (x_i)$, where $i = 1, 2$, and the configuration of the deformed continuum will be described by a two-dimensional displacement field of points in its plane $\vec{u}(\vec{r}) = (u_1, u_2) = (u_i)$ or four-component tensor field of deformations $\varepsilon_{ik}(\vec{r}) = \varepsilon_{ki}(\vec{r})$:

$$\varepsilon_{ik} = \frac{1}{2}(\nabla_i u_k + \nabla_k u_i),$$

$$\nabla_i = \frac{\partial}{\partial x_i}, \quad i,k = 1,2 \qquad (14)$$

Here the components of the displacement fields $u_i(\vec{r})$ and the strain tensor $\varepsilon_{ik}(\vec{r})$ are considered as continuous functions of the space variables $\vec{r} = (x_i)$ in the plane of the continuum.

It should be noted that such a continuum has the property of an infinitely thin elastic film and its small elements can also experience a displacement $w(\vec{r})$ in the third spatial dimension, perpendicular to the plane $x_1 \mathrm{O} x_2$. In the case of an inhomogeneous distribution of displacements $w(\vec{r})$ the bending deformations of the continuum are arised This is a deformation mode specific only for the 2D continuum, it is absent in the 3D continuum. We do not discuss the mode here since the main task of the article is a comparative description of the deformation properties of 3D and 2D solids. We also note that in this section we store the symbols of the previous section to denote the deformation properties and characteristics of the continuum. We emphasize only the differences in the values of the coordinate indices: here $i,k,n = 1,2$ instead of $i,k,n = 1,2,3$ at the preceding part. This makes it possible to display more clearly the differences of the deformation properties of solids with three-dimensional and two-dimensional geometries discussed in the article.

The four-component symmetric tensor ε_{ik} (14) has three independent components ε_q, $q = 1,2,3$:

$$\varepsilon_1 = \varepsilon_{11}, \qquad \varepsilon_2 = \varepsilon_{22}, \qquad \varepsilon_3 = \varepsilon_{12} = \varepsilon_{21} \tag{15}$$

The diagonal components ε_{11} и ε_{22} determine the relative tensile-compression strain along two coordinate axes Ox_i. The sum

$$\varepsilon_{nn} = \varepsilon_{11} + \varepsilon_{22} \tag{16}$$

describes the relative change in the area of a small element in the continuum (two-dimensional dilatation). Nondiagonal components ε_{ik} at $i \neq k$ determine the shear strain in the 2D continuum

Any local deformation in the 2D continuum can be represented as the sum of a two-dimensional dilatation (circular component) ε_{nn} and pure shear $\tilde{\varepsilon}_{ik}$:

$$\varepsilon_{ik} \equiv \frac{1}{2}\varepsilon_{nn}\delta_{ik} + \tilde{\varepsilon}_{ik}, \qquad \tilde{\varepsilon}_{ik} = \varepsilon_{ik} - \frac{1}{2}\varepsilon_{nn}\delta_{ik}, \tag{17}$$

where δ_{ik} – two-dimensional Kronecker symbol ($\delta_{11} = \delta_{22} = 1$, $\delta_{12} = \delta_{21} = 0$), where $\delta_{nn} = 2$. The deviator of the strain tensor $\tilde{\varepsilon}_{ik}$ at $i \neq k$ has only one independent component $\varepsilon_3 = \varepsilon_{12} = \varepsilon_{21}$, a $\hat{\varepsilon}_{nn} = 0$. We should pay attention to the difference in the numerical coefficients in formulas (4) and (17) (accordingly $\frac{1}{3}$ and $\frac{1}{2}$). Exactly this difference after all will be associated with a significant difference in the relationship between the characteristics of the elasticity of 3D and 2D continua.

In the approximations of the linear elasticity theory the two-dimensional free energy density of an isotropic deformed 2D continuum is a function of temperature T and three independent components of the strain tensor ε_q and can be represented as two equivalent quadratic forms:

$$\begin{aligned} F(T,\varepsilon_1,\varepsilon_2,\varepsilon_3) - F_0(T) &= \frac{1}{2}\lambda(T)\varepsilon_{nn}^2 + \mu(T)\varepsilon_{ik}\varepsilon_{ik} = \\ &= \frac{1}{2}K(T)\varepsilon_{nn}^2 + \mu(T)\tilde{\varepsilon}_{ik}\tilde{\varepsilon}_{ik} \end{aligned} \tag{18}$$

Here $F_0(T)$ – equilibrium value of the two-dimensional free energy density and λ, μ, K – two-dimensional analogs of elastic moduli.

The short range interaction between the points of the 2D continuum is characterized by a symmetric internal stress tensor $\sigma_{ik}(\vec{r}) = \sigma_{ki}(\vec{r})$. Each individual component of this tensor has dimension σ_{ik} $\left[\frac{force}{lenght}\right]$, here force is directed along Ox_i axis and acts on the unit element of the dividing line between next regions of the continuum, which has a normal in the direction of the axis Ox_k.

In the symmetrical stress tensor, we distinguish σ_{ik} the circular σ_{nn} and deviatoric $\hat{\sigma}_{ik}$ components:

$$\sigma_{ik} = \frac{1}{2}\sigma_{nn}\delta_{ik} + \tilde{\sigma}_{ik}, \ \tilde{\sigma}_{ik} = \sigma_{ik} - \frac{1}{2}\sigma_{nn}\delta_{ik} \tag{19}$$

Then, according to formulas (6) and (18), Hooke's law for a 2D continuum can be represented in the form of relations:

$$\sigma_{ik} = \lambda\varepsilon_{nn}\delta_{ik} + 2\mu\varepsilon_{ik} = K\varepsilon_{nn}\delta_{ik} + 2\mu\tilde{\varepsilon}_{ik}; \tag{20}$$

$$\sigma_{nn} = 2K\varepsilon_{nn}, \qquad \tilde{\sigma}_{ik} = 2\mu\tilde{\varepsilon}_{ik}, \ i \neq k. \tag{21}$$

The physical dimension of the moduli of elasticity of the 2D continuum λ, μ, K $\left[\frac{force}{lenght}\right]$ coincides with the dimension of the components of the tensor σ_{ik}. It can be seen from the relations (21) that the relative change in the area of a small element of the 2D continuum ε_{nn} is determined by the action of the forces of all-round tension-compression σ_{nn}. Therefore, the parameter K should be regarded as a two-dimensional analog of the bulk modulus. Accordingly, the parameter μ has the meaning of a two-dimensional analog of the shear modulus, since it determines the relationship of pure shear $\tilde{\varepsilon}_{ik}$ and shear forces $\tilde{\sigma}_{ik}$ within the 2D continuum. Comparison of (20) and (21) leads to a relation between the moduli λ, μ and K:

$$K = \lambda + \mu \tag{22}$$

At description of the deformation of plane elastic bodies of limited dimensions, it is also expedient to use two-

dimensional analogues of the Young's modulus *E* and Poisson's ratio ν. Let us consider, for example, the elongation (or compression) of the 2D continuum strip along its longitudinal axis under the action of a two-dimensional stress *P* at its ends and in the absence of load on the side boundaries. Such a band is a two-dimensional analogue of the rod considered in the previous section. At rectangular coordinates system with an axis Ox_2 along the longitudinal axis of the band, the deforming stress in it has only one nonzero component $\sigma_{22}(\vec{r}) = P = const$, created by the stress *P* at the ends. It follows from (20) and (21) that under such a load a uniform deformed state appears in the band $\varepsilon_{ik}(\vec{r}) = const$ with two nonzero components of the strain tensor ε_{11} and ε_{22}. Each of them is proportional to the load *P*, and their relationship can be represented in the form of relationships in which the role of the elasticity parameters is played by two-dimensional analogues of the Young's modulus *E* and Poisson's ratio ν:

$$\sigma_{22} = E\varepsilon_{22}, \quad \varepsilon_{11} = -\nu\varepsilon_{22}. \tag{23}$$

The relationship between *E* and ν with elasticity moduli *K* and μ is defined by:

$$E = \frac{4K\mu}{K+\mu}, \quad \nu = \frac{K-\mu}{K+\mu}. \tag{24}$$

To characterize the deformation properties of an elastic 2D continuum, five parameters can be used λ, μ, ν, *K* and *E*, but since they are related by (22) and (24) only two of them should be regarded as independent.

Topological differences in the deformation properties of 3D and 2D elastic solids

If we carefully compare the basic relationships between the linear elasticity theory of 3D and 2D continuum, we can note the presence of both their similarity (at least visual), and quite significant differences. For example formulas (5) – (8) and (18) - (20), visually coincide, but this similarity is conditional, it is a consequence of the use in both sections of the same symbols for marking radius-vector of physical points $\vec{r} = (x_i)$, of strain tensors ε_{ik} and stress tensors σ_{ik}, elasticity moduli λ, μ, *K*, E and Poisson's ratio ν. Strictly speaking, there is no such similarity: first, the coordinate indices assume the values $i = 1,2,3$ or $i = 1,2$; secondly, the components of the stress tensor σ_{ik} and the elastic moduli λ, μ, *K*, E change their physical dimensions when the spatial dimension of the continuum changes.

Very significant differences, directly related to the general geometry (topology) of the continua. There are also clearly seen when comparing the relationships between the elasticity parameters in Section 3 and in Section 4. In order to more clearly show these differences, it is advisable to give here several relationships between the elasticity parameters of 3D and 2D solids, which are most often used when considering various specific problems of the applied elasticity theory. For elastic 3D solids the parameters λ, μ, *K*, *E* and ν are related by the relations:

$$E = \frac{9K\mu}{3K+\mu} = 3K(1-2\nu) = 2\mu(1+\nu), \tag{25}$$

$$\nu = \frac{3K-2\mu}{2(3K+\mu)} = \frac{E-2\mu}{2\mu} = \frac{3K-E}{6K}, \tag{26}$$

Analogues of these relations for elastic 2D solids have the form:

$$E = \frac{4K\mu}{K+\mu} = 2K(1-\nu) = 2\mu(1+\nu), \tag{27}$$

$$\nu = \frac{K-\mu}{K+\mu} = \frac{2\mu-E}{E} = \frac{2K-E}{2K}, \tag{28}.$$

Comparison of formulas (25) - (26) with formulas (27) - (28) leads to the conclusion that there are significant differences in the deformation properties of elastic continua with different numbers of spatial measurements.

Separately, we should also discuss topological differences in the allowed intervals for the change in the numerical values of the elasticity parameters. The equilibrium values of the elastic moduli λ, μ, *K*, *E* and ν for a particular solid are determined by the physico-chemical characteristics of the interatomic interaction and by the intensity of the thermal motion of the atoms. At the same time, these values should be compatible with the condition of thermodynamic stability common to all solids with respect to arbitrary elastic deformations. A formal mathematical criterion of stability is the positive definiteness of the quadratic forms (5) and (18), which describe the dependence of the free energy of elastic bodies on six (2) or three (15) independent components ε_q of the strain tensor. This criterion imposes certain restrictions on the admissible values of the moduli λ, μ, and *K* as the coefficients of quadratic forms. For example, such restrictions can be obtained if in the formulas (5) and (18) we consider separately two types of homogeneous deformations:

- pure dilation, when $\varepsilon_{ik} = \varepsilon\delta_{ik}$, where $\varepsilon = const$ and $\tilde{\varepsilon} = 0$, and $F - F_0 = \frac{s^2}{2} K \cdot \varepsilon^2$, $s = 2,3$;
- pure shear when $\varepsilon_{nn} = 0$, and $F - F_0 = \mu\tilde{\varepsilon}_{ik}\tilde{\varepsilon}_{ik} = \mu\varepsilon_{ik}\varepsilon_{ik}$.

From this it is clear that the condition of positive definiteness of the deformation component of the free energy $F(T, \varepsilon_q) - F_0(T) \geq 0$ is the positive values of the

moduli $K \geq 0$ and $\mu \geq 0$. It follows from (25) and (27) that this restriction also leads to the condition $E \geq 0$ for both the three-dimensional ($s = 3$) and two-dimensional ($s = 2$) continua.

However, the ranges of values of the Poisson's ratio ν, that satisfy the condition of thermodynamic stability for 3D and 2D continua are significantly different. If we take the limiting values $K = 0$ and $\mu = 0$ for the 3D continuum according to (26), we obtain condition

$$-1 \leq \nu \leq \frac{1}{2}. \qquad (29)$$

and for the 2D continuum, according to (28), condition

$$-1 \leq \nu \leq 1. \qquad (30)$$

Thus, the range of admissible equilibrium values of the Poisson's ratio of elastic solids can be regarded as a kind of topological invariant that varies abruptly from (29) to (30) upon transition from three-dimensional to two-dimensional solid systems.

The above discussion and the conclusions drawn on its basis confirm the advisability of using geometric concepts and methods in the theory of elasticity. They allow a deeper and more comprehensive description of the laws of deformation of elastic solids and reveal additional features of deformation properties.

Appendix [3, 4, 11]

For a reader who does not have a fundamental mathematical education, it is useful to explain the meaning of a number of terms and concepts of geometry that are used in the article, without excessive mathematical rigor of formulations.

Geometry, as a branch of mathematics, is based on the concepts of "point" and "space": a point is an elementary structural unit of a mathematical space G_S, that is the result of continuous and infinitely extended repetition of a point in s dimensions (or conditional "directions"): positive integer values $s = 1, 2\ldots$ give the number of measurements space. It is assumed that any of the points can be considered as the origin, and the position with respect to it of any other point in space is given by a set of real numbers $(x_1, x_2, \ldots x_S) = (x_i)$ – the coordinates of the point (the symbol $i = 1,2\ldots s$ denotes a coordinate index).

In the geometric description of deformations of solids within the framework of the linear elasticity theory it suffices to consider one of the simplest types of a mathematical space – the Euclidean metric space with zero curvature. In this space we introduce the notion of the distance $l^{\alpha,\beta}$ between two points (x_i^{α}) and (x_i^{β}), which is defined by

$$l^{\alpha,\beta} = \sqrt{(x_1^{\alpha} - x_1^{\beta})^2 + (x_2^{\alpha} - x_2^{\beta})^2 + \ldots + (x_S^{\alpha} - x_S^{\beta})^2}\,.$$

In this case, a single point (for example, the origin) can be interpreted as a zero-dimensional space and assume that the distance of any point (x_i^{α}) from itself is equal to zero ($l^{\alpha,\alpha} = 0$).

In the early stages of the development of geometry, it was a mathematical "tool" for analyzing spatial relationships in the surrounding and intuitively perceived three-dimensional empirical space G_3 (or 3D) of the physical world. In this geometry, the topology was called its section, which dealt with a general analysis of the structure of space itself-the presence or absence of continuity discontinuities (holes or point punctures-singularity points) in it, as well as the systematization and general characteristics of the lines and surfaces defined in it with different curvatures, closed or open with the presence or absence of self-intersections etc. Later, the concepts of abstract mathematical spaces described at the beginning of this section as multi-dimensional continua of mathematical points (multidimensional numerical or even functional continua) arose and became established. By analogy with 3D geometry in such spaces, G_S for $s \geq 1$ you can specify different geometric figures by a continuous repetition of points, infinitely extended in one dimension and finite in others: conditional segments, lines, surfaces, volumetric figures. The number, variety and geometric meaning of such figures are different for different values of the number of measurements *s*. In modern geometry, topology is the most general and abstract part of it, in which only properties of space and geometric objects (figures) defined in it are studied that are not related to quantitative characteristics and are preserved for all continuous space deformations and one-to-one transformations of points, invariants with respect to such transformations are systematized [3, 4, 11]. The theorem [3] is formulated and proved, according to which the main topological invariant of the space G_S is the number of dimensions *s*; in other words, changing the dimension of space changes its topology.

Topological analysis of the most common geometric properties of spaces and geometric objects defined in them widely and effectively use various branches of mathematics [11]: symmetry analysis, vector and tensor algebra, analytic and differential geometry, mathematical field theory, theory of partial differential equations. These same branches of mathematics serve in modern physics as the basis for theoretical analysis and description of various physical systems. Moreover, for their comprehensive characterization, it also proved expedient to use geometric concepts of space and its topology [4, 12, 13]. Examples include: classification of 1D, 2D and 3D structures in solid state physics; 4D space-time

continuum in the theory of relativity; phase space in the classical mechanics of material points; functional spaces in quantum mechanics.

The use of the geometric approach and topology methods in theoretical physics helps to describe not the details of the structure and properties of physical systems, but to establish or interpret the most general laws and relationships obtained in various concrete experiments in the study of systems of different physical nature [4, 12, 13]. An important role is played by the development of representations about the relationships and mutual correspondences between abstract spaces in mathematics and their physical analogs - different types of material continuum or physical vacuum [4]. It is possible to separate various real physical systems into extremely small subsystems (regions) and consider them as physical points. They are compared to the points of the abstract mathematical space, but they preserve and bear upon themselves a set of physical characteristics: mass, momentum, potential and kinetic energies, electric charge, and so on. Continuous and infinitely extended repetition of such points creates a physical space that is regarded as an analog of a mathematical space with its geometric and topological properties. Thus, there are prerequisites for the effective use of geometry as a mathematical "tool" in theoretical physics.

The authors are sincerely grateful to S.N. Smirnov for a meaningful and useful discussion of the article, and also want to express gratitude to T.I. Vainblat for help in translating the article.

The article is offered as an addition to the course of lectures for the masters of the Physics Faculty: Prof. Natsyk V.D. "Fundamentals of the elasticity and plasticity theory of solids", kfk.biz.ht – Educational materials.

References

1. L. D. Landau. E.M. Lifshits. Teoriya uprugosti. Nauka. M. (1978). 730 s.
2. D.Ya. Stroyk. Kratkiy ocherk istorii matematiki. Nauka. M. (1978). 335 s.
3. K. F. Kleyn. Elementarnaya matematika s tochki zreniya vysshey. Nauka. M. (1987). 431 s.
4. V.S. Lukianets. Fiziko-matematicheskiye prostranstva i realnost. Naukova dumka. Kiyev (1971). 109 s.
5. I. F. Lyuksutov. A. G. Naumovets. V. L. Pokrovskiy. Dvumernyye kristally. Naukova dumka. Kiyev (1988). 320 s.
6. A. M. Kosevich. Teoriya kristallicheskoy reshetki (fizicheskaya mekhanika kristallov). KhGU Vishcha shkola. Kharkov (1988). 327 s.
7. A. M. Kosevich. Mekhanika kristalichnoï gratki. seriya «Universitetski lektsiï z fiziki tverdogo tila». Nauk. vid. Akta. Kharkiv (2005). 305 s.
8. K. S. Novoselov. UFN 181. 1299 (2011).
9. V.D. Natsik. S.N. Smirnov. FNT. 39. 690 (2013).
10. V. D. Natsik. S. N. Smirnov. V. I. Belan. FNT. 44. 877 (2018).
11. G. Korn. T. Korn. Spravochnik po matematike (dlya nauchnykh rabotnikov i inzhenerov). Nauka. M. 1977. 831 s.
12. M. Nakahara. Geometry. Topology and Physics. IOP Publishing. Bristol 1990
13. A.M. Kosevich. FNT 30. 135 (2004).

Вісник ХНУ, серія «Фізика», вип. 28, 2018. с. 40-45

PACS:

UDC: 530.1/539.8

Quantification and physics of cold plasma treatment of organic liquid surfaces

Edward Bormashenko[1], Victor Multanen[4], Gilad Chaniel[2], Roman Grynyov[2], Evgeny Shulzinger[1], Roman Pogreb[2], Hadas Aharoni[1], Yakir Nagar[3]

1 Ariel University, Engineering Faculty, Chemical Engineering, Biotechnology and Materials Department, 40700, P.O.B. 3, Ariel, Israel
2 Ariel University, Physics Department, 40700, P.O.B. 3, Ariel, Israel
3 Ariel University, Department of Electrical Engineering, 40700, P.O.B. 3, Ariel, Israel
4 Department of Mechanical and Aerospace Engineering within the College of Engineering at The Ohio State University
edward@ariel.ac.il

ORCID: *0000-0003-1356-2486*

DOI: 10.26565/2222-5617-2018-28-02

Plasma treatment increases the surface energy of condensed phases: solids and liquids. Two independent methods of the quantification of the influence imposed by a cold radiofrequency air plasma treatment on the surface properties of silicone oils (polydimethylsiloxane) of various molecular masses and castor oil are introduced. Under the first method the water droplet coated by oils was exposed to the cold air radiofrequency plasma, resulting in an increase of oil/air surface energy. An expression relating the oil/air surface energy to the apparent contact angle of the water droplet coated with oil was derived. The apparent contact angle was established experimentally. Calculation of the oil/air surface energy and spreading parameter was carried out for the various plasma-treated silicone and castor oils. The second method is based on the measurement of the electret response of the plasma-treated liquids.

Keywords: cold plasma, silicone oils, spreading parameter, change in the surface energy, hydrophilization, electret.

Обробка плазмою збільшує поверхневу енергію конденсованих фаз: твердих речовин і рідин. Введено два незалежні методи кількісної оцінки впливу холодної радіочастотної обробки плазмою на властивості поверхні силіконових масел (полидиметилсилоксана) різних молекулярних мас та касторової олії. За першим способом крапля води, вкрита маслами, зазнавала впливу холодної повітряної радіочастотної плазми, що призводило до збільшення поверхневої енергії масла/повітря. Отримано вираз, що зв'язує енергію поверхні нафти і повітря з удаваним кутом контакту краплі води, що вкрита маслом. Явний кут контакту був встановлений експериментально. Розрахунок параметрів поверхневої енергії нафти і повітря проводили для різних оброблених плазмою силіконових і касторових масел. Другий метод заснований на вимірюванні електретного відгуку рідин, оброблених плазмою.

Ключові слова: холодна плазма, силіконові олії, параметр змочування, зміна поверхневої енергії, гідрофілізація, електрет.

The paper is devoted to the blessed memory of Ya. E. Gegusin, Brilliant scientist and teacher, who devoted his life to Kharkov University.

Introduction

Plasma treatment (low and atmospheric-pressure) is widely used for the modification of surface properties of solid organic materials [1]. The plasma treatment creates a complex mixture of surface functionalities which influence surface physical and chemical properties; this results in a dramatic change in the wetting behaviour of the surface [2]. It was suggested that hydrophilization of organic surfaces by plasmas may be at least partially related to the re-orientation of hydrophilic moieties constituting organic molecules [2i, 3-4]. Oxidation of plasma-treated surfaces and removal of low-mass weight fragments present on organic surfaces also contribute to hydrophilization [4]. Much effort has been spent in understanding the interaction of plasmas with solid organic surfaces, whereas data related to plasma treatment of liquids are scarce [5].

An interest in plasma treatment of liquid organic surfaces arose due to various practical reasons, including the possibility of de-contamination of liquids by plasmas [5] and microfluidics applications of these surfaces, stipulated by the extremely low contact angle hysteresis exhibited by liquid/liquid systems including oil/water ones [6]. Quantification of the impact exerted by plasmas on liquid surfaces faces serious experimental challenges [7]. Our paper focuses on the modification of surfaces of

organic liquids exposed to cold radiofrequency plasma by two independent techniques, namely the measurement of the apparent contact angle and study of their electret response.

Experimental

Quantification of the interaction of cold plasma with organic liquid surfaces was carried out with silicone-impregnated micro-porous polymer surfaces, manufactured as described in Refs. 8. Polypropylene (PP) films (the thickness 25 μm) were coated with honeycomb polycarbonate (PC) films, by the fast dip-coating process. As a result, we obtained typical "breath-figures" self-assembly patterns, depicted in Figure 1. Honeycomb PC

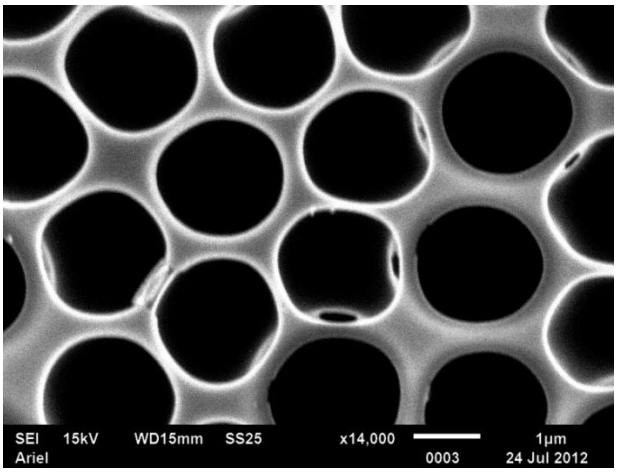

Fig. 1. Polycarbonate honeycomb coating of polypropylene film , obtained with "breath-figures" self-assembly, carried out in a humid atmosphere. Scale bar is 1 μm.

coating was obtained according to the protocol described in detail in Refs. 8. The average radius of pores was about 1.5 μm. The average depth of pores as established by AFM was about 1 μm.

Polydimethylsiloxane (PDMS) oils with molecular masses of 5600, 17500, 24000 $g \cdot mol^{-1}$, and silicone oil for MP & BP apparatus (the molar mass was not identified), denoted for brevity in the text respectively as PDMS1, PDMS2, PDMS3 and PDMS4 were supplied by Aldrich. Castor oil was supplied by Vitamed Pharmaceutical Industries Ltd. PC porous coatings were impregnated by all kinds of aforementioned PDMS oils and castor oil, as shown in Figure 2. The thickness of PDMS/Castor oil layers was established by weighing as 20±2 μm.

A water droplet with a volume of 8 μl was deposited on surfaces impregnated with the abovementioned oils as depicted in Figure 2. The water droplet was encapsulated by silicone and Castor oils, as depicted in Figure 3 and as discussed in detail in Ref. 7.

Water droplets, encapsulated by all kinds of the oils used in our study, were exposed to a radiofrequency

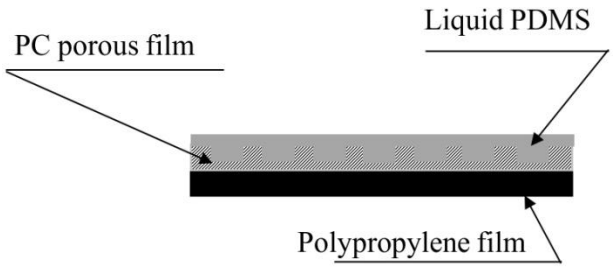

Fig. 2. Scheme of the silicone oil impregnated PP substrates used in the investigation.

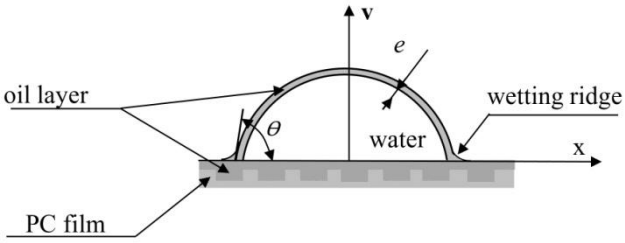

Fig. 3. Water droplet encapsulated by the oil layer. θ is the apparent contact angle. *e* is the thickness of the oil layer

(13.56MHz) inductive air plasma discharge under the following parameters: pressure 266 Pa, power 18 W, ambient temperature. It should be stressed that the encapsulation of water droplets by oils prevented their evaporation in the plasma vacuum chamber, which made the entire experiment possible. The time of plasma treatment was varied within 30-60ms; the duration of a single pulse was 30ms.

Apparent contact angles of the water droplets encapsulated with the above oils were measured before and after the plasma treatment by a Ramé-Hart Advanced Goniometer (Model 500-F1).

Surface tensions of oils used in our investigation were established with the pendant droplet method by a Ramé-Hart Advanced Goniometer (Model 500-F1).

The electret response of oils exerted to the plasma treatment was studied with lab-made device depicted in Figure 4. PP films coated by PC porous films, filled by silicone and castor oils were exposed to cold plasma under the aforementioned parameters. Plasma treated samples were placed between two copper plates, mounted into a faradaic cage (see Figure 4).

The use of PP films possessing excellent dielectric properties in these experiments prevented possible artifacts due to the short circuiting across the sample. The lower plate was accelerated periodically by a vibration generator, therefore during the measurement the film was loaded with a dynamic oscillating force. The output signal of voltage between the charged surfaces was registered by a lock-in amplifier (7260 DSP). The vibration generator and lock-in amplifier were modulated by a function

generator (Model DS345) at the frequency 107.77 Hz. Time dependencies of the electrical potential measured on the surface of the wet side of the samples were registered.

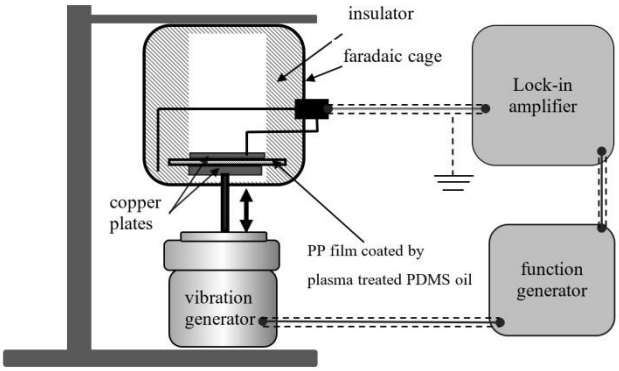

Fig. 4. Scheme of the experimental lab-made unit for measuring of electret response of plasma-treated silicone oils.

Results and discussion

Influence of plasma treatment on the wetting regimes inherent for PDMS

Water droplets deposited on silicone oils were encapsulated with them, as demonstrated in Refs. 7, 9. This wetting situation is well explained by the analysis of the spreading parameter *S* governing the wetting situation [10]:

$$S = \gamma - (\gamma_{oil} + \gamma_{oil/water}), \quad (1)$$

where γ, γ_{oil} and $\gamma_{oil/water}$ are interfacial tensions at water/vapor, oil/vapor and oil/water interfaces respectively. Interfacial oil/water tensions for the studied oils, summarized in Table 1, were extracted from the literature data [11].

Table 1.

Interfacial properties of oils used in the investigation.

Oil	Surface tension, γ_{oil}, mJ·m^{-2}	Interfacial tension, $\gamma_{oil/water}$ mJ·m^{-2}
PDMS1	20.7±0.3	23-24
PDMS2	21.2±0.3	23-24
PDMS3	21.1±0.5	23-24
PDMS4	21.1±0.5	23-24
Castor oil	35.4±0.2	14.8

Substituting the aforementioned values of interfacial tensions in Equation (1), we obtain $S > 0$; in this case, both the silicone and castor oils are expected to completely coat the water droplet. This was indeed observed: water droplets were coated by silicone and castor oils.

We have already demonstrated, that cold plasma treatment increased the surface energy of silicone liquids [7]. The natural measure of the surface energy is an apparent contact angle, so-called APCA [10]. When the effects of disjoining pressure *P(e)* and wetting ridge (see Figure 3) are neglected, the APCA for oils/water pairs in the situation of complete coating of a water droplet by oil, is given by the following expression [7]:

$$\cos\theta = \frac{\gamma_{oil} - \gamma_{oil/water}}{\gamma_{oil} + \gamma_{oil/water}}, \quad (2)$$

The contact angle θ appearing in Equation (2) is an equilibrium contact angle [7, 10]. First of all we made sure that the APCAs observed for the studied oil/water pairs demonstrated properties inherent for equilibrium contact angles. Equilibrium contact angles do not depend on external fields, including gravity [10, 12]. Hence they are independent of the volume of a droplet [10]. We varied the volume of water droplet in the range of 3-8 μl with a step of 1 μl for all investigated water/oils pairs, and proved that the established APCAs are independent of the volume of the water droplets within the experimental accuracy of the measurement. Thus, it was reasonable to suggest that the established APCAs are the equilibrium ones.

Equation (2) may be exploited for the calculation of the surface energy of the oil. Rewriting of Equation (2) immediately yields:

$$\gamma_{oil} = \gamma_{oil/water} \cot^2 \frac{\theta}{2}, \quad (3)$$

Thus, measurements of APCAs allow calculation of γ_{oil} according to Equation (3), when $\gamma_{oil/water}$ is known from the independent measurements, such as those carried out in Refs. 11. If the value of $\gamma_{oil/water}$ is not affected by plasma treatment and θ is established experimentally, Equation (3) immediately supplies the value of γ_{oil}. The idea that $\gamma_{oil/water}$ was not essentially modified by plasma treatment seems reasonable, due to the fact that cold plasmas affect only the external nanometrically scaled layer of a surface [1-2].

It should be emphasized that Equation (3) permits direct calculation of γ_{oil} from the value of the APCA, because the APCA depends on the pair $\gamma_{oil}, \gamma_{oil/water}$ and not on the triad of interface tensions as it occurs for wetting of solid surfaces, described by the famous Young formula [10,12].

As it is seen from the data, summarized in Table 2, the APCA decreased markedly with the time of plasma treatment for all kinds of oils used in our investigation. It should be stressed that in the present paper the time span of the plasma treatment was controlled precisely with a step of 30 ms. The decrease of APCA is also illustrated in Figure 5.

We observed the gradual decrease of the volume of the water droplet in the course of plasma treatment.

Table 2.

Dependence of APCA, θ, surface tension γ_{oil}, and spreading parameter S on the time of plasma treatment.

Oil	Time of plasma treatment, ms	Contact angle θ, degrees	γ_{oil}, mJ·m^{-2}	S, mJ·m^{-2}
PDMS 2	0	95	20.7	28.3
	30	73	42.8	6.1
	60	69	48.7	0.2
PDMS 3	0	95	21.2	27.7
	30	87	25.5	23.4
	60	77	36.4	12.6
PDMS 4	0	96	21.1	27.8
	30	73	42.0	6.9
	60	70	46.9	2.0
Castor oil	0	70	35.4	21.7
	30	61	42.7	14.5
	60	54	57.0	0.1

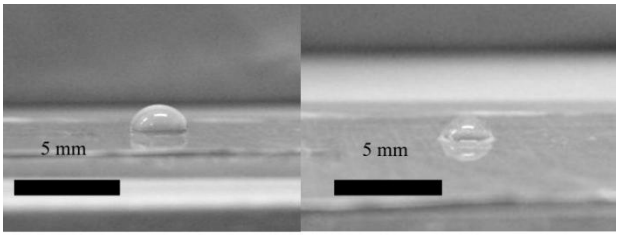

Fig. 5. Images of a water droplet coated with PDMS2 silicone oil: a). before plasma treatment; b) the same droplet after 60 ms of the cold plasma treatment. In both cases the water droplet is coated by PDMS2 oil.

However this change in the droplet volume does not prevent the calculation of γ_{oil} according to Equation (3), due to the fact that the equilibrium APCA is insensitive to the volume of a droplet, as dicussed above [10].

As it may be expected, γ_{oil} increased with the time of plasma treatment, as it is clearly seen from data supplied in Table 2.

It was also instructive to deduce the dependence of the spreading parameter S on the time of plasma treatment. The spreading parameter S was calculated with Equation (1) for values of γ_{oil}, and estimated with Equation (3) from the experimental data, supplied in Table 2. It is seen, that the spreading parameter S decreases with growth of the time of plasma treatment and approaches zero. This is quite understandable, when the increase in the oil/air surface energy arising from the plasma treatment is taken into account. When the spreading parameter approaches zero, the continuation of plasma treatment becomes impossible; silicone oil does not coat a water droplet and it is evaporated in the plasma chamber.

The maximal value of γ_{oil} established for all kinds of silicone oils used in our study was close to $\gamma_{oil} = 49\text{mJ} \cdot \text{m}^{-2}$. It should be emphasized that this is not the "saturation value" of the oil/air interfacial tension. The saturation value of γ_{oil} remains unachievable under the applied technique, due to the decrease of the spreading parameter finally approaching zero, resulting in the evapotation of a droplet, as explained above.

The important advantage of the proposed method of establishment of the surface energy of oils is stipulated by the low contact angle hysteresis, inherent for liquid/liquid systems, associated with the weak pinning of the contact line, intrinsic for these kinds of systems [6].

Electret response of plasma-treated oils

As it was demonstrated in the previous section plasma treatment increases the surface energy of organic oils. But what is the physical mechanism responsible for this increase? It is well accepted that the plasma treatment creates a complex mixture of surface functionalities which influence physical and chemical properties of a polymer surface, resulting in the jump in its surface energy [2]. In our paper we focus on one of the possible sources of this increase, namely the modification of electrical properties of oils by the plasma. Recent investigations demonstrated that plasmas modify essentially electrical properties of solid polymers including PDMS, PP and polyethylene [13]. We studied the electret response of the plasma-treated oils with the device, shown in Figure 4, already exploited by our group for the study of the electret response of plasma-treated solid polymers [13b].

The literature data related to the electret properties of liquids are scanty (an electret is a material that has a macroscopic electric field at its surface) [14]. It should be emphasized that all studied organic oils demonstrated the pronounced electret response. The initial voltage V_0, established immediately after the plasma treatment, registered for plasma-treated oils was on the order of magnitude of 100 μV. However, this voltage decays with times, as shown in Figures 6a-b, as it takes place on plasma-treated solid polymers [13b]. The temporal decay of voltage may be exponentially fitted by exponential dependence:

$$V(t) = V_0 + \tilde{V} \exp(-\frac{t}{\tau_e}), \qquad (4)$$

where τ_e is the characteristic time of the decay of electret properties, $\tilde{V}$ is the fitting parameter. The characteristic

times established for investigated organic oils are summarized in Table 3.

The open question to be addressed in future investigations: what are the microscopic sources of both of the hydrophilization of oils (discussed in the previous Section) and electret behavior of the oils observed on our experiments and illustrated with Figure 6 a-b).

Table 3.

Characteristic times of the electret reponse τ_e decay established for various organic oils.

Oil	τ_e, ±2.5 min
PDMS1	18.0
PDMS2	17.4
PDMS3	12.5
PDMS4	12.8
Castor oil	19.9

Generally, the observed behavior may be related to following effects: orientation of groups of polymer chains by plasma [15], resulting in a non-zero dipole moment, oriented perpendicular to both the chain axis and the plane of the films, as it occurs with the poled PVDF [16],

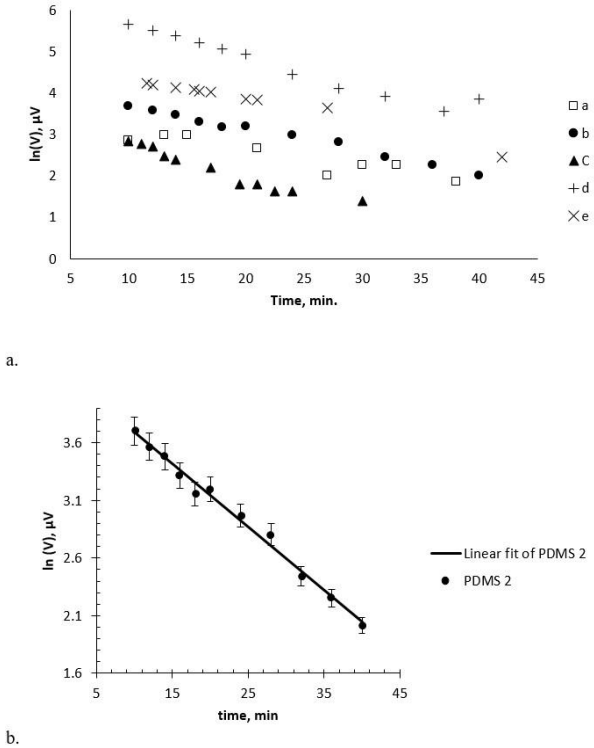

Fig. 6. a) Semi-*ln* dependence of the electret response (voltage) on time: a - PDMS1, b - PDMS 2, c - PDMS 3, d – PDMS 4, e – castor oil; b) The example of the linear fitting of the semi-*ln* dependence of the voltage on time for PDMS 2. Parameters of fitting are $\ln(V) = (4.24 \pm 0.04) + \frac{t}{18.2 \pm 0.6[\text{min}]}$; the squared coefficient of correlation for the fitting is $R^2 = 0.989$.

and the charging of polymer films by the plasma [13, 17]. It is also possible that both of these effects act in parallel.

We incline to suggest that the charging of the surface by plasma is the main mechanism responsible for the modification of the electrical properties of a surface. Indeed, consider first the interaction of dipole groups of polymer chains with the electrical field of the plasma. Assume that the surface is built of moieties possessing the dipole moment $\vec{p}$. It seems reasonable to relate relate at least partially the hydrophilization of the surface to the orientation of these moieties by the electric field of the plasma sheath $\vec{E}$, formed in the vinicity of a treated liquid [18]. The dimensionless parameter ς, describing the interaction of the dipoles constituting the surface with the electric field of the plasma $\vec{E}$, is given by [19]:

$$\varsigma = \frac{pE_s}{k_B T}, \qquad (5)$$

where T is the temperature. The upper value of the achievable electric field of the plasma sheath may be estimated as $E_s^{\max} \cong \frac{\Phi_S}{\lambda_{De}} \cong \frac{100\text{V}}{10^{-4}\text{m}} = 10^6 \text{V}\cdot\text{m}^{-1}$, where $\Phi_S \approx 100\text{V}$ is the potential of the liquid surface, and $\lambda_{De} \approx 10^{-4}\text{m}$ is the Debye length of the cold plasma [18]. Substituting $p \cong 1\text{D} \cong 3.3\times10^{-30}\text{C}\cdot\text{m}$, which is typical for moieties constituting polymer surfaces [20], we obtain the upper estimation of ς for room temperatures: $\varsigma \cong 10^{-3}$. This means that the observed hydrophilization of liquid surfaces by cold plasmas could hardly be related to orientation of the dipole moieties forming the surface by the electrical field of a plasma sheath. This orientation will rapidly be destroyed at ambient conditions by the thermal agitation of dipole groups. Hence, the reasonable mechanism of the modification of liquid surfaces by plasma should be related to the charging of the surface by plasma [13]. The kinetic model of charging was proposed recently in Ref. 21.

Electrical charge gained by a liquid surface is lost with time. The similarity of the electret response and hydrophobic recovery time scales [7] hints that the physical processes responsible for hydrophobic recovery and decay of the electret response are generally the same. However, the precise identification of these processes remains quite challenging.

Conclusions

We conclude that measurements of the apparent contact angle and the electret response could be exploited for the establishment of the surface energy of liquids, in the situation where the spreading parameter is positive. We tested these methods with water/silicone and

water/castor oil systems. Silicone and castor oils coated and encapsulated the water droplets. This enabled exposure of water/silicone oil "sandwiches" to the cold radiofrequency air plasma. We demonstrated recently that radiofrequency plasma increases the surface energy of the liquid polymers. An expression relating the oil/air surface energy to the apparent contact angle of a water droplet coated with oil was derived. This expression allowed quantification of the impact exerted by cold plasma treatment on the surface energy of the oil/air interface. Calculation of the oil/air surface energy and spreading parameter was carried out for different time spans of plasma treatment for silicone oils possessing various molecular weights and also for the castor oil.

The increase in the surface energy of plasma-treated organic liquid surfaces may be at least partially related to the charging of liquid surface by plasma. Plasma-treated liquid surfaces demonstrated a strong electret response, decaying with time. The similarity of the electret response and hydrophobic recovery time scales leads to the conclusion that physico-chemical processes responsible for a hydrophobic recovery and decay of the electret response are generally the same.

Acknowledgements

We are thankful to Mrs. Y. Bormashenko for her help in preparing this manuscript. The Authors are thankful to Mrs. N. Litvak for SEM imaging of PC substrates. The work was partially supported by the ACS Petroleum Research Fund (Grant 52043-UR5).

References

1. a) H. K. Yasuda, J. Wiley & Sons, New York (1984); b) M. Strobel, C. S. Lyons, K. L. Mittal (Eds), VSP, Zeist, The Netherlands (1994); c) M. Thomas, K. L. Mittal (Eds), Wiley, Beverly, USA (2013); d) M. Lehocky, H. Drnovska, B. Lapcikova, A. M. Barros-Timmons, T. Trindade, M. Zembala, L. Lapcik Jr., *Colloids Surf., A.***,** *222*, 125 (2003); d) E. C. Preedy, E. Brousseau, S. L. Evans, S. Perni, P. Prokopovich, *Colloids Surf. A.*, *460*, 83 (2014); e) R. M. Cámara, E. Crespo, R. Portela, S. Suárezd, L. Bautista, F. Gutiérrez-Martín, B. Sánchez, *Catalysis Today*., *230*, 145 (2014).
2. a) E. Occhiello, M. Morra, F. Garbassi, D. Johnson, P. Humphrey, *Appl. Surf. Sci*. *47*, 235 (1991); b) R. M. France, R. D. Short, *Langmuir*, *14*, 4827 (1998); c) R. M. France, R. D. Short, *J. Chem. Soc., Faraday Trans.***,** *93*, 3173 (1997); d) S. Wild, L. L. Kesmodel, *J. Vac. Sci. Technol. A.*, *19*, 856 (2001); e) E. Kondoh, T. Asano, A. Nakashima M. Komatu, *J. Vac. Sci. Technol. B*., *18*, 1276 (2000); f) J. P. Fernández-Blázquez, D. Fell, El. Bonaccurso, A. del Campo, *J. Colloid Interface Sci***.,** *357*, 234 (2011); g) D. Hegemann, H. Brunner, Ch. Oehr, *Nucl. Instr. And Meth. In Phys. Res B. 208*, 281 (2003); h) B. Balu, V. Breedveld, D. W. Hess, *Langmuir*, *24*, 4785 (2008); i) A. Kaminska, H. Kaczmarek, J. Kowalonek, *Eur. Polym. J*., *38*, 1915 (2002); j) E. Bormashenko, R. Grynyov, *Colloids Surf., B*., *92*, 367 (2012); k) E. Bormashenko, G. Chaniel, R. Grynyov, *Appl. Surf. Sci*., *273*, 549 (2013).
3. J. Garcia-Torres, D. Sylla, L. Molina, E. Crespo, J. Mota, L. Bautista, *Appl. Surf. Sci*., *305*, 292 (2014).
4. Y. Ladner, F. D'Orlye, C. Perreard, B. Da Silva, C. Guyon, M. Tatoulian, S. Griveau, F. Bedioui, A. Varenne, *Plasma Process. Polym*., *11*, 518 (2014).
5. a) N. Shainsky, D. Dobrynin, U. Ercan, S.G. Joshi, H. Ji, A. Brooks, G. Fridman, Y. Cho, A. Fridman, G. Friedman, *Plasma Process. Polym*. *9*, 1 (2012); b) D. Staack, A. Fridman, A. Gutsol, Y. Gogotsi, G. Friedman, *Angew. Chem. 120*, 8140 (2008); c) D. Staack, A. Fridman, A. Gutsol, Y. Gogotsi, G. Friedman, *Angew. Chem. Int. Ed. Engl. 47*, 8020 (2008); d) D. P. Park, K. Davis, S. Gilani, C.-A .Alonzo, D. Dobrynin, G. Friedman, A. Fridman, A. Rabinovich, G. Fridman, *Current Appl. Phys*., *13*, 19 (2013).
6. a) C. Shillingford, N. MacCallum, T.-S. Wong, Ph. Kim, J. Aizenberg, *Nanotechnology*, *25*, 014019 (2014); b) T.-S. Wong, S. H. Kang, S. K. Y. Tang, E. J. Smythe, B. D. Hatton, A. Grinthal, J. Aizenberg, *Nature*, *477*, 443 (2011); c) A. Grinthal, J. Aizenberg, *Chem. Mater. 26*, 698 (2014**)**; d) M. Nosonovsky, *Nature*, *477*, 412 (2001); e) A. Eifert, D. Paulssen, S. N. Varanakkottu, T. Baier, St. Hardt, *Adv. Materials Interfaces*, *1*, 1300138 (2014); f) E. Bormashenko, R. Pogreb, Ye. Bormashenko, R. Grynyov, O. Gendelman, *Appl. Phys. Lett*., *104*, 171601 (2014).
7. V. Multanen, G. Chaniel, R. Grynyov, R. Y. Loew, N. Siany, E. Bormashenko, *Colloids Surf. A*, *461*, 225 (2014).
8. a) E. Bormashenko, R. Pogreb, O. Stanevsky, Y. Bormashenko, Y. Socol, O. Gendelman, *Polym. Adv. Technol*., *16*, 299 (2005); b) E. Bormashenko, Al. Malkin, Al. Musin, Ye. Bormashenko, G. Whyman, N. Litvak, Z. Barkay, V. Machavariani, *Macromol. Chem. Phys.*, *209*, 567 (2008).
9. a) D. Smith, R. Dhiman, S. Anand, E. Reza-Garduno, R. E. Cohen, G. H. McKinley, K. K. Varanasi, *Soft Matter*, *9*, 177 (2013); b) S. Anand, A.T. Paxson, R. Dhiman, J. D. Smith, K. K. Varanasi, *ACS Nano*, 6, 10122 (2012).
10. a) P. G. de Gennes, F. Brochard-Wyart, D. Quéré, *Capillarity and Wetting Phenomena*, Springer, Berlin (2003); b) H. Y. Erbil, *Surface Chemistry of Solid and Liquid Interfaces*, Blackwell, Oxford (2006); c) E. Bormashenko, *Wetting of Real Surfaces*, de Gruyter, Berlin (2013).
11. a) P. Than, L.Prezosi, D.D. Joseph, M. Arney, *J. Colloid Interface Sci*., *124*, 552 (1988); b) H. Chung, T. W. Kim, M. Kwon, I. C. Kwon, S. Y. Jeong, *J. Controlled Release*, *71*, 339 (2001).
12. R. Tadmor, Pr. S. Yadav, *J. Colloid Interface Sci.*, *317*, 241 (2008).
13. a) A. Eifert, J. Petit, T. Baier, El. Bonaccurso, St. Hardt, *Appl. Surf. Sci.***,** *330*, 104 (2015); b) E. Bormashenko, R. Pogreb, G. Chaniel, V. Multanen, A. Ya. Malkin, *Adv. Eng. Mat*., DOI: 10.1002/adem.201400445 (2014).

14. a) L. S. McCarty, G. M. Whitesides, *Angew. Chem., 120*, 2218 (2008); b) L. S. McCarty, G. M. Whitesides, *Angew. Chem. Int. Ed. Engl., 47*, 2188 (2008).
15. H. E. N'guessan, A. Leh, P. Cox, Pr. Bahadur, R. Tadmor, Pr. Patra, R. Vajtai, P. M. Ajayan, Pr. Wasnik, *Nature Comm., 3*, 1242 (2012).
16. H. Kawai, *Jpn. J. Appl. Phys., 8*, 975 (1969).
17. L. K. Koopal, *Adv. Colloid & Interface Sci., 179*, 29 (2012).
18. M. A. Lieberman, A. J. Lichtenberg, *Principles of plasma discharges and materials processing*, J. Wiley & Sons, Hoboken, (2005).
19. L. D. Landau, E. M. Lifshitz, *Electrodynamics of Continuous Media* (Volume 8 of *A Course of Theoretical Physics*) Pergamon Press, (1960).
20. D. W. van Krevelen, *Properties of polymers*, Elsevier, Amsterdam, (1997).
21. E. Bormashenko, G. Whyman, V. Multanen, E. Shulzinger, G. Chaniel, *Journal of Colloid and Interface Science, 448*, 175 (2015).

Вісник ХНУ, серія «Фізика», вип. 28, 2018. с. 40-45

PACS:
UDC: 539.1.074.5: 620.179.152

Dead layer in living CsI crystal

A.M. Kudin[1], D.I. Zosim[2], A.Yu. Yemelyanov[2]

1. National University of civil protection of Ukraine, 94 Chtrnyshevska str., 61023 Kharkiv, Ukraine a.m.kudin@gmail.com
2. Institute for scintillation materials National Academy of Science, 60 Nauki ave., 61001, Kharkiv, Ukraine

ORCID: *0000-0003-4788-6665*

DOI:10.26565/2222-5617-2018-28-03

Representations of dead layer (DL) nature in CsI:Na crystals are considered. To eliminate the contradictions between the models of DL, degradation of the conversion efficiency (η) for surface layers has been studied. Simultaneously, the DL profile and its evolution under aging were studied using X-rays of different energies. It has been shown that immediately after surface polishing the η is increased for 5.9 keV photons (depth of 90% attenuation is equals ~7.6 μm). Anion vacancies are responsible for η increase, whose concentration in the disturbed layer is comparable with the concentration of the activator C_A. Decay of supersaturated vacancy solid solution results in extremely inhomogeneous distribution of the η due to the local distortion of the C_A. The consequence of this is the disappearance of the full absorption peak in the pulse height spectrum. Despite the loss of energy resolution and detection efficiency (at photopeak) the total counting rate remains constant for α-particles. The dead layer itself (the loss of full detection efficiency) is formed after the diffusion of sodium to the free surface, approximately after 6 months and more.

Keywords: dead layer; detection efficiency; conversion efficiency; light yield non-uniformity.

Розглянуто уявлення про природу мертвого шару (МШ) в кристалах CsI:Na. Для усунення розбіжностей між моделями МШ вивчено деградацію конверсійної ефективності (η) поверхневих шарів. Одночасно з цим вивчено профіль МШ і його еволюцію під час старіння, використовуючи рентгенівські кванти різної енергії. Показано, що безпосередньо після полірування поверхні η збільшена для фотонів з енергією 5,9 кеВ (глибина 90% послаблення ~ 7.6 мкм). За збільшення η відповідають аніонні вакансії, концентрація яких у спотвореному шарі порівняна з концентрацією активатора C_A. Розпад пересиченого розчину вакансій призводить до вкрай неоднорідного розподілу η через локальні порушення C_A. Наслідком цього є зникнення піку повного поглинання в амплітудному спектрі. Незважаючи на втрату роздільної здатності а також пікової ефективності реєстрації, швидкість рахунку α- часток по всьому спектру залишається постійною. Власне МШ (втрата повної ефективності реєстрації) утворюється через 6 місяців і більше, після дифузійного виходу натрію на вільну поверхню.

Ключові слова: мертвий шар; ефективність реєстрації, конверсійна ефективність; неоднорідність світловиходу.

Introduction

The figurative expression "living crystal" has long been firmly established in the scientific literature [1] with the easy hand of Ya.E. Geguzin. The term "dead layer" (DL) is also widely used in technology for functional materials and implies the absence of a useful signal from the surface layers of the active element. For example, the concept of DL was introduced in [2] for semiconductor crystal phosphors and is explained by the distortion of the band structure near the surface.

Despite the fact that the term DL has firmly entered the scientific lexicon, seems that different authors put into this concept a somewhat different meaning. First of all it should be noted that spectrometry is the most important section of scintillation technique. As to spectrometry in our opinion the term DL means a sharp decrease (by one order or more) of the registration efficiency ε at the peak of total absorption, as this concept is used in [3, 4] especially for weakly penetrating radiations.

On the other hand, it is known that the conversion efficiency η is reduced commonly for low-energy photons. This fact was discovered long ago, for the first time in [5] for NaI:Tl scintillator. It was a decrease of η by approximately 20% (without a change in the ε) and there were no grounds for using the term DL. Since this decrease concerned only the region of soft X-ray radiation and did not affect the volume characteristics of scintillator, the nature of this phenomenon was not dealt with in detail.

Nature of the DL and mechanism of its formation were considered in [6, 7] for hygroscopic crystals of NaI:Tl. In present paper, let us dwell on the features of the DL manifestation in the CsI:Na scintillation material. The goal of our present consideration is to review modern ideas

about the nature of the dead layer, its evolution over time, and also about measures to prevent its occurrence.

The dead layer manifestations in CsI:Na

Initially, the DL idea and its effect on the detection of short-range radiation arose on the basis of a study of light yield degradation. It is well known, that CsI:Na crystals, despite its successful application for γ-ray detection, are not recommended as an α-particle counter. Let us explain this conclusion by two examples. Fig. 1 shows the pulse height spectra excited by α-particles in the CsI:Na scintillation material [8]. It is clear seen that the degradation of the light yield L_α begins immediately after manufacturing (finishing polishing) of the sample and continues until the crystal is almost completely lost by the ability to register short-range particles**.** A distinctive feature of pulse height spectra at a late stage of degradation is that, the peak of the total absorption (see curve 4) is not so much shifted to the low-energy region as it spreads to such an extent that it is practically impossible to correctly determine the half-width. After a few days,

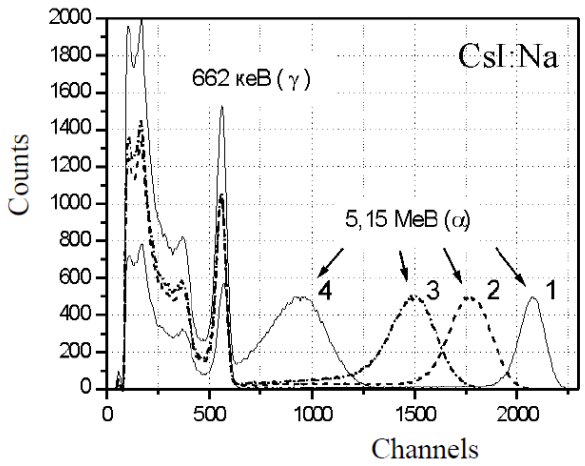

Fig.1 – Change of pulse height spectrum during the crystal storage at ambient conditions. Spectra are recoded after one hour (1) of finishing polishing, 12 hours (2), 3 days (3) and 6 days (4). Note that position of the photopeak for 662 keV γ-rays do not change [8]

depending on the temperature and relative humidity, the full absorption peak disappears.

The aging degradation kinetics of the light yield is shown in Fig. 2. Curve 1 presents the change in light yield for α-particle L_α at temperature of 18°C and relative humidity of ~ 80%. It is clear seen that the L_α is continuously reduced and after 25 days is only 30% of the initial value.

A distinctive feature of the degradation process is not so much a reduction in light yield as a significant deterioration in the energy resolution (*R*). The measurements were terminated due to the fact that the *R* values exceeded 50% and it was impossible to determine correctly the position of the maximum and the peak half-width. This means that the CsI:Na crystal loses the ability to identify the particles on energy (by the position of the full absorption peak) after three weeks of aging (see curve 1 in Fig. 2). It should be noted that a collimator with a hole diameter of 0.5 mm was used in our experiments. It means that the α-particles penetrated into the crystal perpendicular to its surface. Apparently, the registration of oblique particles leads to the fact that the degradation of L_α occurs in a few days [10] under normal conditions.

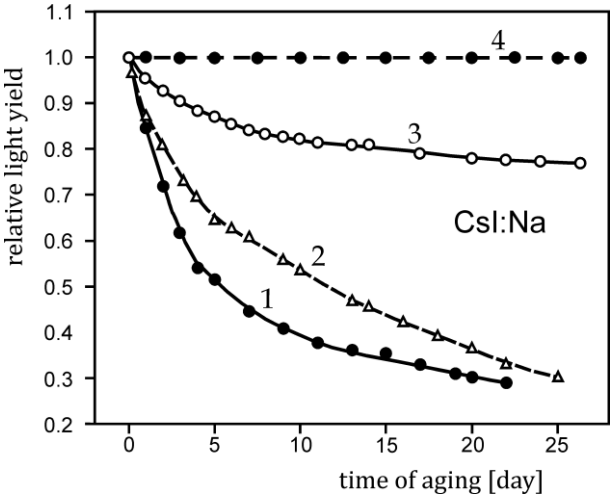

Fig. 2 – Relative light yield degradation during CsI:Na crystals aging at 25°C and relative humidity 70 (1), 30 (2) and 5% (3). Curves 1, 2 and 3 correspond to excitation by α-particles (^{239}Pu), curve 4 by γ-rays (^{137}Cs)

Diffusion model of the DL in CsI:Na

Representations of the DL formation mechanism due to the Na^+ diffusion from the crystal volume to free surface were originally formed when studying thin-film detectors [11], which have obvious advantages in the detection of α-particles, protons and soft X-rays, when the thickness of the scintillator is sufficiently small. The development of works in this direction [12] led to the creation of production for CsI:Tl epitaxial layers, which have been successfully used so far.

It turned out, however, that CsI:Na thin films are not stable and degrade in a short period of time in contrast to CsI:Tl one which exhibit the stability of the spectrometric characteristics. To explain this phenomenon, a diffusion mechanism for DL formation due to the sodium release from the volume to surface has been proposed in [3, 13].

The experimental facts underlying the mechanism are the following:

- during the aging of CsI:Na films, the parameters η and ε deteriorate sharply during 2-4 days;
- distribution profile of activator in the aged sample shows a sharp Na concentration increase at the surface;
- the NaI phase is formed on the surface itself;

- sodium precipitates are formed in the near-surface layer.

It was concluded in [13] that all these facts also hold for single crystals taking into account that the diffusion processes are inhibited. The typical time needed for NaI phase formation on free surface is 6 months or more. A visual experimental confirmation was obtained in [14], see Fig.3. When the aged CsI:Na crystal is excited, a strong dependence of the spectral composition of the luminescence on the penetration depth of X-rays is observed. It has been shown that a 304-nm emission, typical for CsI-pure, rather than 420 nm, characteristic of the CsI:Na, is excited near the surface. According to our data, a sample of 3.8-mm-thick loses its spectrometric properties at excitation by 662 keV γ-rays after 13 years of storage under ambient conditions. When this sample is excited with 60-keV X-rays (90% depth of attenuation is ~0.65 mm) the 420 nm luminescence of CsI:Na does not appeared, but only 304 nm emission is clearly recorded.

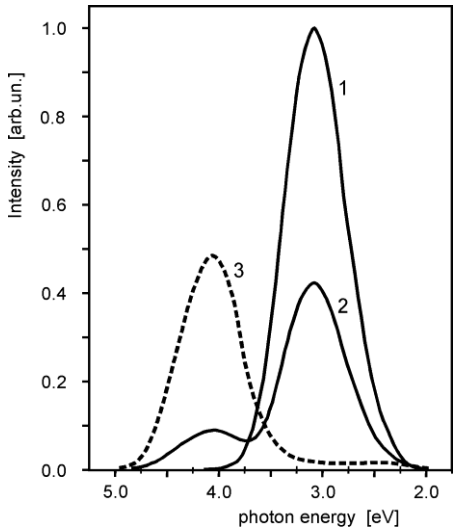

Fig.3. Radioluminescence spectra of CsI:Na crystal at aging. 1 – one day of storage; 2 – 10 years; 3 – 14 years of storage, curve 3 is multiplied by factor 5. Emission is excited by 60 keV γ-rays from ^{241}Am source.

On the surface of aged samples, there is an appearance of matte areas with a characteristic size of up to one millimeter. The micro-X-ray analysis of such areas shows that they are a film of baking soda ($NaHCO_3$) on the polished surface [15]. The $NaHCO_3$ product is observed in centers of nucleation, where the formed NaI phase actively adsorbs water and dissolves in it. The arid puddles of a saturated solution are visible to the naked eye like the shiny spines of a clamping hole [16]. In our opinion, it is with this fact that the concepts of the hygroscopicity of CsI: Na crystals are related. In solution, NaI hydrolyses to form NaOH, this process is especially active in the light [7]. Then the carbonization process proceeds according to a known reaction:

$$NaOH + CO_2 = NaHCO_3, \quad (1)$$

as a result of which baking soda is formed. Similar results on the nature of the precipitates on the surface of CsI:Na crystals are presented recently in [17].

The diffusion model of DL proposed by Tchaikovsky and Rosenberg [3, 13] can be considered proven, since both the formation of the NaI phase on the surface and the depletion of the near surface layer by the activator, are observed experimentally.

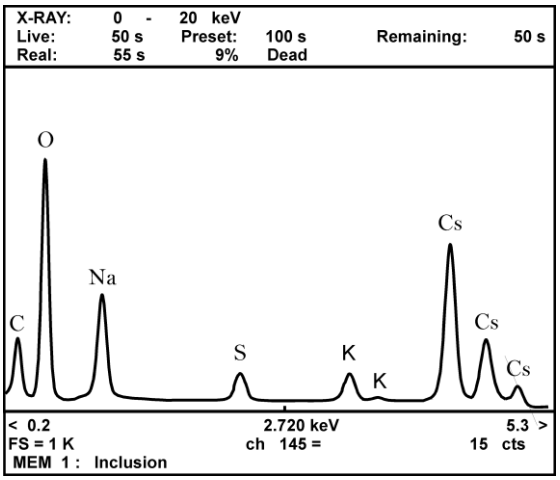

Fig.4. Spectrum of characteristic X-ray emission which excited in matted regions formed by the inclusion of new phase on internal surface of crystal

However, it soon became clear that the loss of crystal spectrometric properties does not coincide in time with the diffusion of sodium to the free surface of sample. The light output decrease at excitation by α-particles in the course of aging follows the exponential law $L_\alpha \sim \exp(-t/\tau)$ with the parameter $\tau \approx 4$ days [4], which is clearly not enough for a noticeable enrichment of the surface with sodium. The essential signs of sodium enrichment appeared after a few months of storage. The authors of [4] explained their results from the opposite point of view they proposed the diffusion of quenching impurities (like OH^- ions) into the crystal lattice. Note that our results (see Fig. 2) confirm both the data [4] as well as [3, 13] (see Fig. 4).

Distorted layer in living crystal

To solve this contradiction a DL profile and its evolution in time have been studied. Simultaneously the degradation of light output L_α has been studied too. To obtain the profile we replaced L_α by η, using first approximation: $\eta = L_\alpha/E_\alpha$. We expected that a sharp decrease in the conversion efficiency will be observed near the surface, as it follows from the data of [18], where the dependence of η *vs* E_p was studied in the range of proton energy $20 \le E_p \le 540$ keV.

Fig. 5 shows the data [18], but the original energy scale was recounted by us into the proton range. It can be seen that the η decrease is observed for protons of the lowest energies. Characteristic depth d_0 of DL (d_0 corresponds to attenuation of the η in 2,71 times) is approximately 2 μm for CsI:Na and only 0.2 μm for CsI:Tl crystal. It should be noted that conversion efficiency is normalized in Fig. 5, the η value is equal to unity for protons of biggest energy.

In present work the DL profile has been investigated using X- and low energy γ-rays. Obtained profiles of DL are shown in Fig.6 for CsI:Na crystal at different stages of aging. Original data are presented in paper [9], here we have recalculated energy scale to a depth of 90% attenuation (d_{90}) of X-rays. It should be noted that dependence η *vs* E_γ (where E_γ is an energy of X-ray) has a nonmonotonic character in the region of the K-edge of iodine (~ 30 keV). It has been shown, however, that after scale replacement ($E_\gamma \rightarrow d_{90}$) this feature is smoothed out [19].

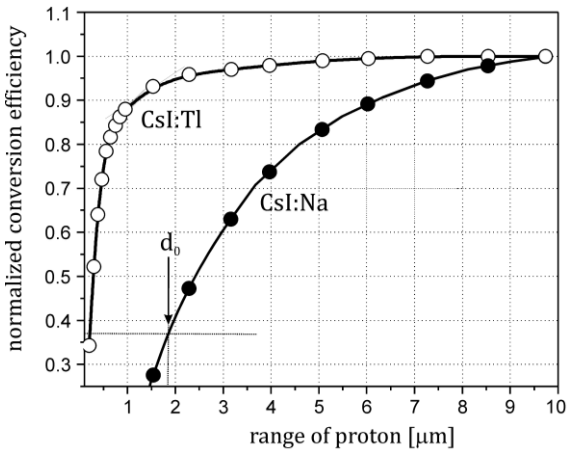

Fig.5. Profile of dead layer in CsI:Na and CsI:Tl crystals after 10 months of aging. Excitation by protons [18]

The course of the dependence η *vs* d_{90} for X-rays after 20 days of storage is similar to curves 1 and 2 in Fig. 5. A distinctive feature of curve 1 in Fig. 6 is that for the quanta of the lowest energies (5.9 keV with the d_{90} = 7.6 μm), an increase in the η value is clearly seen. This increase in conversion efficiency is temporary and disappears after several days of aging. As can be seen from the data in Fig. 6, the alignment of the η values occurs after 19 days.

Contrary to curve 3 in Fig.6 which corresponds to profile of the DL, the curve 1 illustrates the layer with increased conversional efficiency. By analogy with [1] we propose that such a profile be called a ″living layer″. During aging the living layer relaxes and after some days the η values correspond to conversion efficiency in volume, after that the actual dead layer is formed. After 25 days of storage, the crystal practically loses its ability to detect weakly penetrating radiation, which is manifested in the sharp degradation of ε and *R* for photons with energy of 5.9 keV.

The nature of the living layer is associated with an

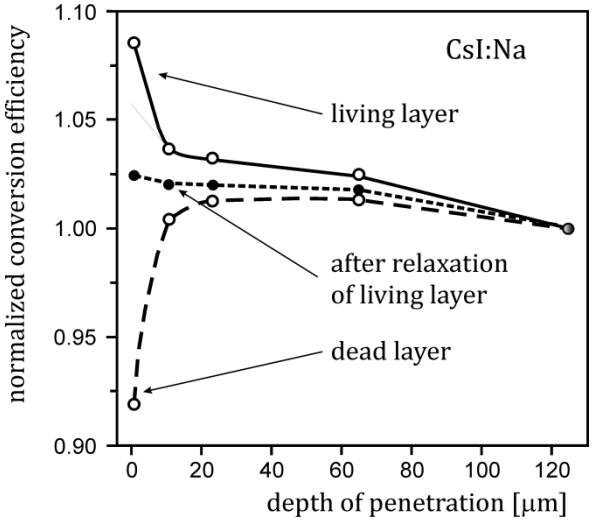

Fig. 6. Dead layer profiles at different stage of CsI:Na crystal aging. 1 – one day of storage; 2 – 19 days; 3 – 22 days of storage

increase in the number of luminescence centers in the near-surface distorted layer. The fact is that the blue luminescence of CsI:Na crystals is associated not only with the activator (Na^+), but also with anion vacancies [20]. Cation (V_C^+) and anion (V_A^-) vacancies easily arise during plastic deformation [20] of CsI crystal. Well known that mechanical treatment causes the plastic deformation in near-surface layer. It was shown that, with a greater degree of deformation, a greater yield of blue luminescence [15, 20]. Estimates made in [15, 21] show that the concentration of vacancies (C_V) in the living layer after ″soft polishing″ is comparable to the sodium content (C_A) in the volume of crystal.

Two-stage mechanism of DL formation

The DL model in CsI:Na crystals, proposed by Tchaikovsky and Rosenberg [3, 13], is schematically shown in Fig. 7. Curve $C_A(d)$ denotes the profile of activator distribution on the depth of crystal. It is well known that sodium diffusion towards free surface results in formation near boundary of the zone depleted by the activator. Boundary between *CsI pure* layer and *CsI:Na* volume has to shifts towards crystal depth according low $d_0 \sim t^{1/2}$ [22]. However, as we saw above for single crystals $d_0 \sim 1–exp(–t/\tau)$. According data [4] as well as our results shown in Fig. 2 the parameter τ is equal to 4 days for sample stored at ambient condition and 6 days for aging at dry room. These values of τ are in good agreement with data [10, 15] also.

A decrease in the light yield by 30% (see curve 3 in Fig. 2) cannot lead to a significant broadening of total

absorption peak and to a catastrophic deterioration in energy resolution (see Fig. 1). It is natural to assume that in the near-surface layer an inhomogeneous distribution of emission centers is formed not only along the depth of layer, but also in the cross-sectional area. An obvious sign of such non-uniformity is the presence of sodium precipitates, which appear in the DL [3, 13]. Sodium precipitates are not typical for crystals with an optimal Na concentration: $C_A = 9.5 \cdot 10^{17}$ см$^{-3}$. It should be noted that we used an ingot with uniform activator distribution in whole volume, sodium concentration in all samples was: $C_A = 8{,}6 \cdot 10^{17}$ см$^{-3}$.

Existence of the living layer near the surface at initial stage of aging implies a revision of mechanism of DL formation, since a supersaturated solid solution of vacancies should disintegrate first of all. Obvious sinks for vacancies are the free surface and dislocations. Let's explain the above with a simple example.

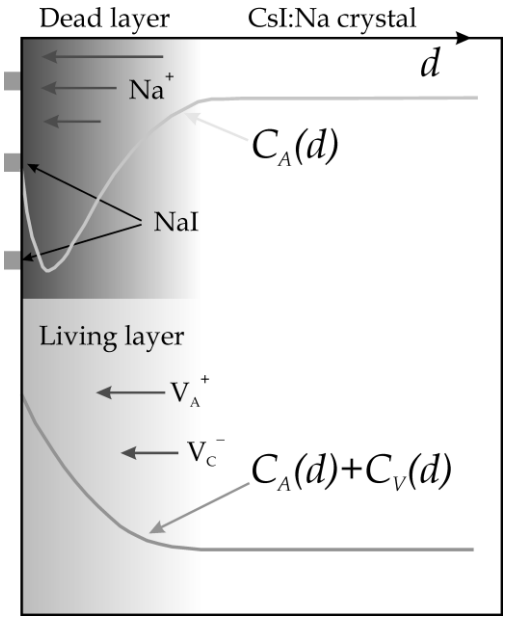

Fig.7. Model of Dead Layer in CsI:Na crystal after aging [13], curve *"$C_A(d)$"* shows the distribution profile of Na Proposed model of Living Layer, curve *"$C_A(d)+ C_V(d)$* shows profile of distribution of emission centers

Free surface itself is a natural sink for excess vacancies. Within a few days towards the interface, a gradual weakening flow of vacancies will be directed. Vacancy flow will lead to a predominant shift of Na^+ cation in the opposite direction. Another consequence of the living layer relaxation is, perhaps, the penetration of foreign impurities, for example, OH^- ions, from the surface into the crystal lattice. A similar displacement of impurity ions occurs in any part of the crystal where there is a directed vacancy flow [22].

As a result, the sodium distribution along depth will change. Schematically, the change in the profile of sodium distribution is shown in Fig.8. In disappearing living layer the zone enriched by sodium should form. Since even a small (within + 20%) increase in Na concentration causes the decay of solid solution [23], in noted zone the sharply inhomogeneous activator distribution is appeared. Sodium precipitates are just an experimental manifestation of such non-homogeneity on microscopic level [3]. Vacancy claster can play role of nucleation center for decay of solid solution. It is known that such clasters appeared easy in CsI [24] after plastic deformation as a result supersaturated vacancy solution decay.

So, proposed model of DL and mechanism of living layer transformation to dead one can be checking experimentally. New model supposes that the formed dead layer (peak of total absorption in which is absent on the pulse height spectrum) is still a solid solution of sodium in CsI. It means that α-particles should be detected even in course of the decay of solid solution. So, CsI:Na crystal can detects α-particles in counting mode but cannot identify them on energy.

To check this assumption the pulse height spectra have been measured. To select needed level of discrimination the pulse height spectrum was measured for CsI-pure crystal. Then the high discrimination threshold was chosen such that the total absorption peak in spectrum

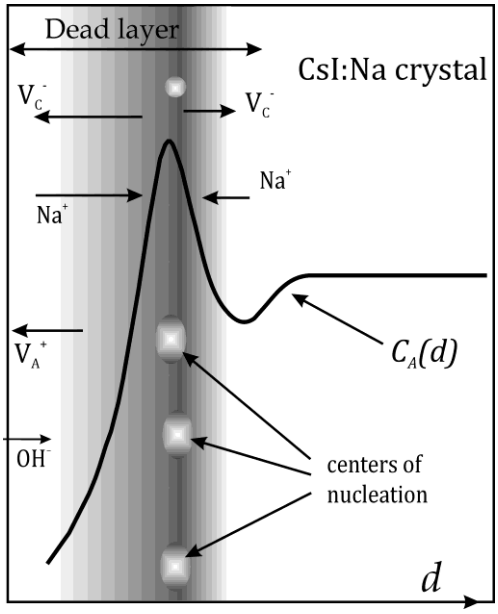

Fig.8. Profile of dead layer in CsI:Na. Curve *"$C_A(d)$"* shows the proposed distribution of Na after relaxation of supersaturated solid solution of vacancies

disappeared. Figuratively speaking, we made artificially the CsI crystal dead. As for the CsI:Na crystals, they still recorded and distinguished α-particles at such a high threshold. The measurements were continued after 30 days. Despite the absence of a full absorption peak in the

spectrum, the crystal registered the α-particles in counting mode, the total detection unchanged.

So, the term DL means first of all a loss of energy resolution, rather than a light output or detection efficiency. The scintillation technique distinguishes the total and peak detection efficiency. Returning to the meaning of term DL, one can concretize that a crystal with a dead layer loses its peak not total registration efficiency. Total efficiency of α-particles registration CsI:Na loss throughout the year formation a CsI-pure layer. The thickness of the CsI-pure layer should not be less than the range ℓ of $\alpha-$ particles in CsI ($\ell = 32\ \mu m$ for energy 5.15 MeV from ^{239}Pu source).

Conclusion

Representations of dead layer nature in CsI:Na crystals are considered. To eliminate the contradictions between two existing models of DL, degradation of the conversion efficiency in near surface layer has been studied. Simultaneously, the DL profile and its evolution under aging were studied using X-rays of different energies. It has been shown that immediately after surface polishing, the η is increased for 5.9 keV photons (depth of 90% attenuation is equals ~7.6 μm). Anion vacancies are responsible for η increase, whose concentration in the disturbed layer is comparable with the concentration of the activator C_A. Decay of supersaturated vacancy solid solution results in extremely inhomogeneous distribution of the η due to the local distortion of the C_A. The consequence of this is the disappearance of the full absorption peak in the pulse height spectrum. Despite the loss of energy resolution and detection efficiency (at photopeak) the total counting rate remains constant for α-particles. The dead layer itself (the loss of full detection efficiency) is formed after the diffusion of sodium to the free surface, approximately after 6 months and more.

References

1. Ya.E. Geguzin. Living crystal, 2-nd ed., Nauka, Moscow (1987), 192 p.
2. A.M. Gurvich. Introduction to physical chemistry of crystal-phosphors, Vysshaya shkola, Moscow (1971), 336 p.
3. G.Kh. Rosenberg, Yu.T. Vydai, G.V. Ptitsyn, E.F. Tchaikovsky. Bul. Academy of Science of USSR, phys., 41, 2365 (1977).
4. V.V. Averkiev, V.K. Lyapidevsky, V.A. Prorvich, A.V.Sartory. Instr. & Exp. Technique, 3, 152 (1982).
5. W.G. Kaizer, S.I. Baiker, A.J. MacKay and I.S. Sherman. IEEE Trans. Nucl. Sci., 9, 3, 22 (1962).
6. A.M. Kudin. In: Scintillation materials. Obtaining, Property, Application, ed. by B. Grinyov, Ukraine, Kharkov, Institute for Single Crystals (2007), p. 320.
7. K.A. Kudin, A.V. Shkoropatenko, A.Yu. Voloshko, D.I. Zosim, A.M. Kudin. Phys. Surface Engineering, 9, 256 (2011).
8. A.M. Kudin, E.P. Sysoeva, L.N. Trefilova, D.I. Zosim. NIMA, A537, 105 (2005).
9. A.M. Kudin, A.A. Ananenko, Y.T. Vyday, V.Yu Gres', B.G. Zaslavsky, D.I. Zosim, Problems of Atomic Science and Technology, 4, 111 (2001).
10. K.V. Shakhova, A.N. Panova, V.I. Goriletsky, Y.A. Prikhod'ko, V.P. Gavrylyuk, S.P. Korsunova, N.N. Kosinov. Rad. Measurements, 33, 769 (2001).
11. Yu.T. Vyday, G.V. Ptitsyn, G.Kh. Rosenberg, E.F. Tchaikovsky. Single Crystals and Tech., Ukraine, Kharkov, VNII Monokristallov, 17, 228 (1976).
12. A. Fedorov, A. Gektin, A. Lebedynskiy, P. Mateychenko, A. Shkoropatenko. Rad. Measurements, 56, 163 (2013).
13. G.Kh. Rosenberg. Autoreferat diss. candidate fis.-mat. nauk: 01.04.10. – Kharkov, 21 p. (1980).
14. L.E. Dinca, P. Dorenbos, J.T.M. de Haas, NIMA, A486, 141 (2002).
15. V.Yu. Gres'. Autoreferat diss. candidate tech. nauk: 05.02.01. – Kharkov, 18 p. (2002).
16. B.V. Grinyov, V.P. Seminozhenko. Scintillation detectors of ionizing radiation for hard operation conditions, Osnova, Kharkov (1998), 155 c.
17. Pin Yang, Charles D. Harmon, F. Patrick Doty, and James A. Ohlhause. IEEE Trans. Nucl. Sci., 61, 2, 1024 (2014).
18. Yu.I. Usikov, Yu.T. Vyday, G.I. Primenko, Yu.A. Tsyrlin. Instr. & Exp. Technique, 1, 86 (1984).
19. A.M. Kudin, B.V. Grinyov, V. Yu. Gres, A.I. Mitichkin. Functional Materials, 13, 54 (2006).
20. A.V. Gektin, N.V. Shiran, V.Y. Serebryannyi, T.A. Charkina. Opt. & Spectroscopy, 72, 1061 (1992).
21. A.M. Kudin, L.A. Andryushchenko, V. Yu. Gres', A.V. Didenko, T.A. Charkina. J. Opt. Technology, 77, 300 (2010).
22. Ya.E. Geguzin. Diffusion zone, Nauka, Moscow (1979), 343 p.
23. A.N. Panova, E.L. Vinograd, V.I. Goriletsky, S.P. Korsunova, N.N. Kosinov, K.V. Shakhova. Func. Materials, 5, 480 (1998).
24. A.V. Gektin, T.A. Charkina, N.V. Shiran, V.Ya. Serebryanyi, Opt. & Spectroscopy, 67, 1075 (1989).

Вісник ХНУ, серія «Фізика», вип. 28, 2018. с. 46-52

PACS: 81.07.Gf
UDC: 530.1/539.8

Ultrathin ZnO nanowires fabricated by using low-temperature pulsed laser deposition

A. Shkurmanov

Peter Grünberg Institute for Semiconductor Nanoelectronics (PGI-9), Research Center Jülich, 52425 Jülich, Germany
(previously: Felix-Bloch-Institute for Solid State Physics, Universität Leipzig, Linnéstraße 5, 04103 Leipzig, Germany)

ORCID: *0000-0001-8751-0924*

DOI:10.26565/2222-5617-2018-28-04

Recently, numerous devices use ZnO nanowires (NWs) as building blocks, for example, light emitters, pressure and gas sensors, resonators and many others. However, for integrations of the NWs into such devices, a high level of NW diameter control is needed. In this work, an opportunity to adjust the NW diameter by using differently doped by Al or Ga seed layers is presented. Moreover, a change of the doping concentrations allows to optimize the growth temperature. Thus, ultrathin NWs, i.e. with a diameter of d < 10 nm can be fabricated by using temperature of T = 400°C. This temperature is far below than those typically used for the fabrication of NWs by pulsed laser deposition.

Keywords: nanowires, ZnO, pulsed laser deposition

Нанодроти з ZnO використовуються в якості ключових елементів для розробки численних пристроїв, таких як світловипромінювачі, сенсори тиску газу, резонатори і багато інших. Для інтеграції нанодротів в такі пристрої потрібна висока точність в регулюванні їх діаметра. Більш того, температура зростання нанодротів грає ключову роль для їх інтеграції. Дані про особливості росту нанодротів при температурах нижче T = 550 ° C і інформація про механізми їх зростання дуже обмежені. У цій роботі доведена можливість регулювання діаметра нанодротів за допомогою використання підкладок, легованих Al або Ga. Встановлено, що варіація концентрації домішок в підкладці дозволяє оптимізувати температуру зростання нанодротів. Показано, що можуть бути виготовлені ультратонкі нанодроти з діаметром d <10 nm при температурі T = 400 ° C. Ця температура значно нижче значення, яке зазвичай використовується для зростання нанодротів методом імпульсно-лазерного осадження.

Ключові слова: нанопроволоки, ZnO, імпульсно-лазерне осадження.

Introduction

ZnO is a transparent conductive oxide which attracts a lot of scientific interest in the last years. This material mostly crystallizes in the hexagonal wurtzite structure by using an ambient pressure and temperature. In the ZnO lattice structure each Zn ion is encircled by a tetrahedral of O ions, and vice-versa which causes a polar symmetry along the hexagonal axis, i.e. ZnO tends to form c-oriented structures with Zn-terminated (0001) or O-terminated ($000\bar{1}$) polar faces [1]. The polarity is responsible for most of ZnO properties, e.g. piezoelectricity and spontaneous polarization [1, 2]. Additionally, a wide bandgap of about 3.37 eV, optical transparency in the visible spectrum range, large exciton binding energy of about 60 meV at room temperature [3], self-grown properties, radiation hardness, biocompatibility and high melting point of T = 1950°C make the ZnO favorable semiconductor material for the fabrication of the numerous nanostructures with further integration of them in different applications [1,4].

Fabrication of the cylindrical elongated ZnO nanostructures such as nanowires (NWs) is of a special interest in this work. The NWs have a high surface-to-volume ratio, can be grown dislocation-free and have many potential applications, e.g. light emitters [5], electromechanical resonators [6], pressure and 3D imaging sensors [7,8]. The desired geometry of the NWs is determined by the applications. For instance, for the pressure sensors, thick NWs with a diameter of d > 100 nm are favorable for compression-force application, whereas thin NWs (d < 100 nm) are interesting to be used for a bending-force application. Additionally, thin NWs are desired for gas sensors, since sensing is strongly depends on the surface-to-volume ration of the nanostructures. For the ultrathin NWs with a diameter comparable with a Bohr radius, i.e. d < 10 nm, quantum confinement effects are expected and these NWs can be used for a fabrication of qubits [9].

Recently, most of the known growth methods use a vapor to solid phase transfer with an epitaxial fabrication of the NWs on the solid substrate. The growth mechanisms can be splitted into two main groups - mechanisms which require presence of a catalyst, or a catalyst-free growth [10]. A catalytic material changes the melting and evaporation points of ZnO, and supports a

chemical reaction. However, the main disadvantage of using a catalyst for the growth process is its diffusion and incorporation into the NW which can lead to a change of the material properties, e.g. conductivity, optical transmission, etc. Obviously, that for a control of chemical purity of the ZnO NWs, which can be required for many of their possible applications, a catalyst-free growth is desired. However, this desired growth mechanism is technically challenged for the most known growth techniques [10,11].

Methods

In order to grow the NWs by a catalyst-free epitaxial growth, a two-steps fabrication process was used. In the first step, a planar Al- or rather Ga-doped ZnO seed layers were fabricated on the a-plane sapphire substrates by using a conventional low-pressure pulsed laser deposition (LP PLD) with a growth temperature of about T = 720°C and oxygen partial pressure of p = 0.01 mbar. These seed layers have a doping concentration in a range of x = 0 – 7 at% and a thickness of about 200 nm [12]. For the second step, a combination of the sapphire substrate with a seed layer was put into the high-pressure pulsed laser deposition chamber (HP PLD). For more than a decade, the high pressure pulsed laser deposition is using for the NW and other quasi 1-dimensional nanostructure growth [13]. This growth method is technically simple, allows to obtain the NWs by a direct transfer of the depositing ZnO from the vapor to the solid phase without using any catalyst and chemical reaction [10]. Also, a selective growth of the nanostructures is possible by using HP PLD technique [15]. In contrast to the conventional LP PLD method, the high pressure one exploits an internal gas flow which support the transfer of the particles from the target to the substrate, increases a supersaturation of the ZnO particles over the substrate and thus, leads to the growth of the quasi 1- or rather 3-dimensional structures [10, 11]. The HP PLD growth chamber used for this research is schematically presented in Fig. 1. The body of the chamber is made by quartz and the design of the chamber supports the transfer of the ZnO particles to the substrate.

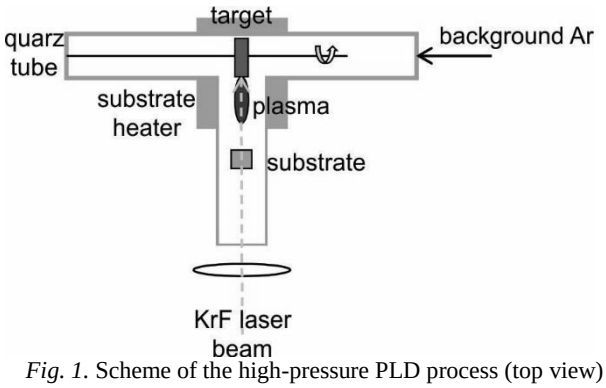

Fig. 1. Scheme of the high-pressure PLD process (top view)

A pulsed high-power excimer laser beam with a wavelength of λ = 248 nm is focused by a UV lens onto the ZnO target, which is evaporated, excited and ionized. The plasma plume propagates with angle of about 30° towards the substrate's surface. The argon particles are mixed with Zn^+ and O^- ions, reduce their energy and thus the ZnO molecules and clusters can be formed during the transfer to the substrate and be deposited there. After reaching the surface of the substrate, Ar with an excess of the ZnO clusters can be removed in the end of the quartz chamber. Note, that the pressure of the Ar flow is about 150 mbar [13].

However, the most of the reports which use the HP PLD process show the growth of thick NW arrays with typical diameter in a range between 60 and 600 nm [13,15,16,17]. Here, an opportunity to obtain ultrathin NWs by using a different compositions of the underlying seed layers will be shown. Moreover, a choice of the seed layer has a strong impact on the growth temperature

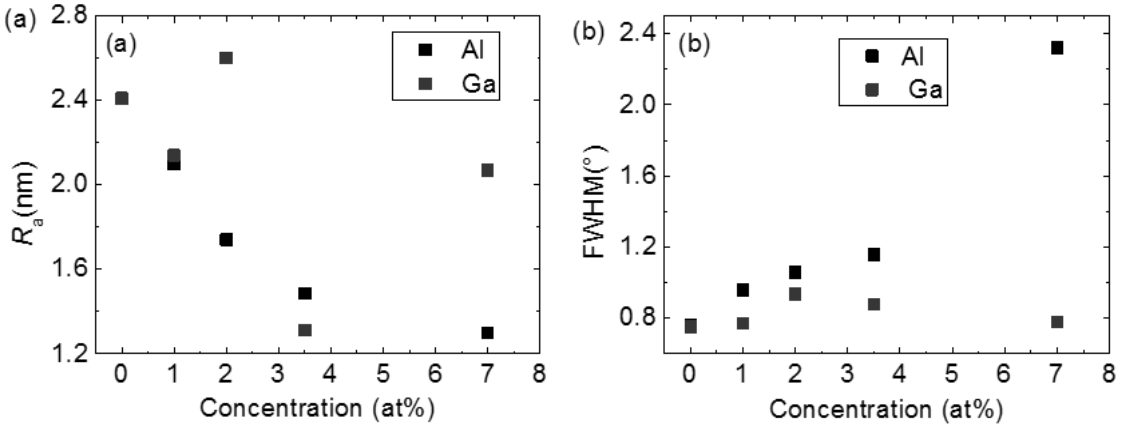

Fig. 2. Surface roughness (a) and the FWHM of rocking curves (b) of the seed layers as a function of the Al or rather Ga concentrations

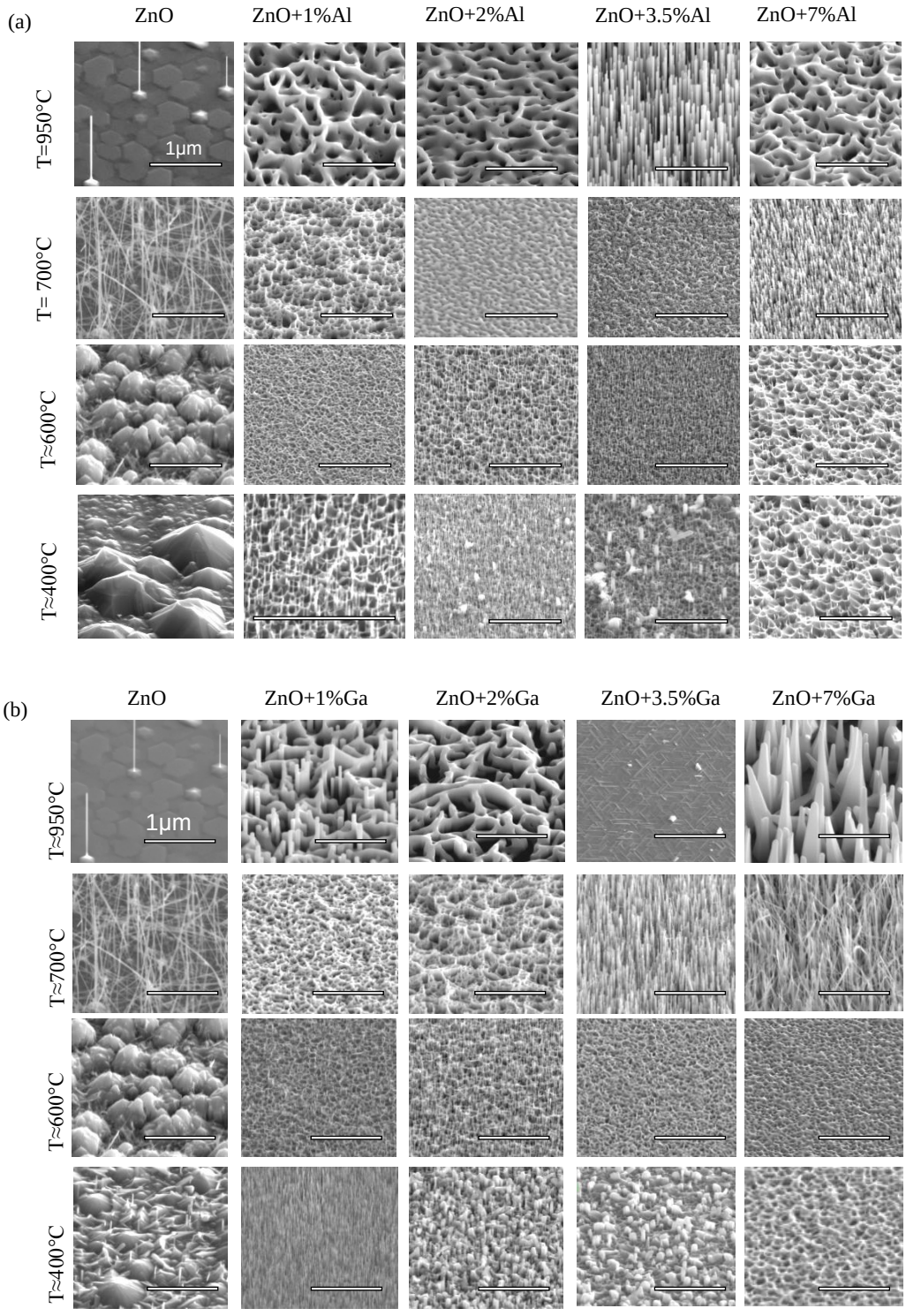

Fig. 3. SEM images of the growth results obtained on the Al-doped (a) or Ga-doped ZnO seed layers (b) by using different temperatures. The scale bar corresponds to 1μm

which can be strongly reduced from the typical T = 950°C to T = 400°C. This relatively low growth temperature can preserve complementary metal-oxide-semiconductor (CMOS) structure [18] and thus, ZnO NWs can be integrated in these technology.

Results

The surface morphology and the crystalline quality of the obtained seed layers were investigated by atomic force microscopy (AFM) and X-ray diffraction (XRD) measurements, respectively, since the surface can influence the NW's growth [19]. For both types of the seed layers, a quite smooth surface was obtained, as shown in Fig. 2a. However, for the Al-doped ZnO seed layers, a decrease of the average surface roughness from 2.4 to 1.3 nm with increasing Al concentration can be seen. For the Ga-doped seed layers, there is no clear behavior of the average surface roughness as a function of

the doping concentrations and the surface roughness fluctuates typically between 2.0 and 2.6 nm and only for the layer doped with x = 3.5 at% of Ga, a reduction of the surface roughness to R_a= 1.3 nm can be observed.

The full width half maximum (FWHM) of the rocking curves as a function of the Al and Ga doping concentrations is presented in Fig. 1b. For the undoped ZnO seed layer, FWHM of about 0.8° is observed. For the Al-doped seed layers, an increase of the FWHM up to 2.4° for x = 7at% is seen whereas for the Ga doping, there is no strong dependence on the Ga concentration. In this case, the FWHM was determined to be in the range of 0.8°–1.0°. The FWHM values are strongly depend on the grain size [20,21] and their tilting, therefore the sizes and tilt of the grains for the Ga-doped seed layers are similar, whereas for the Al-doped layers they increase with increasing of doping concentration.

Scanning electron microscopy (SEM) images of the grown nanostructures are shown in Fig. 3. By using an undoped ZnO seed layer and the high growth temperature of T = 950°C, a low density of vertically oriented NWs is obtained as expected from the previous results [22,23]. These NWs have a diameter of about 70 nm and an aspect ratio of about 25. By reducing the growth temperature down to T=700°C, diameter of the NWs decreases to 16 nm and aspect ratio increases up to 300. However, in contrast to the NWs prepared by using the highest growth temperature, these NWs are randomly oriented. For the low temperature growth at T = 400°C, a suppression of the NWs can be observed, and only very thin and short NWs with a diameter of 24 nm and aspect ratio of 6 were obtained.

By using Al- and Ga-doped seed layers, the growth results are different compared to that one observed for the undoped ZnO seed layers. In the case of Al-doped layers and highest growth temperature of T=950°C, a well-oriented growth of vertically aligned NWs is observed but only for Al-concentration of x = 3.5 at%. These NWs have a diameter of about 80 nm and an aspect ratio of 30. For other doping concentrations, the NW growth is suppressed and only growth of honeycomb-like structures is obtained. These honeycomb-like structures were not observed on the undoped seed layers and are typical for the growth on the doped seed layers. Interestingly, that with reduction of the growth temperature to T = 700°C, NWs were obtained on the seed layer with a concentration of x = 7 at% only and the growth on the seed layers with x ≤ 3.5 at% is suppressed. A further reduction of the growth temperature leads to decrease of the optimum Al concentration which supports the growth of NWs, i.e. at T = 600°C NWs are obtained for the doping concentration of x = 2 and x = 3.5 at%, whereas for T = 400°C, the growth is observed on the seed layers with x = 1 and 2at%. Note, all NWs are well-oriented vertically, and for

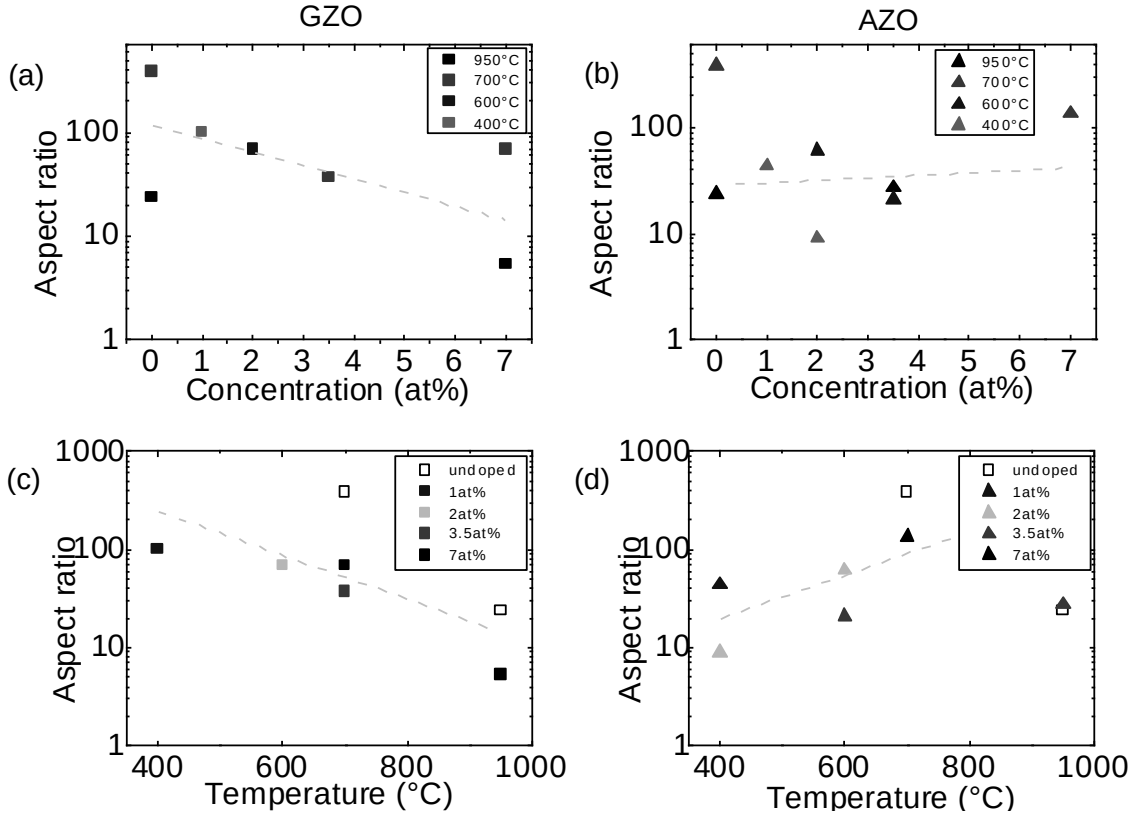

Fig. 4. NW aspect ratio as a function of the doping concentration (a,b) and growth temperature (c,d) for the Ga-doped (a,c) and Al-doped seed layers (b,d).

T = 400°C, NWs are grown as an ultrathin array with a diameter of d ≤ 7 nm and an aspect ratio of 45. For the concentrations which does not support the growth of NWs at given temperature, the growth of a honeycomb-like structures is observed.

The growth on the Ga-doped seed layers is slightly different at temperature of T=950°C compared to that one observed on the Al-doped layers. For this growth temperature, there are no NWs are observed on the seed layer doped with x=3.5at%. However, for the doping concentration of x = 7at%, growth of elongated pyramid-like structure was obtained. For other concentrations and growth temperatures, the results are mostly similar to those ones grown on the Al-doped seed layers. Growth of ultrathin NWs with a diameter d ≤ 7 nm and an aspect ratio of about 100 was obtained on the seed layer doped with x = 1 at% of Ga and by using growth temperature of T = 400°C.

In the work of Kaebisch et al [17], an impact of the Al dopants in the seed layer on the NW growth process is observed as well. They attributed this behavior to a change of the surface polarity from an O-terminated surface of the undoped ZnO layer to a Zn-terminated one of the Al-doped layers. In their case, on the doped layers, the honeycomb-like structures were fabricated instead of NWs. The observed growth of the honeycomb structure for the Al- and Ga-doped layers in the experiments presented here, would also indicate such a change of the surface polarity. In order to verify the change, the polarity of the seed layers were determined by using an etching method described in Ref. 24. Accordingly to that method, the seed layers were etched in a diluted HCl acid with a concentration of 1:100 for 30 s and the etching pattern indicates a type of the polarity. Note, that for the mentioned concentration, an etching rate is expected to be of about 1 nm/s. This experiment revealed that only for the undoped seed layer as well as for Al-doped layers with x = 1 at%, an O-terminated surface was found which manifested itself by a pyramidal etching pattern. Other seed layers have a crater-like pattern which indicates a Zn-termination. However, in contrast to the conclusions made by Käbisch et al., the change of the polarity of the surface seems to be unlikely for the difference of the observed growth behaviors since the NWs are able to be fabricated even on the Zn-terminated surfaces.

A change of the observed NW growth results can be caused by a variation of the growth mechanism [10,11] via a change of the free energy, which can be given by: $\Delta F = F_m + F_i - F_s$ [25]. Here F_m, F_i, and F_s represent the free energy of the depositing material, the interface, and the surface, respectively. Obviously, the surface roughness and crystal quality described above, have an impact on the surface free energy. However, their impact is not sufficient in order to change the entire growth

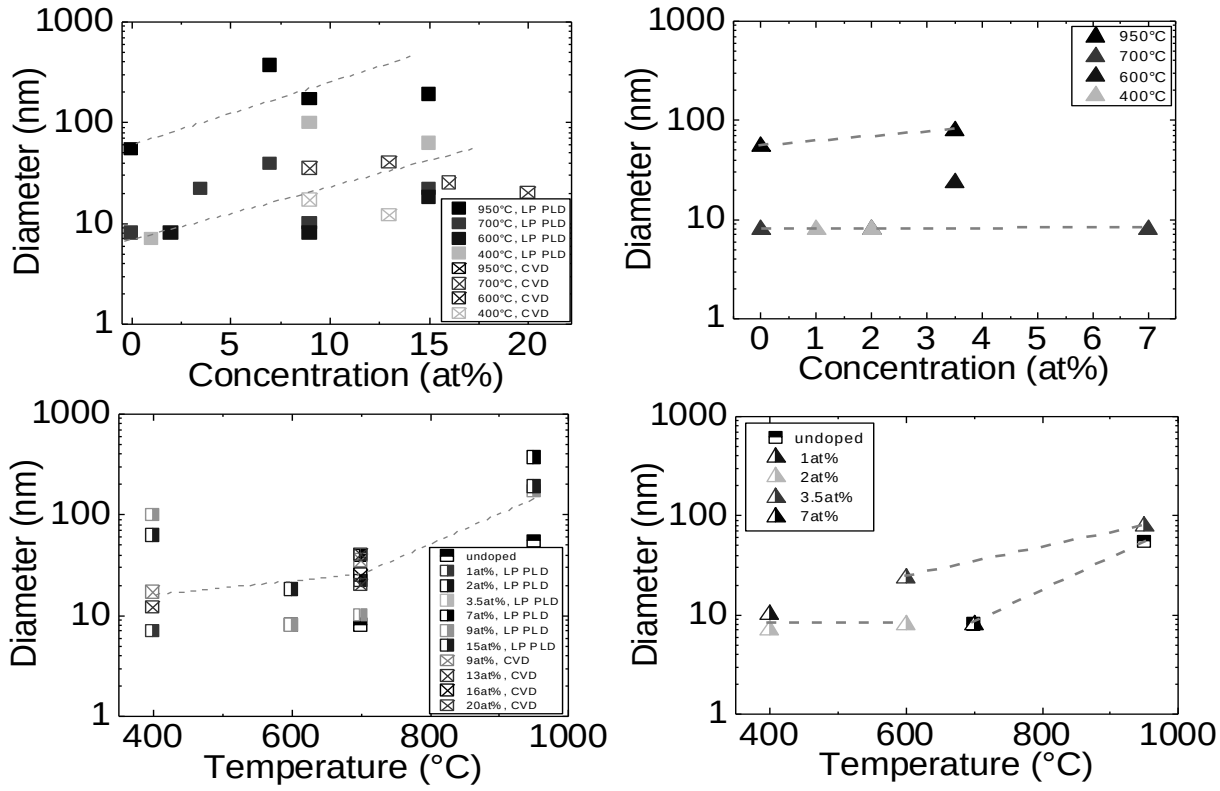

Fig. 5. The diameter of the NWs as a function of the doping concentration (a,b) and growth temperature (c,d) for the Ga-doped (a,c) and Al-doped seed layers (b,d).

mechanism. For example, for the Ga-doped seed layers, the grain size was determined almost the same, whereas for the Al-doped ZnO layers, the grain size increases with increasing Al concentration. However, for both types of the seed layers, the growth results are observed almost the same and fabricated NWs have similar diameter and aspect ratio. This result is in a contradiction to the results obtained by Ting et al. [26] which conclude that the NW diameter increases with the grain size. Moreover, neither an increase of the diameter of the NWs with decreasing of the surface roughness [19] nor another correlations were found. Note that a change of the surface roughness and the grain size caused by the elevated temperature during the growth process can be excluded since XRD and AFM measurements performed on the reference samples and annealed under deposition conditions did not reveal a sufficient change of the seed layer morphology.

Thus, a sum of the free energy of the depositing material (i.e. F_m,) and the free energy of the interface of deposited ZnO (F_i) has a strong and significant impact on the change of the growth mechanism. However, the experimental determination of these free energies is technically challenging by using mentioned HP PLD chamber. For the F_m investigation a mass spectrometer should be integrated inside the chamber, whereas for the F_i determination, a theoretical model based on the Monte Carlo simulations is needed [27].

In Fig 4 and 5, aspect ratio and diameter of the grown NWs as a function of the doping concentration of the seed layers and the growth temperature are presented respectively. The aspect ratio of the NWs grown on Ga-doped ZnO layers decreases with increasing doping concentration, whereas it decreases with increasing temperature. At the same time, an increase of the NW diameter with increasing Ga concentration and growth temperature is observed. For the growth on the Al-doped layers, a slightly different situation occurs. Here, the NW aspect ratio has no behavior as a function of the Al doping concentration but increases with the growth temperature.

Thereby, the Ga doping of the ZnO seed layer has a stronger impact on the NW diameter than the doping of the layers with Al. This effect might be explained by the larger size of Ga dopants which are probably more attractive for the deposited ZnO particles, i.e. the particles remain close to the surface of the seed layer and their motion toward the NW axis is suppressed. Thus, the lateral growth rate is enhanced, i.e. the NW diameter increases, whereas the vertical growth is reduced, i.e. the NW length decreases. Also, seems that the kinetic energy of the moving ZnO particles, i.e. particles which were deposited but not yet crystallized, strongly depends on the growth temperature. Low kinetic energy might be responsible for the lateral mobility and the lateral growth rate of the NWs on the both types of the seed layers.

Conclusions

In order to summarize the work, following conclusions should be made:

1) Al and Ga dopants in the ZnO seed layers have a significant impact on the NW growth process. They effect on the surface free energy via surface morphology, crystal quality of the layers and other surface parameters and thus can change the growth mechanism of the NWs.
2) The NWs can be fabricated at T = 400°C. This temperature is far below the typical PLD-used temperature, allows to protect metallic contact lines in the CMOS structure and thus, the NWs can be integrated into this technology.
3) By using a low-temperature process, a well-oriented vertical array of ultrathin NWs can be obtained on the seed layer doped with x = 1at% of Al or Ga. These NWs have a typical diameter d < 10 nm, which is comparable with a Bohr radius.

References

1. V. A. Coleman and C. Jagadish, Basic Properties and Applications of ZnO, edited by C. Jagadish and S. Pearton, The Netherlands, Amsterdam, Elsevier Limited, Chapter 1, (2006).
2. A. R. Hutson, Phys. Rev. Lett., 4, 10, 505, (1960).
3. C. P. Dietrich and M. Grundmann, Wide Band Gap Semiconductor Nanowires: Low-Dimensionality Effects and Growth, edited by V. Consonni and G. Feuillet, USA, Hoboken, Wiley-ISTE, Chapter 22, (2014).
4. M. Grundmann, The Physics of Semiconductors, Germany, Heidelberg, Springer-Verlag, 3 edition, (2016).
5. S. Xu, et al., Adv Mater., 22, 4749, (2010).
6. J. Mei, et al., Procedia Eng., 47, 462, (2012).
7. R. Dauksevicius, et al., Procedia Eng., 120, 896, (2015).
8. Z.L. Wang, Mater. Sci. Eng. R, 64, 33, (2009).
9. S. M. Frolov, et al., MRS Bulletin, 38, 809, (2013).
10. J. S. Horwitz and J. A. Sprague, Pulsed Laser Deposition of Thin Films, edited by D. B. Chrisey and G. K. Hubler, USA, New York, 229, Wiley-Interscience, (1994).
11. M. Lorenz, Zinc oxide as transparent electronic material and its application in thin film solar cells, edited by K. Ellmer, A. Klein and B. Rech, Germany-USA, Berlin-Heidelberg-New York, Springer, Chapter 6, (2006).
12. A. Shkurmanov, et al., Nanoscale Res. Lett., 12, 134, (2017).
13. M. Lorenz, et al., Appl. Phys. Lett., 86, 14, 143113, (2005).
14. A. Shkurmanov, et al., Procedia Eng., 168, 1156, (2016).
15. T. Michalsky, et al., Eur. Phys. J. Appl. Phys., 74, 30502, (2016).
16. M. Willander, et al., Nanotechnology, 20, 332001, (2009).
17. S. Käbisch, et al., Appl. Phys. Lett., 23,10, (2013).

18. S. Sedky, et al., IEEE Trans. on Elec. Dev., 48, 2, 377, (2001).
19. H. Ghayour, et al., Vacuum, 86, 101, (2011).
20. A. Patterson, Phys. Rev., 56, 978, (1939).
21. A. P. Samantilleke, et al., Nanoscale Res. Lett., 6, 309, (2011).
22. A. Rahm, et al., Appl. Phys. Lett., 88, 31, (2007).
23. Y. W. Heo, et al., J Nanosc. Nanotech. 14, 12, 9020, (2014).
24. A.N. Mariano and R.E. Hanneman, J. App. Phys., 34, 2, 384, (1963).
25. A.A. Chernov, Modern crystallography III – Crystal Growth, edited by E. Givargizov, Germany, Berlin-Heidelberg, Springer, (1984).
26. J.M. Ting, et al., J. Am. Ceram. Soc. 92, 11, 2718, (2009).
27. A. Shkurmanov, ZnO-based nanostructures by PLD: growth mechanism, doping and geometry, Universität Leipzig, 2017

Вісник ХНУ, серія «Фізика», вип. 28, 2018. с. 53-62

PACS:
UDC 53.216.2

Temperature effects in nanostructured carbon-copper films deposited by magnetron sputtering

A. A. Onoprienko

Frantsevich Institute for Problems of Materials Science, National Academy of Sciences of Ukraine
3 Krzhyzhanovsky Str., 03142 Kiev, Ukraine
onopr@ipms.kiev.ua

DOI: 10.26565/2222-5617-2018-28-05

Nanostructured carbon-copper films were deposited by direct current magnetron sputtering of composed graphite-copper or pure graphite and copper targets. The evolution of film structure on annealing in a vacuum at temperatures in the range of 300-600^{o}C and upon deposition at 600^{o}C has been studied by transmission and scanning electron microscopy and electron diffraction. Three types of thin annealed films were studied, namely: mixed C+Cu (type 1), two-layer C/Cu (type 2), and nanostructured (type 3). Also two types of thick films were prepared by deposition of mixed carbon-copper film onto substrate at room temperature and then annealing in a vacuum (type 4), and by deposition of mixed carbon-copper film onto pre-heated substrate (type 5).

The as-deposited films of type 1 (containing 8-22 at. % Cu) exhibited amorphous structure with copper atoms uniformly distributed over the film volume. Annealing in the range of 300-600^{o}C resulted in precipitation of copper into the set of particles with average particle size depending on copper content and annealing temperature, and in development of diffusion coalescence within the set of particles. The coalescence occurred more slowly than it is predicted by the theory. Upon annealing at 600^{o}C of type 2 film the copper layer disintegrated and the set of copper particles formed. The diffusion coalescence of particles also took place. Like type 1 film, in the type 2 film the coalescence occurred also more slowly than it is predicted by the theory. The structure of type 3 film was stable upon annealing at 600^{o}C for period up to 15 h. The specific microstructure of carbon film-matrix greatly slowed down the diffusion coalescence of copper particles in the films of types 1 and 2 and prevented it in type 3 film.

Upon annealing of the film of type 4 the amorphous structure of carbon matrix preserved, and the set of copper particles formed on its surface. The film deposited onto pre-heated substrate (type 5) exhibited clearly columnar structure of carbon matrix with the set of copper particles located both in the film volume and on its surface.

Keywords: film; amorphous carbon; nanostructure; coalescence; diffusion; electron microscopy.

Наноструктурні плівки в системі „вуглець-мідь” одержані методом магнетронного на постійному струмі розпилення мішені, складеної із графіту та міді, а також чистих мішеней із графіту та міді. Еволюцію структури при відпалі в інтервалі температур 300-600^{o}C, а також при осадженні при температурі підкладку 600^{o}C вивчали методами електронної просвічу вальної та скануючої мікроскопії, а також електронографії. Досліджували три типи тонких плівок після відпалу, а саме; змішана C+Cu (тип 1), двошарова C/Cu (type 2) та наноструктурна (тип 3). Були досліджені також товсті плівки двох типів, одержані осадженням змішаної C+Cu плівки на підкладку при кімнатній температурі та наступним відпалом в вакуумі (тип 4), а також осадженням змішаної C+Cu плівки на наперед нагріту підкладку (тип 5).

Осаджені плівки 1-го типу (які містили 8-22 ат. % Cu) мали аморфну структуру, в якій атоми міді були розподілені рівномірно по об'єму плівки. Відпал в інтервалі температур 300-600^{o}C призвів до виділення міді в ансамбль частинок зі середнім розміром, який залежав від концентрації міді в плівці та температури відпалу, а також до розвинення процесу коалесценції частинок. Коалесценція протікала повільніше, ніж передбачено теорією. При відпалі при 600^{o}C плівки 2-го типу шар міді розпався і на поверхні сформувався ансамбль острівців міді. В ансамблі острівців також розвинувся процес коалесценції, який протікав також повільніше, ніж передбачено теорією. Структура плівки 3-го типу виявилась стійкою до відпалу при 600^{o}C протягом 15 годин. Специфічна структура вуглецевої плівки-матриці істотно уповільнювала дифузійну коалесценцію в ансамблі частинок міді в плівках 1-го та 2-го типів, та заблокувала коалесценцію в плівці 3-го типу.

При відпалі плівки 4-го типу аморфна структура плівки зберігалася, і на її поверхні сформувались частинки міді. В плівці, осадженої на попередньо нагріту підкладку (тип 5), сформувалась стовпчаста структура вуглецевої матриці, а частинки міді сформувались як на поверхні плівки, та і в її об'ємі.

Ключові слова: плівка; аморфний вуглець; наноструктур; коалесценція; дифузія; електронна мікроскопія.

The ideological ground for present work is the theoretical and experimental research which was carried out under leadership of Prof. Ya. E. Geguzin at the chair of crystals physics of Kharkov university on the problem of diffusion mass transfer in discrete metal films located on the surface of real crystal.

Introduction

An interest in the composite carbon films that contain nanosized metal particles stems from the prospects in application of such films. The diamond-like (DLC) and amorphous (a-C) carbon films themselves have unique properties, such as high hardness, chemical inertness, high electrical resistance, transparency in infrared spectrum. An introduction in such films of nanosized particles opens new areas for application films, e. g. creation of the media for information recording in case of particles of magnetic material. The composite carbon/metal films are promising wear-resistant material with low friction coefficient for tribological application, and also as an electrode material for electrochemistry.

The metal-containing carbon films can be produced by different techniques, such as dc/rf magnetron sputtering,

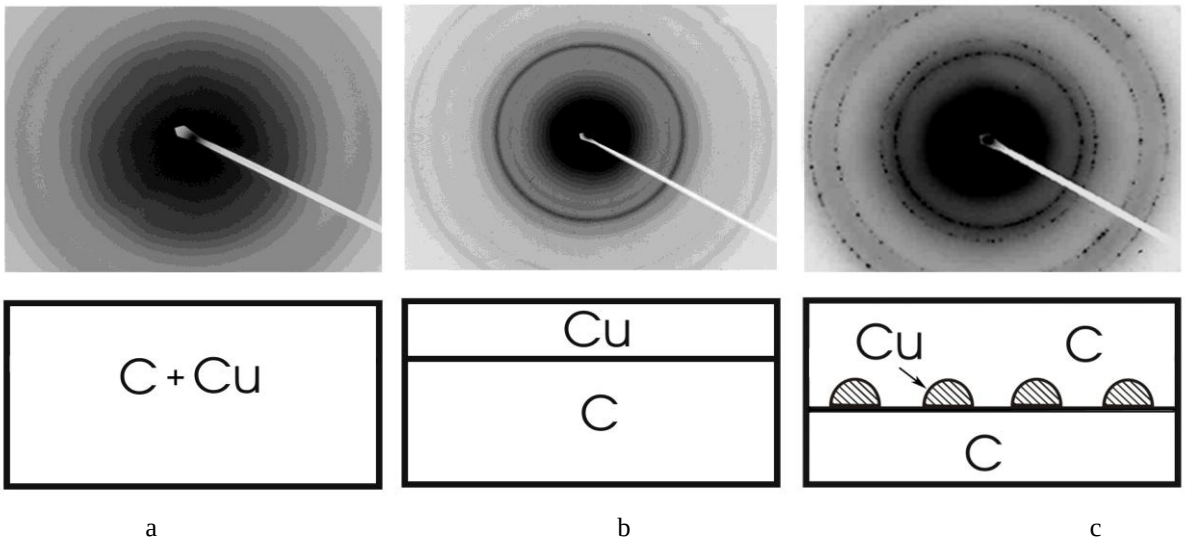

Fig. 1. Schematic representation and electron diffraction patterns of as-deposited carbon/copper films: (a) mixed (type 1); (b) two-layer (type 2); (c) nanostructured (type 3).

cathode vacuum-arc process, mass-separated ion-beam deposition, combined magnetron sputtering with chemical vapor deposition, etc [1-6]. However, when depositing carbon films the problem often arises connected with high compressive stress which tends to detach the film from the substrate when film thickness exceeds definite critical value. One of the ways to reduce the internal stress is addition of new element in the a-C matrix, e. g. the copper because it is highly ductile metal and it does not form hard carbides.

There are a number of works on the effect of copper doping on the properties of composite carbon/copper films [1, 6-10]. In Ref. [7], it was demonstrated that adding of a small amount of copper (Cu:C ratio <1:100) to a-C:H film results in an increase in the Vickers hardness and improvement of film adhesion to the silicon substrate. At the same time, in Ref. [1] the adding 11 at. % copper to a-C:H film was shown to decrease the film hardness, increase the critical load in the adhesion tests, reduce the film stress, and increase the film toughness. In Ref. [7], the optical properties of carbon/copper films have also been studied, and it was shown that copper atoms not only passivate the dangling bonds but also create a favorable environment for sp^3 structure of amorphous carbon. In Ref. [8], the hardness of a-C:H/Cu films decreased with increase in copper content up to 60 at.% while the Young's modulus did not change. In Ref. [9, 10], the microstructure of copper nanoparticles encapsulated into carbon shell has been studied, and it was shown that the size and morphology of particles depend on the deposition and subsequent annealing conditions.

Since the carbon and copper are mutually insoluble, so to mix them it is necessary to create non-equilibrium conditions for deposition copper-containing carbon film. The magnetron sputtering technique provides with such conditions. In this chapter, the microstructure of as-deposited and annealed in a vacuum composite carbon/copper films has been studied by transmission electron microscopy (TEM) and electron diffraction (ED). The hardness of films was also measured by indentation method.

Experimental details

The carbon/copper films were sputter deposited using conventional planar balanced direct current (dc) magnetron units. The target composed from graphite disk (60 mm in diameter and 4 mm thick) and copper chips, and also pure graphite target of the same dimensions and copper target (60 mm in diameter and 1.5 mm thick) were used for film deposition. The target-to-substrate distance was 50 mm. The sputtering gas was 99.97 % pure argon at constant pressure 1 Pa. The single crystal wafers of (100) NaCl (fresh cleavages) and (100)-oriented plates of single-crystalline silicon were used as substrates. Prior to film deposition, the targets were pre-sputtered on the shield in order to remove contaminations from the target surface and stabilize the magnetron discharge parameters. The magnetrons operated at about 100 W power, and this allowed achieving of reasonable deposition rate while minimizing non-controllable heating of growing film by plasma radiation and bombardment with positive ions [11]. Under above deposition conditions, the substrate temperature during film condensation did not exceed 50^{o}C. No biasing voltage was specially applied to the substrate during deposition.

Five types of specimens for structure study were prepared as follows. The films of type 1 were mixed C+Cu ones (Fig. 1a) deposited by sputtering of the target composed of graphite disk and copper chips attached to

its surface in the sputtering zone. As substrates, the single crystal NaCl (100) plates were used. To produce the films with different copper content, the amount of copper chips was varied in different experiments. The thickness of these films was about 100 nm (for TEM and ED studies).

The type 2 film was two-layer C/Cu one deposited by successive sputtering of graphite and copper targets. In this case, the deposition rates of pure carbon (≈0.2 nm/sec) and copper (≈2.5 nm/sec) were pre-determined. The carbon layer was first deposited onto NaCl substrate for 450 sec and then the copper layer was deposited for 2 sec, so that the copper layer was 5 nm thick and the whole two-layer film specimen was near 100 nm thick (Fig. 1b).

The type 3 film was nanostructured C/Cu/C one produced as follows. A carbon layer was first deposited onto NaCl substrate for 180 sec to be about ~36 nm in thickness. Next, the copper layer was deposited onto carbon film for 2 sec to be about 5 nm in thickness. Then the carbon film with copper layer was separated from the substrate by dissolving the latter in distilled water, and placed onto a special copper mesh used in electron microscopy. This mesh material was selected because the carbon and the copper neither dissolve each other nor form carbides, and so there should not be additional doping of the film with copper during annealing. The mesh with two-layer C/Cu film was annealed in vacuum ($P \approx 1.33 \cdot 10^{-3}$ Pa) at 600°C for 1 h in order to the copper layer disintegrated into separate islands under effect of surface tension. After cooling to room temperature, the above C/Cu film was again placed in vacuum chamber and new carbon layer was deposited over the copper islands for 180 sec. As a result, the test specimen was composite C/Cu/C film of about 77 nm thick, in which individual nanosized copper particles-islands were between two carbon layers (Fig. 1c). The thickness of the layers was adjusted so that the carbon completely covered the copper particles but the whole composite film was thin enough to be examined with a transmission electron microscope.

The as-deposited carbon/copper films of types 1 and 2 were also removed from NaCl substrate by dissolving the latter in distilled water and placed onto aforementioned copper meshes. The dried meshes with films were placed in a vacuum chamber, and after pumping to a pressure of $1.3 \cdot 10^{-3}$ Pa they were annealed stepwise at temperatures 300-600°C for up to 15 h. After each annealing step and cooling to room temperature the specimens were extracted from the chamber and studied in a transmission electron microscope JEM-100CX II (JEOL) operating at 100 kV.

The specimen of type 4 was the thick carbon-copper film (like the films of type 1) deposited onto the Si substrate at room temperature, and then annealed in a vacuum ($1.3 \cdot 10^{-3}$ Pa) at 600°C for 1 h. The specimen of type 5 was the thick carbon-copper film (like the films of type 1) deposited onto the Si substrate pre-heated to 600°C. After cooling to room temperature, the surface and cross section of specimens were studied in a scanning electron microscope.

Results and discussion

Films of type 1

To study the structure evolution upon annealing of copper-doped carbon films, the specimens were prepared containing 8 to 22 at % Cu, as determined by Auger-electron spectroscopy. TEM and ED studies showed that the as-deposited films were amorphous irrespective of the copper content examined. In particular, the respective electron diffraction patterns (Fig. 1a) contained only few halos peculiar to amorphous carbon films deposited by magnetron technique under conditions identical to those used in present experiments, and TEM images did not reveal any signs of the structure. This observation indicated that the copper atoms and possibly clusters were

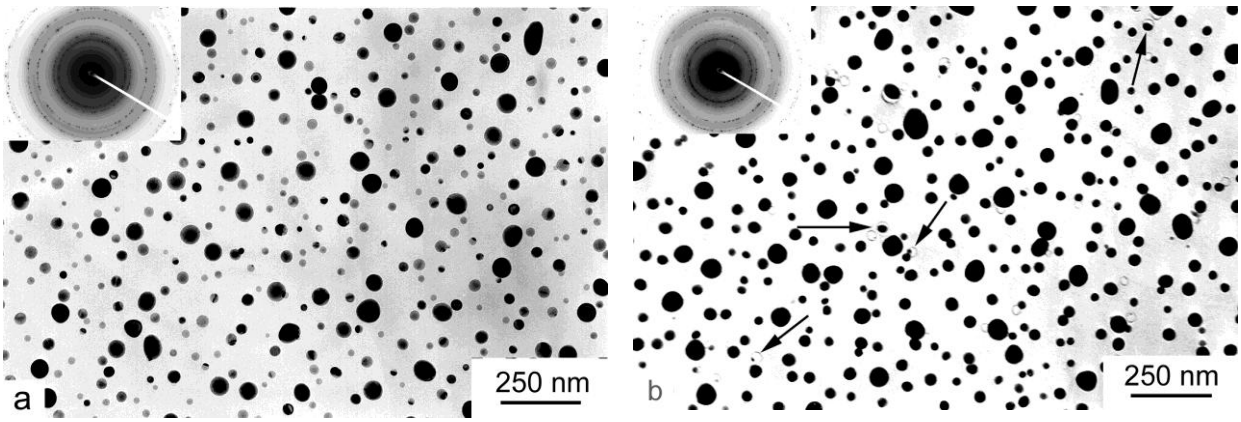

Fig. 2. TEM images and respective ED patterns taken from type 1 carbon/copper (8 at. % Cu) film after annealing in vacuum at 600°C for (a) 1 h and (b) 5 h. Arrows show the pits from partially or totally dissolved copper particles.

uniformly distributed over the volume of the as-deposited films. Annealing in a vacuum at temperatures in the range 300-600°C for 1 h drastically changed the film structure. In particular, a set of round-shaped nanoparticles formed in the film, and ED proved these to be the copper particles. The spherical shape of copper particles was clearly seen in the electron-microscopic images of the edge of film rolled up under effect of electron beam (not shown here). In Fig. 2a, the typical carbon film with copper particles after annealing under above conditions is shown.

The analysis of particle distribution with respect to their diameters has revealed that for specified copper content the average particle size in the set (determined as an average arithmetic value of diameters of all the particles involved in plotting respective size distribution graphs) decreased with increase in annealing temperature (Table 1). This sudden at first sight result will be explained further. Also, with increase in copper content in the film the average particle size in the set increased under otherwise equal annealing conditions (Table 1). This is predictable result, because it is clear that the more copper in the film, the more copper atoms will precipitate in particles during annealing.

Table 1.

Dependence of average Cu particles diameter on copper content and annealing temperature for type 1 carbon films

Cu, at. %	T_{ann}, °C	$\bar{d}$, nm
8.0	300	31.3
	450	27.2
	600	24.8
12.4	300	42.4
	450	38.3
	600	35.1
16.8	300	48.7
	450	46.5
	600	41.2
22.6	300	51.7
	450	48.6
	600	44.0

The behavior of C+Cu films upon prolonged annealing was followed with the film containing 8 at. % Cu. For this purpose, the film on a copper mesh was stepwise annealed at 600°C in a vacuum. Periodically the annealing was interrupted, and after cooling to room temperature the specimen was extracted from the chamber and studied by TEM and ED.

The size (diameter) distribution showed that after the first annealing step for 1 h the majority of particles had diameters in the range of 10-30 nm with average over the set particle diameter of 24.8 nm (Fig. 3a). The next annealing step for 1 h resulted in changes within particle set, namely the total number of particles increased somewhat, more small particles with diameters in the range of 10-30 nm and the particles with larger diameters (60-70 nm) appeared (Fig. 3b). The average over the set particle diameter became 24.5 nm. This means that not all of the copper atoms have precipitated in particles during the first annealing step (for 1 h), and this process

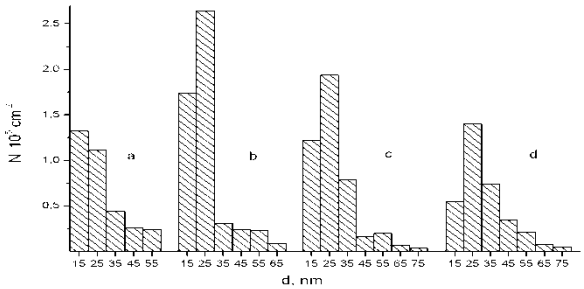

Fig. 3. Size-distribution plots for copper particles normalized for area unit of type 1 film surface after annealing at 600°C for (a) 1, (b) 2, (c) 3.5, and (d) 5 h.

continued in the second annealing step with formation of new particles. Some decrease in the average particle diameter is just the result of formation of additional small (10-30 nm in diameter) particles in the second annealing step. The above feature in behavior of particle set explains the observed decrease in average particle size in the film with specified copper concentration with increase in the temperature upon annealing for one-hour period (Table 1). During annealing, the copper atoms precipitate primarily at the sites which are the most appropriate for particle nucleation, i. e. on the film free surface and at structural defects, and then at sites where the probability of particle nucleation is less. The higher the annealing temperature, the higher mobility of copper atoms, and the more small particles nucleate within the first one-hour period of annealing. Therefore, the average particle size should decrease with increase in annealing temperature for films with specified copper content as it was observed in present experiments.

Further annealing for 1.5 h resulted in the decrease in the total number of particles, in the majority of particles to have the diameters in the range of 10-40 nm with average particle diameter over the set of 26.5 nm, and also in the appearance of the particles with diameters in the range of 70-80 nm (Fig. 3c). After the next annealing step for 1.5 h, the total number of particles further decreased and the average particle size increased to 30.3 nm (Fig. 3d).

The features of histograms in Fig. 3 allowed suggestion that in the second annealing step the process of copper particles precipitation stopped and further only the process of diffusion coalescence (i. e. growth of some particles at the expense of dissolution others) within the set of particles continued. This is evidenced by the decrease in the number of small particles and in the total number of particles within the set, as well as by the

increase in the average particle diameter over the set and formation of particles of larger diameters (Fig. 3c, d). The occurrence of coalescence is also confirmed by the pits free of particles and by small particles in the pits of larger size in carbon film thus indicating that some copper particles have totally or partly dissolved upon annealing (Fig. 2b).

The observed structure evolution of copper-doped carbon film can be explained based on the hetero-diffusion concept. As noted above, the copper atoms are distributed uniformly over the volume of as-deposited C+Cu films. In accordance with the results of our earlier study [11], the as-deposited at low (near room) substrate temperature carbon films consist of nanoclusters with chaotically oriented and distorted aromatic rings and graphite-like fragments within them. Subsequent annealing at temperatures up to 650°C results only in the local transformation of distorted aromatic rings into regular-shaped ones and in ordering of them within graphite-like nanoclusters in the substrate plane without increase in the size of clusters [12]. These results allowed the conclusion that the as-deposited amorphous carbon films contain large amount of structural defects, and the annealing at 650°C does not result in considerable reconstruction of the carbon film structure. Formation of copper particles can therefore be only the result of diffusion processes for copper atoms within the carbon film.

The idea of calculation of three-dimensional diffusion coalescence kinetics, i. e. variation with time of the average size in the set of particles, was first formulated in [13] in which the authors have developed a theory for coalescence within the set of inclusions in the bulk of crystal, based on the assumption that the change in inclusion radii with time is a consequence of interaction of inclusions with generalized field of atoms of inclusion substance. That field is characterized by the averaged atom concentration $\bar{\xi}$ which depends on the size distribution function $f(R,t)$ for inclusions, and it is in equilibrium with inclusions of critical radius R^*. Since near the inclusions with radius $R<R^*$ the equilibrium atom concentration is $\xi_R>\bar{\xi}$, then those inclusions have to dissolve while the inclusions with $R>R^*$ have to grow since $\xi_R<\bar{\xi}$ in this case. The average inclusion radius within the set was shown has to vary with time as $\bar{R}^3 \sim t$ [13].

Similar approach has been applied to the problem of two-dimensional coalescence in a conservative system, namely in the set of "islands" of one substance onto the surface of crystal of another substance [14]. It was shown that if the island substance mass transfer via gas phase is negligibly small compared with that over the crystal surface, then the average particle radius within the set has to increase as $\bar{R}^4 \sim t$.

As suggested above, after the second annealing step only the diffusion coalescence within the particle set occurred in type 1 films. The fact that the total amount of substance in particles, which was determined as a sum of volumes of all the particles (which was suggested to have spherical shape) within the specified surface of carbon film, i. e. $\frac{\pi}{6}\sum n_i \bar{d}_i^{\,3}$, first increased with time and after the second annealing step was virtually unchanged, allowed the assumption that the carbon-copper film under study is an analog of the conservative system considered in [13,14].

We attempted to determine the mechanism for diffusion transport of the particle substance (copper) during coalescence. Since the equilibrium pressure at 600°C for copper is negligibly low ($P = 9.78\cdot10^{-9}$ Pa), then one can neglect mass transfer via gas phase and consider the copper atoms diffusion occurring only within the film volume or onto its surface. In these cases, as was shown in [13, 14], the average particle radius in the set has to vary with time as $\bar{R}^3 \sim t$ or $\bar{R}^4 \sim t$, respectively. Shown in Fig. 4 is the dependence of log $\bar{R}$ on log *t*, from which it is evident that for annealing steps starting from the second

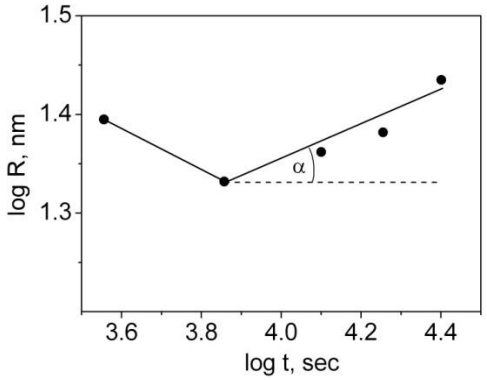

Fig. 4. Dependence of average radius of copper particles on annealing time for type 1 film.

one (i. e. when only the coalescence process is suggested to took place within the system "film-set of particles") the tangent of slope angle for best fitted straight line is about $\frac{1}{5}$ and not $\frac{1}{3}$ or $\frac{1}{4}$ as it should be in case of diffusion only within the volume or only onto the surface of film, i. e the mass transfer occurred substantially more slowly. This finding can be explained through reasoning from the following argumentation. The results in [13, 14] were

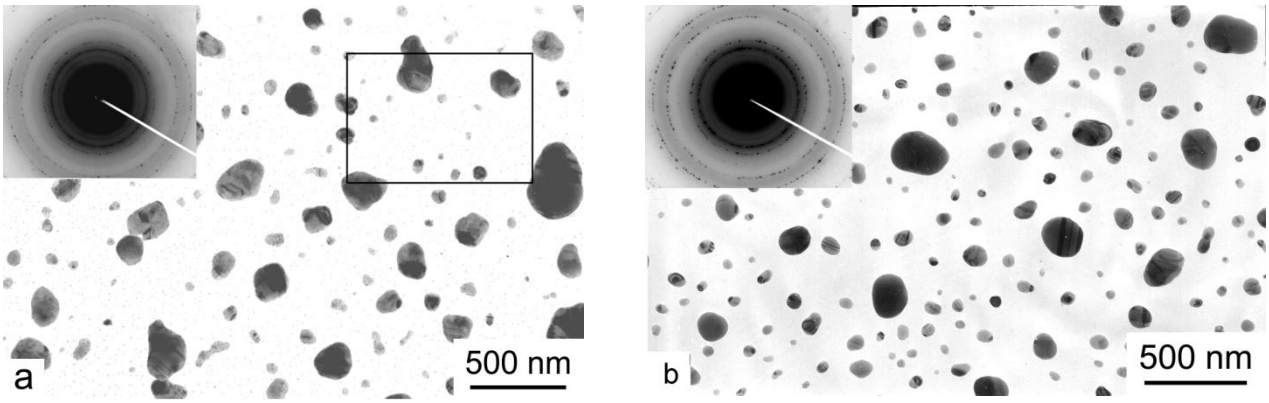

Fig. 5. TEM images and respective ED patterns for two-layer (type 2) film annealed at 600 °C for (a) 1 h and (b) 7 h.

obtained from consideration of diffusion in the spatially homogeneous medium or on atomic-smooth surface, respectively. In our case, as noted above, the as-deposited carbon film contained a large amount of structural defects that are not eliminated by annealing and hinder the diffusion transfer of copper atoms. Moreover, the pits from dissolved particles (Fig. 2b) indicate that the copper particles were partly immersed into the carbon film at different depths. So, based on above results one can suggest that the mass transport is apparently of a mixed nature, i. e. it occurs in both the film bulk and on its surface. In aggregate, all these factors determine observed by experiment the dependence of particle average size on annealing time.

Film of type 2

To elucidate the question: what is the real mechanism of mass transfer upon annealing within the set of copper particles located on the surface of carbon film, the two-layer specimen has been prepared.

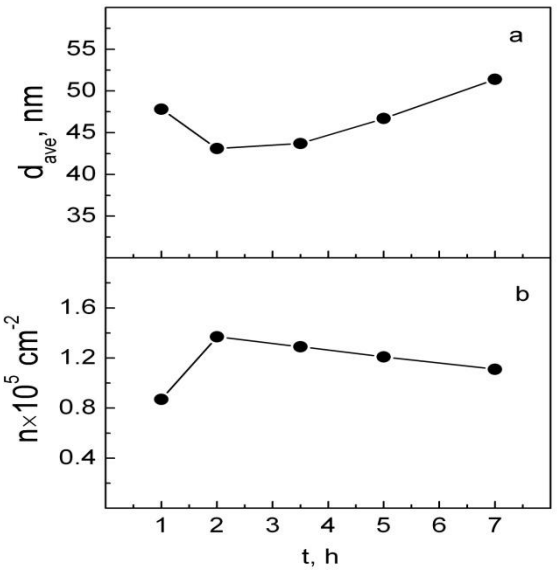

Fig. 6. Dependence of average diameter (a) and surface density of copper particles (b) on annealing time for type 2 film.

TEM and ED study of this film showed that the initial (as-deposited) film consisted of amorphous carbon layer and continuous polycrystalline copper layer (Fig.1b). Annealing in vacuum at 600°C for 1 h fundamentally changed the film structure. In particular, the copper layer disintegrated due to the surface tension force and the set of particles formed on the surface of carbon film-substrate. The ED proved them to be copper nanoparticles (Fig. 5a). The particles were almost equi-axial and acquired well-defined internal structure (grain boundaries, twins, etc.). After long-term annealing the particles loss their inner sub-structure and gained more rounded shape while the carbon film remained amorphous as is evidenced by halos in ED pattern (Fig. 5b).

The behavior of the set of particles upon annealing in films of this type is also of two-stage nature like that in the films of type 1. In the first stage, after the originally continuous copper layer has disintegrated, the average size of particles decreased and their number increased during the second one-hour step of annealing (Fig. 6). Upon further annealing the diffusion coalescence developed, in particular the average diameter of particles increased and their number decreased. Since the copper layer was initially located over the carbon layer, one can assume that the particles formed as a result of copper layer disintegration are also located onto the carbon film surface. Therefore, in this case the coalescence that leads to changes in the set of copper particles seems to proceed through only the surface hetero-diffusion mechanism.

Size distribution of copper particles is of two kinds. There are particles several tens of nanometer on average (Fig. 5a) and very fine particles visible only under much higher magnification (Fig. 7). For statistical processing of TEM images the pictures should be taken under magnification that would ensure the optimum ratio between the size and number of particles. However, in this case very fine particles are not visible in the pictures,

so they cannot be accounted in statistical processing, but these seem to be nevertheless involved in coalescence process. In the first stage of annealing the very fine particles coalesce due to diffusion of copper atoms and,

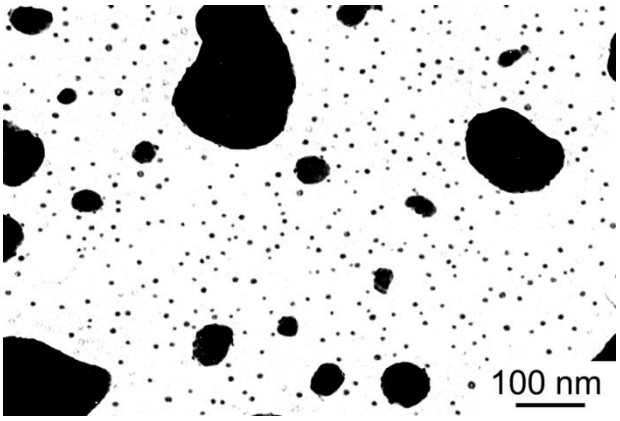

Fig. 7. TEM image with higher magnification of area shown in insert in Fig. 5a.

thus, contribute to formation of additional small particles which are now accounted in statistical processing of images. Just the formation of new small particles causes the decrease in average diameter and increase in particle density in the first annealing stage comprising two one-hour annealing steps. In the second stage, the contribution from formation of small particles at the expense of finest particles becomes essentially less, and predominant is the diffusion coalescence within the set of larger particles which are accounted upon statistical processing of TEM images. As a result, the average diameter of particles increased (Fig. 6a) and the surface density of particles decreased (Fig. 6b). (Note that after prolonged annealing the finest particles disappeared and were not longer seen in electron microscopic images of particles set.)

Analysis of the dependence of particle average diameter on annealing time ($log\,\bar{R}$ vs. $log\ t$ plot) has shown that the average radius in the set obeys again the law $\bar{R}^5 \sim t$ (like that for type 1 film) and not $\bar{R}^4 \sim t$ as it might be expected for the case of coalescence by the mechanism of surface diffusion of copper atoms [14]. We believe that deviation of the experimental coalescence law from the theoretical one is because of the real microstructure of carbon layer-substrate. As noted above, in [14] the law $\bar{R}^4 \sim t$ was derived based on the hetero-diffusion concept over the homogeneous and atomic-smooth surface. The as-deposited under conditions used in present experiments real carbon layer consists of chaotically oriented and internally strongly disordered graphite-like clusters, and that structure preserves upon annealing. So, the diffusion of copper atoms over the surface of such carbon layer seems to be hindered and therefore occurred more slowly than it is predicted by the theory.

As mentioned above, in the mixed carbon-copper films (type 1) the particles formed due to diffusion precipitation of copper atoms from the volume of carbon film. It was suggested that the process of particles set formation finished to the end of the first one-hour annealing step, and further only the diffusion coalescence of particles occurred. Based on the results obtained with films of type 2, it is now reasonable to suggest that in the type 1 films the processes of particle formation and diffusion coalescence occur simultaneously. In the first stage (two successive one-hour annealing steps) the process of particles set formation was predominant, and in the next stage predominant became diffusion coalescence of particles in the set, so that the average particle diameter increased.

Film of type 3

To verify the suggestion about surface diffusion mechanism for coalescence, the film of type 3 was examined, in which the pre-formed set of copper particles was located between carbon layers. In this case, the near

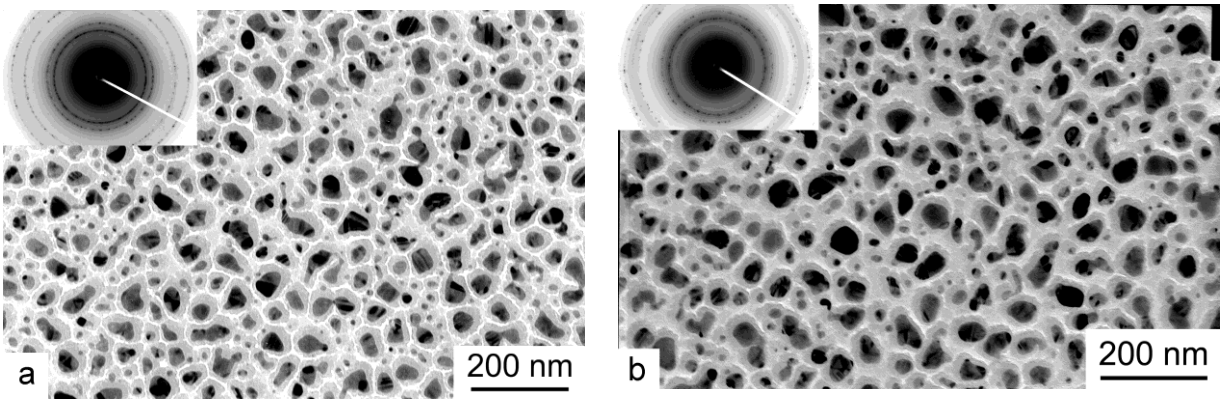

Fig. 8. TEM images and respective ED patterns for nanostructured (type 3) initial (a) and annealed at 600°C for 15 h (b) films.

regular-shaped copper particles were initially surrounded by amorphous carbon matrix thus simulating volume conditions.

Shown in Fig. 8a is TEM photograph of initial film. The copper particles gained a certain crystallographic orientation during specimen preparation annealing step, which is evidenced by the point reflections in ED pattern.

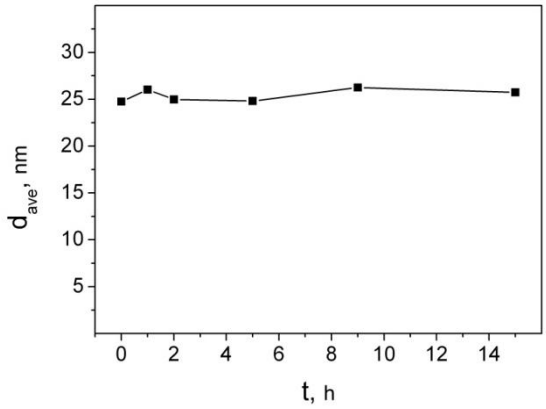

Fig. 9. Dependence of average diameter of copper particles on annealing time for type 3 film.

The coarser particles exhibit structural defects (grain boundaries, twins). Subsequent long-term annealing didn't result in any noticeable changes in the shape of copper particles (Fig. 8b).

An analysis of size distribution of copper particles has shown that the average diameter of particles was actually unchanged after annealing at 600°C even for 15 h (Fig. 9). This evidence unambiguously indicates absence of coalescence in these films, which can be explained based on aforementioned reasoning (see par. 3.1). In this case, the copper particles are surrounded by the quasi-amorphous carbon matrix with highly distorted structure which is resistant to annealing. So, the diffusion transfer of copper atoms whose size in addition is much larger than that of carbon atoms is greatly hindered because of structural imperfection of carbon matrix.

Films of types 4 and 5

The structure of annealed carbon-copper films of type 1 was formed due to the features of specimen preparation. To be appropriate for TEM study, the carbon films must be rather thin (no more than 100 nm). As was shown, the copper atoms were uniformly distributed over the carbon matrix in the as-deposited films. Since the copper forms neither solid solutions with carbon nor carbides, then upon annealing copper atoms strived to segregate into particles in order to lower the total energy of the system. Naturally, the most suitable place for particle formation is free surface of thin film, and thus the copper particle set formed just onto the carbon matrix surface with average particle diameter in the sets in the range from about 25 nm to about 52 nm depending on copper concentration in C-Cu films. However, the question remained open as to whether the copper particles form only on the carbon film surface during annealing or that process can occur also in the carbon film-matrix volume during deposition?

To give answer to above question we studied the peculiarities of structure formation in thick composite carbon-copper films in which free surface is of less importance. In view of aforesaid as to the effect of annealing on the behavior of thin carbon-copper films, we chose the highest copper content at about 22 at. % Cu and the treatment temperature of 600°C in order to ensure the film structure formation process to be the most expressive and the results comparable with those reported above for films of type 1.

Shown in Fig. 10 is the SEM image of type 4 C-Cu film deposited at low temperature and then annealed at 600°C for 1 h. It is evident that like the thin carbon-copper films of type 1, in this case the set of copper particles also formed on the film surface. The fact that these particles are metal (copper) ones is proved by the image obtained in back-scattered electrons. The estimated size of copper particles is about 120 nm, i. e. noticeably larger than for particles formed in thin type 1 carbon-copper films. This discrepancy in particle sizes can be explained based on the following argumentation. In thin film the reserve of copper is much less than in thick film due to film small volume. Upon annealing, that reserve quickly run out, and after the set of particles formed the predominantly diffusion coalescence of particles

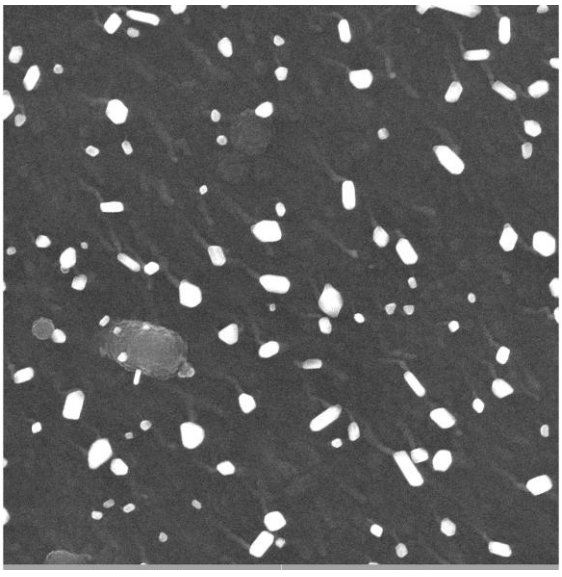

Fig. 10. Copper particles on the surface of thick type 4 carbon-copper film deposited at room temperature and annealed in vacuum at 600°C for 1 h: image in secondary electrons (left) and back-scattered electrons (right).

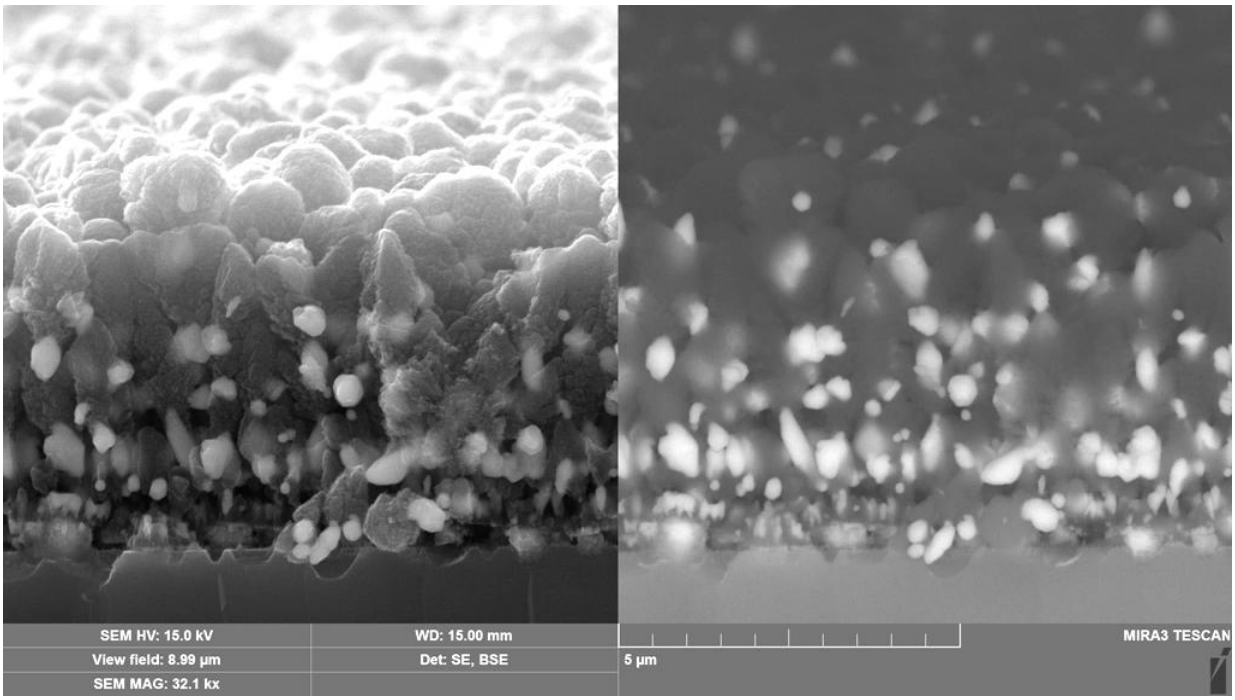

Fig. 11. SEM cross-section of thick type 5 carbon-copper film deposited at substrate pre-heated to 600°C: images in secondary electrons (left) and back-scattered electrons (right).

developed. In thick film the reserve for copper is essentially larger, and more atoms are able to precipitate in particles thus resulting in greater particle size.

The following observation in the specimen cross section (not shown here) attracted attention. The film volume adjacent to the film free surface contained less amount of particles compared to deeper film volume. This observation means that the copper atoms diffused from the sub-surface layers to free film surface and precipitated there in particles. Another remarkable feature is the structure-less nature of the film. This fact is also consistent with the results in [12] where it was shown that the amorphous structure of carbon film deposited at low substrate temperature is stable to subsequent annealing at temperatures up to 600°C.

The structure of type 5 carbon-copper film deposited onto the substrate pre-heated to 600°C is shown in Fig. 11. The film exhibits clearly expressed columnar structure of carbon matrix. That structure agrees with the results obtained in [12], where ordering of aromatic rings and growth of graphitic clusters at deposition temperatures of ≈500°C and higher was observed. Also, the copper particles formed during film deposition are distributed over the whole film volume and onto its surface. The estimated size of copper particles is about 500 nm. It is notable that particle density decreases from the bottom to the surface of film. The latter fact is consistent with the results in [15] and indicates that part of copper atoms diffused from the sub-surface carbon matrix layer and precipitated in particles onto free film surface.

Conclusions

In dc magnetron sputtering of composite graphite/copper target, the copper-doped amorphous carbon films are deposited with uniform distribution of copper atoms and clusters over the film volume. Annealing of films in a vacuum at 300-600°C results in precipitation of copper particles and accompanies by changes within the set of copper particles because of diffusion coalescence. As a consequence of this, the density of copper particles decreased and their average over the set size increased. The coalescence occurred more slowly than it is predicted by the theory. With increase in copper content in the film the average particle size in the set increased with other annealing conditions being equal. With specified copper content the average particle size in the set decreased with increase in annealing temperature. The coalescence mechanism is suggested to be of mixed nature and includes the mass transfer in both the film volume and over its surface. The structure defects in carbon film reduce greatly the rate of diffusion displacement of copper atoms within the carbon film.

In the two-layer film an annealing in a vacuum at 600°C resulted in two-stage microstructure evolution. In the first stage, the copper layers disintegrated into separate “islands”-particles. In the second stage, the process of diffusion coalescence developed within the set of copper particles. As a result, the density of copper particles decreased and their average size increased. The coalescence in two-layer carbon-copper film occurred

also more slowly than it is predicted by the theory and obeyed the same low as for the mixed copper-doped carbon films of type 1. This is because the strongly disordered structure of carbon film preserves upon annealing at 600^{o}C and reduces greatly the rate of diffusion transport of copper atoms over the surface of carbon matrix. In the three-layer film, upon annealing the copper layer also disintegrated into particles of strongly irregular shape. The process of coalescence was not observed because of specific morphologic and structural features of copper particles and carbon layers.

In nanostructured films the average size of copper particles didn't change upon annealing. This is because the copper particles were initially surrounded with carbon matrix whose real structure effectively hindered the diffusion transfer of copper atoms and thus prevented the coalescence of copper particles by volume diffusion mechanism. So, the results obtained with types 1 to 3 carbon/copper films make it possible to conclude that upon annealing the mass transfer within the set of copper particles occurs predominantly by the surface hetero-diffusion mechanism.

The thick carbon-copper film deposited at low temperature and then annealed at 600^{o}C for 1 h preserved the amorphous structure of its carbon matrix, and the set of copper particles formed onto its surface. The film deposited onto pre-heated to 600^{o}C substrate exhibited well-defined columnar structure of carbon matrix with the set of copper particles in the film volume and onto its surface. The substrate temperature during deposition and/or post-deposition annealing is critical for copper precipitation both in the carbon film volume and on film surface.

References

1. C.C. Chen, F.C.N. Hong, Structure and properties of diamond-like carbon nanocomposite films containing copper nanoparticles, Appl. Surf. Sci., 94 (2005) 261-269.
2. J.M. Ting, H. Lee, DLC composite thin films by sputter deposition, Diamond Relat. Mater., 11 (2002) 1119-1123.
3. Gy. J. Kovács, G. Sáfrán, O. Geszti, T. Ujvári, I. Bertóti, G. Radnóczi, Structure and mechanical properties of carbon-nickel and CN_x-nickel nanocomposite films, Surf. Coat. Technol., 180-181(2004) 331-334.
4. D.Y. Wang, K.W Weng, S.Y. Hwang, Study on metal-doped diamond-like carbon films synthesized by cathodic arc evaporation, Diamond Relat. Mater., 9 (2000) 1762-1766.
5. F.C. Fonseca, A.S. Ferlauto, F. Alvarez, G.F. Goya, R.F. Jardim, Morphological and magnetic properties of carbon-nickel nanocomposite thin films, J. Appl. Phys., 97 (2005) 0443131-7.
6. H. Hofsäss, H. Binder, T. Klumpp, E. Recknagel, Doping and growth of diamond-like carbon films by ion beam deposition, Diamond Relat. Mater., 3 (1993) 137-142.
7. P.A. Chen, Characteristics of copper-incorporated amorphous carbon film, Thin Sol. Films, 182 (1989) 261-263.
8. Y. Pauleau, F. Thièry, Deposition and characterization of nanostructured metal/carbon composite films, Surf. Coat. Technol., 180-181 (2004) 313-322.
9. J. Jiao, S. Seraphin, Carbon encapsulated nanoparticles of Ni, Co, Cu, and Ti, J. Appl. Phys., 83 (1998) 2442-2448.
10. T. Cabioc'h, A. Naudon, M. Jaouen, D. Thiaudiére, D. Babonneau, Co-sputtering C-Cu thin film synthesis: microstructural study of copper precipitates into a carbon matrix, Phil. Mag., B 79 (1999) 501-516.
11. A.A. Onoprienko, V.V. Artamonov, I.B. Yanchuk, Effect of magnetron discharge power on the resistivity and microstructure of carbon films. Surf. Coat. Technol., 200 (2006) 4174-4178.
12. A.A. Onoprienko, V.V. Artamonov, I.B. Yanchuk, Effect of deposition and anneal temperature on the resistivity of magnetron sputtered carbon films, Surf. Coat. Technol., 172 (2003) 189-193.
13. I.M. Lifshitz, V.V. Slyozov, The kinetics of precipitation from supersaturated solid solutions, J. Phys. Chem Sol., 19 (1961) 35-50**.**
14. Ya.E. Geguzin, Yu.S. Kaganovsky, V.V. Slyozov, Determination of the surface heterodiffusion coefficient by the method of mass transfer, J. Phys. Chem Sol., 30 (1969) 1173-1178.
15. A. A. Onoprienko, N. I. Danilenko, I. A. Kossko, Structure evolution on annealing of copper-doped carbon film, Thin Sol. Films, 515 (2007) 6672-6675.

Вісник ХНУ, серія «Фізика», вип. 28, 2018. с. 63-67

PACS: 81.40.Ef ; 62.25.+g ; 62.20.F.
UDC: 530.1/539.8

Mechanical properties of the nanostructured Ti processed by combination of the severe plastic deformation methods

E.D. Tabachnikova[1], A.V. Podolskiy[1], S.N. Smirnov[1], M.A. Tikhonovsky[2], P.A. Khaimovich[2], N.I. Danylenko[3], S.A. Firstov[3].

[1]*B.Verkin Institute for Low Temperature Physics and Engineering, Nauky Ave. 47, Kharkiv 61103, Ukraine, e-mail: tabachnikova@ilt.kharkov.ua*
[2]*National Science Center «Kharkov Institute of Physics and Technology» of National Academy of Sciences of Ukraine, 1 Academicheskaya street, Kharkov, 61108, Ukraine*
[3]*Frantsevich Institute for Problems of Materials Science NASU, 3, Krzhizhanovsky str., Kyiv, 03680, Ukraine*
ORCID: *0000-0002-1866-7941, 0000-0001-6846-3130, 0000-0001-5889-0366, 0000-0002-2523-9726, 0000-0001-6655-2404*

DOI: 10.26565/2222-5617-2018-28-06

The polycrystalline Ti Grade2 was subjected to combination of different methods of the severe plastic deformation, such as equal channel angular pressing, quasi hydro extrusion and rolling, and eight different structural states were produced. For each state were measured the following parameters: average grain size, microhardness (at 300 K) and mechanical characteristics in uniaxial compression at 300, 77 and 4.2 K. The concept of mutually complementary modes of plastic deformation differing in the set of active slip systems is introduced. The combination of the modes of plastic deformation was found, which gives the maximal values of the mechanical characteristics at temperatures 300, 77 and 4.2 K. It was shown that decrease of temperature of the preliminary deformation from 300 down to 77 K leads to improvement of the mechanical characteristics of the Ti Grade 2 samples in the whole studied temperature range.

Keywords: deformation, polycrystalline Ti Grade2, equal angular pressing, quasi-extrusion, rolling, mechanical characteristics

У полікристалічному Ti Grade 2, шляхом комбінації різних методів інтенсивної пластичної деформації при 300 і 77 К, таких як рівноканальне кутове пресування, квазігідроекструзія і прокатка, були отримані вісім різних структурних станів. Для кожного стану виміряні наступні параметрп: середній розмір зерен в мікроструктурі, значення мікротвердості (при 300 К) і механічні характеристики в ході одновісного стиску при 300, 77 і 4,2 К. Введено уявлення про взаємно додаткові моди пластичної деформації, що відрізняються набором діючих систем ковзання. Знайдений набір мод пластичної деформації, дія яких призводить до максимально високих значень механічних характеристик при температурах 300, 77 і 4,2 К. Показано, що зниження температури попередньої деформації від 300 до 77 К призводить до поліпшення механічних характеристик зразків Ti Grade 2 у всьому дослідженому температурному інтервалі.

Ключові слова: деформація, полікристалічний Ti Grade 2, рівноканальне кутове пресування, квазіекструзія, прокатка, механічні характеристики.

Introduction

Development of the new methods for production of the high strength states of materials by grain refinement is one of the actual tasks of modern material science. For this purpose the treatment of the various metallic materials is used by means of severe plastic deformation (SPD), which allows produce microstructures with submicron, and in some cases with nanoscaled grain sizes [1-17]. While, using the SPD methods at ambient temperature leads to saturation of the process of grain refinement at strains of $e \sim 8$-10 due to intensification of the dynamic recovery processes at large strains. But influence of the dynamic recovery on the microstructure changes during SPD can be decreased by decrease of the SPD temperature down to cryogenic values, which leads to increase of the yield and ultimate strength of the deformed materials [1, 2]. Additional decrease of average grain sizes and increase of the strength in metallic materials can be achieved by consequent change of deformation mode during SPD, which leads to activation of the new slip systems. So, in [3] for Al–0.13 wt.%Mg alloy, subjected to ECAP (strain ~10) at 298 K, which followed by compression at 77 K, the record small average grain size of ~ 180 nm was achieved.

The present paper is devoted to investigation of the possibilities of grain refinement and corresponding increase of the yield and ultimate strength of the polycrystalline Ti Grade 2 by consequent application of the mutually complementary modes of the severe plastic deformation: the simple shear (during ECAP), the axisymmetric deformation (during quasi hydro extrusion at 300 and 77 K), and also by the pure shear (during rolling at 77 K). The polycrystalline Ti Grade 2 was chosen as investigation material due to its wide applications, and due to different acting slip and twinning systems, which can be activated by different deformation types, used in this work.

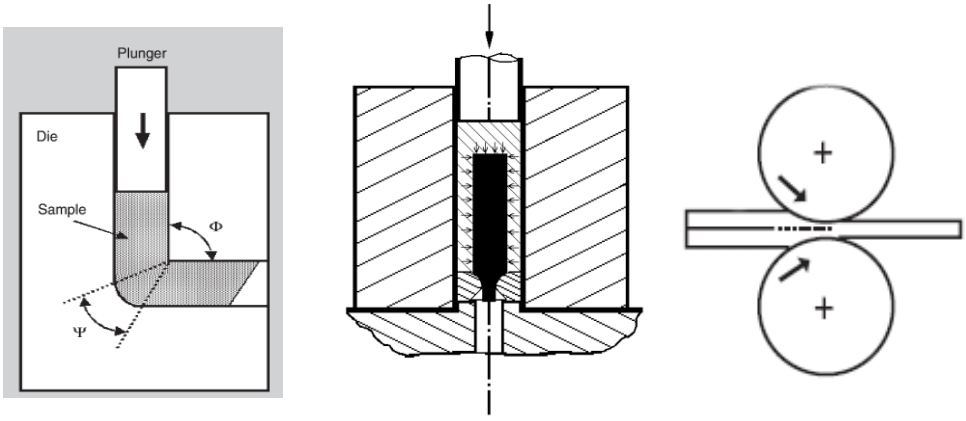

a b c

Fig. 1. Types of the severe plastic deformation used in this work: a) Equal channel angular pressing (ECAP); b) Quasihydroextrusion (QHE), working substance – metallic indium; c) Cryorolling (CR) in liquid nitrogen (77 K).

Materials and methods

The polycrystalline rods of Ti Grade 2, produced by hot forging, with average grain size of 20 μm were used as the initial material (**state 1**). Content of main impurities (in wt. %): O – 0.25; N – 0.03; C – 0.08.

From this material by combination of different types of the severe plastic deformation, which are schematically shown in Fig. 1 and described in [1, 2, 12], were produced seven different structural states (states 2-8).

State 2 was produced by 8 ECAP passes at 720 K.

States 3 and 4 were produced by QHE at 300 K by strain e ~ 32% (state 3) and e ~ 55% (state 4).

States 5 and 6 were produced by QHE at 77 K by strain e ~ 38% (state 5) and e ~ 52% (state 6).

State 7 was produced by consequent application of ECAP (8 passes at 720 K) and QHE (e ~ 57 % at 77 K).

State 8 was produced by consequent application of ECAP (8 passes at 720 K) and rolling at 77 K to 50 %.

Vickers microhardness was measured by PMT-3 instrument with load of 100 g and time 10 s. Mechanical tests were carried out in uniaxial compression with initial strain rate $4 \cdot 10^{-4}$ s^{-1} at cylindrical samples of 6 mm length and 3 mm diameter at deformation machine MRK-3 (stiffness $7 \cdot 10^6$ N/m) at temperatures 300, 77 and 4.2 K. During compression deformation the yield strength, ultimate strength and corresponding ultimate strain were registered. Measurements of the grain sizes were realized by electron microscope JEM-100CX II.

Experimental results

The average grain sizes and values of yield strength of the Ti Grade 2 samples in uniaxial compression of different structural states at the three temperatures are shown in Table 1. It should be noted that in state 8 after rolling the plate width was 1 mm, which is not sufficient for compression test and it was not carried out for this state.

Analysis of the experimental data listed in Table 1 shows the significant dependence of $\sigma_{0.2}$ and d on different SPD parameters: its type, value and temperature. It is turned out that minimal average grain sizes and maximal values of the yield strength for all studied temperatures were observed for state 7, which was produced by subsequent application of the mutually complementary modes of the severe plastic deformation:

Table 1.

Average grain sizes d and yield strength $\sigma_{0.2}$ in compression of Ti Grade 2 at temperatures 300, 77 and 4.2 K for the different structural states.

Temperature, K	Yield Strength $\sigma_{0.2}$, GPa						
	1.Initial, d≈20 μm	2.ECAP (8 passes at 720 K) d≈0.4 μm	3. QHE, (300 K, 32 %), d≈2 μm	4. QHE, (300 K, 55 %), d≈1.5 μm	5. QHE, (77 K, 38 %), d≈0.5 μm	6. QHE, (77 K, 52 %), d≈0.4 μm	7. ECAP, (8 passes at 720 K+ QHE, 77 K, 57 %), d≈0.1 μm
300	0.42	0.64	0.52	0.60	0.63	0.73	0.86
77	0.67	1.05	0.82	0.89	0.86	1.00	1.22
4.2	0.74	1.22		0.99			1.38

simple shear (ECAP, 8 passes at 720 K) and axisymmetric deformation (carried out by QHE at 77 K to 57 %). For this structural state the typical stress – strain curves in uniaxial compression at temperatures 300, 77 and 4.2 K are shown in Fig. 2.

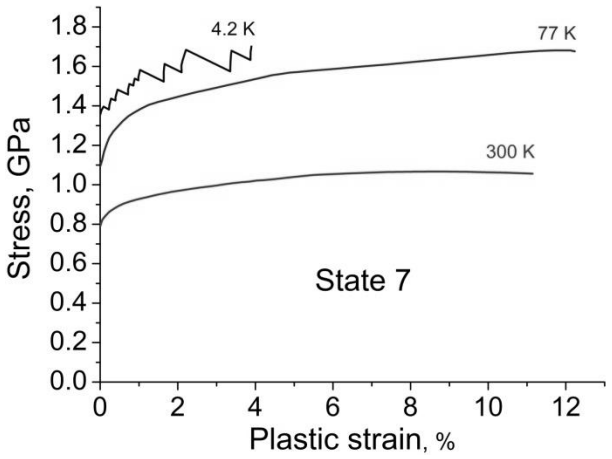

Fig. 2. Typical stress-strain curves in compression of Ti Grade 2 in state 7 for temperatures 300, 77 and 4.2 K

It can be seen from Fig. 2 that the smooth type of plastic deformation is changed by serrated, jump-like deformation at temperature 4.2 K. Such changes of the stress-strain curve type during transition to the liquid helium temperatures are typical [18] for deformation of titanium in this temperature range.

Yield strength values for different structural states of Ti Grade 2 in the forms of diagrams (for temperatures 300, 77 and 4.2 K correspondently) are shown in Fig 3 (a-c).

In Fig. 4 the microhardness values can be seen of Ti Grade 2 for different structural states, measured at 300 K.

It can be seen from Fig. 3 and 4 that values of microhardness and yield strength for the different studied structural states are in good correlation. And the maximal values of microhardness and yield strength at 300 K were observed for the state 7, produced by the consequent application of the mutually complimentary modes of the severe plastic deformation: simple shear (ECAP, 8 passes at 720 K) and axisymmetrical deformation, realized by QHE at 77 K to 57 %.

In Fig. 5 the typical microstructures are shown for the two structural states: state 2 (after ECAP) (a) and state 7 (after ECAP + QHE at 77 K) (b).

As follows from Fig. 5 a, the structure with grain sizes of ~ 0.4 μm is formed in the result of ECAP. Azimuth blurring of reflexes, observed in the diffraction pattern (insert to Fig. 5a), is caused by stresses from defects both inside the grains and at grain boundaries. Typical

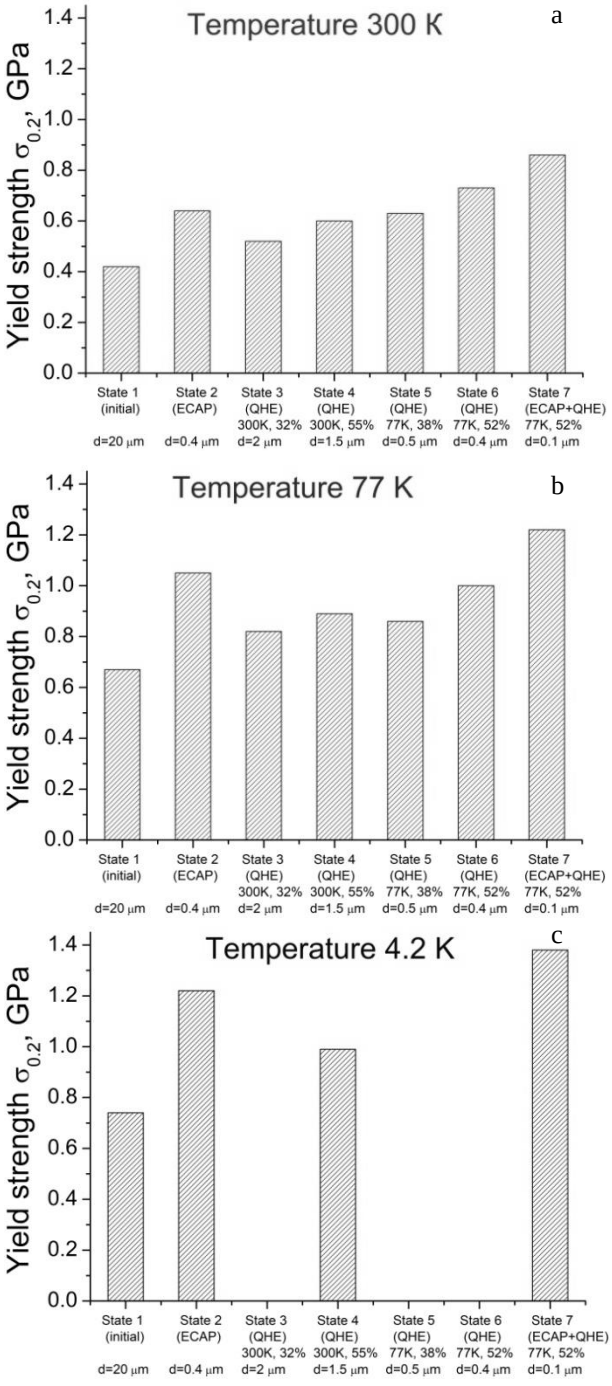

Fig. 3. Yield strength in compression of the Ti Grade 2 in different structural states at temperatures 300 K (a), 77 K (b), 4.2 K (c).

microstructure of the state 7 (ECAP + QHE at 77 K) indicates the significant grain refinement (Fig. 5 b) down to ~ 0.1 μm. Diffraction pattern in this case (insert to Fig 5b) has specific circular dot pattern, typical for the unltrafine grained structure.

Discussion of results

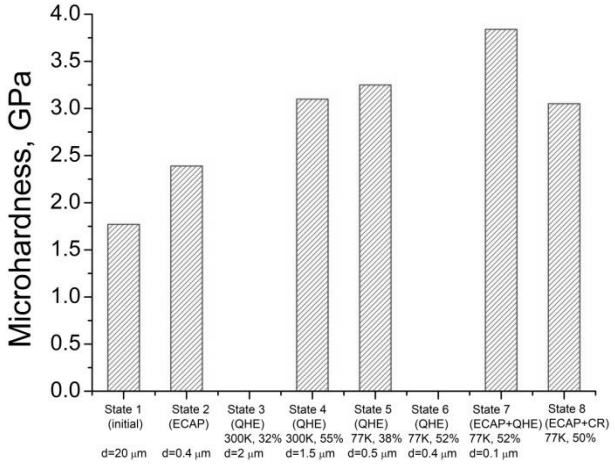

Fig. 4. Vickers microhardness at 300 K of the Ti Grade 2 in different structural states

It is known that the processes of mechanical treatment of metals can be described by combinations of different modes of plastic deformation, such as axisymmetrical deformation, simple and pure shear [1, 10, 19-23] etc. In this work the set of plastic deformation modes was realized by the consequent application of different deformation methods – ECAP, rolling and QHE.

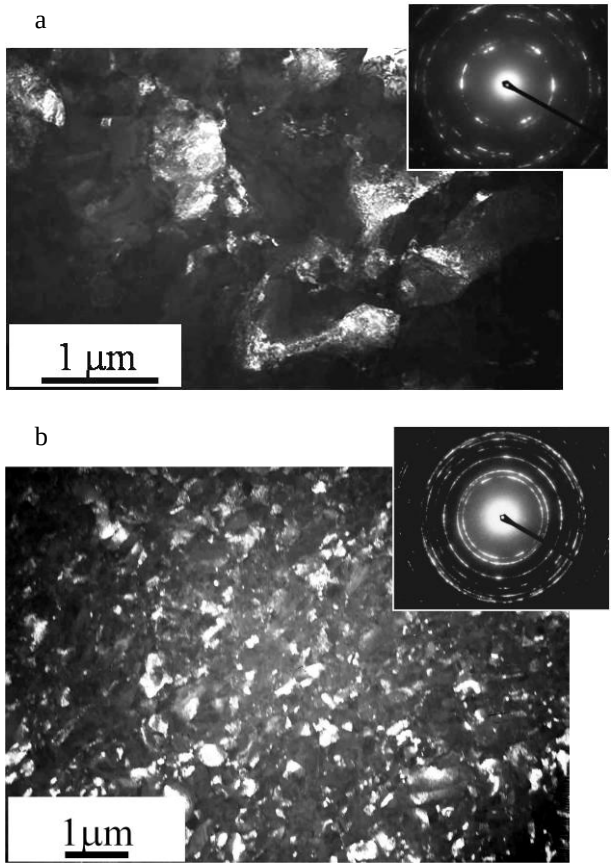

Fig. 5. Typical dark field transmission electron microscopy images and correspondent diffraction patterns of the Ti Grade 2 structure: state 2 (after ECAP) (a); state 7 (ECAP + QHE at 77 K) (b).

It is reasonable that the consequent application of these deformation methods should provide the activation of maximal quantity of the slip systems [2], i.e. maximal accumulation of deformation in the material, maximal grain refinement and obtaining the high yield strength values. The experimental results of this work confirm these suggestions and indicate the influence of the SPD temperature on the measured parameters. It is seen from the Table 1 that combination of ECAP (simple shear deformation) and QHE (axisymmetrical deformation), i.e. use of mutually complimentary deformation modes of SPD, significantly increase the influence of SPD on the microstructure and mechanical properties. So, in this case (Table 1, state 7) grain size values are decreased in comparison with the initial state from 20 μm down to d = 0.1 μm, and $\sigma_{0.2}$ values at 300 K increased in two times – from 0.42 GPa to 0.86 GPa (Table 1, states 1 and 7).

The consequent action of other deformation types: ECAP + rolling (state 8) (i.e. simple and pure shear) also significantly (almost at ~ 20%) increased the microhardness value (Fig. 4).

The case of QHE can be used to consider the influence of the SPD temperature on the values d and $\sigma_{0.2}$. It is seen (Table 1, states 4 and 6) that decrease of QHE temperature from 300 down to 77 K leads to decrease of d in 4 times (from 2 μm down to 0.5 μm), while the $\sigma_{0.2}$ increases at 20 %.

More strong grain refinement at lower temperature of SPD is realized due to decreas e of the dynamic recovery processes, which are caused by thermally activated cross slip or climbing of dislocations. Moreover, as follow from [1], increase of grain boundary mobility with decrease of SPD temperature influences on the grain refinement. Physical mechanism of such increase of the grain boundary mobility during SPD at cryogenic temperatures is not clear yet [1]. The authors of [1] suggested, based on the results of molecular dynamic simulation [24, 25] that at cryogenic temperature at conditions of active loading, the structure of the boundaries is heavily disordered. In the result, the grain boundaries are in nonequilibrium state, which can lead to increase of the diffusion coefficients and to accelerated grain boundary migration [25]. However, this suggestion needs additional confirmation, as the question about the activation energy, required for grain boundary diffusion at cryogenic temperatures [1] is not clarified yet.

One of the possible hypothesis, explaining the origin of the high mobility of grain boundaries at cryogenic temperatures, consists in counting of difference in coefficients of the thermal expansion of the grain boundary area and the grain interior: coefficient of the thermal expansion of the grain boundary area in several

times larger in comparison with the coefficient of the grain interior [25, 26]. According to the Gruneisen relation [27], it leads to the increased isothermal compressibility of the grain boundary area, which was experimentally found for nanocrystalline iron [28] and nanocrystalline nickel [29]. Difference in the coefficients of thermal expansion of the grain boundary area and of the grain interior during the cooling below 300 K, should lead to the uniform compression of the grain boundary area and to increase of atomic volume in the grain boundary area [29]. This effect simplifies the diffusional mobility of atoms and decreases the resistance to the grain boundary sliding at cryogenic temperatures, which can explain the high mobility of the grain boundaries in these conditions. It is obvious, that these peculiarities can amplify the processes of grain refinement at cryogenic temperatures.

Conclusions

1. The concept is suggested of influence of the mutually complementary modes of plastic deformation, which are characterized by different sets of acting slip systems, on the microstructure and mechanical properties of Ti Grade 2.

2. The combination of the SPD methods is found, which leads the polycrystalline Ti Grade 2 to the nanostructured state with the minimal average grain size and with the maximal values of the yield strength. So, by consecutive use of simple shear (during ECAP) and axisymmetrical deformation (during QHE at 77 K) the decrease of average grain sizes is registered from 20 μm in initial state down to 0.1 μm, which accompanied by increase in two times of the yield strength values (from 0.42 GPa to 0.86 GPa).

3. Use of the cryodeformation during QHE allows to slow down the dynamic recovery. In the result, after QHE at 77 K, the resulted average grain size (0.5 μm) is in 4 times smaller, than after QHE at 300 K (2 μm), and the yield strength after QHE at 77 K increases at 20 %.

4. The explanation is suggested of the mobility increase of grain boundaries at cryogenic temperatures, which simplify of process of grain refinement.

References

1. R.Z Valiev, I.V Aleksandrov. Nanostrukturnye materialy, poluchennye intensivnoj plasticheskoj deformaciej, Logos, M. (2000), 272 p.
2. E.G. Pashinskaja. Fiziko-mehanicheskie osnovy izmel'chenija struktury pri kombinirovannoj plasticheskoj deformacii, Doneck: izd-vo «Veber», (2009), 352 p .
3. Y. Huang, P.B. Prangnell. Acta Materialia, 56, 7, 1619 (2008).
4. V. V. Stolyarov, Ya. E. Beigel'zimer, D. V. Orlov, R. Z. Valiev. The Physics of Metals and Metallography, 99, 2, 204 (2005).
5. S. Zherebtsov, M. Ozerov, N. Stepanov, M. Klimova 1 and Y.Ivanisenko. Metals,7, 507, (2017).
6. M. Greger, V. Masek.AMME, 18, 1, 103 (2006).
7. A.V.Makarov,N.A.Pozdeeva, R.A.Savray,A.S.Jurovskih,I.Y.Maligina. Izvestia Samarskogo Nauchnogo Zentra RAN, 13,4, 800 (2011).
8. A.V.Makarov, P.A.Skorinina,E.G. Volkova, A.L Osinzova.Vektor Nauki TGU 4,38, 12 (2016).
9. M.A. Tikhonovsky, I.F. Kislyak, O.I. Volchok and etc. Fizika ana Tehnika Visokih Davlenii, 99, 2, 105 (2008).
10. V.M.Segal,V.I.Reznikov,V.I.Kopilov, D.A.Pavlik,V.F.Malishev " Prozessi plastichesko go strukturoobrazovania metallov, Minsk: Nauka and Tecknika, (1994), 232 p.
11. V.A. Beloshenko, A.N. Pilipenko, V.V. Chishko. Obrabotka metallov davleniem, 1, 44 , 56 (2017).
12. P. A. Khaimovich. Low Temperature Physics, 44, 5, 349 (2018).
13. I.F. Kislyak, K.V. Kutniy, V.S. Okovit, M.A. Tikhonovsky, P.A. Khaimovich, I.V. Kolodiy, A.S. Kalchenko. PAS, 1562, 109 (2018).
14. M.A. Tikhonovsky, P. A. Khaimovich, K.V.Kutniy, I.F. Kislyak, V.S. Okovit, T.U. Rudcheva, Low Temperature Physics, 39, 11, 1261 (2013).
15. E.D. Tabachnikova, V.Z. Bengus, A.V. Podolskiy, S.N. Smirnov, V.D. Natsik, K. Csach, J. Miskuf, D.V. Gunderov, R.Z Valiev., Rev. on Adv/ Materials Science,10, 3, 229 (2005).
16. V.Z. Bengus, S.N. Smirnov, E.D. Tabachnikova, V.V. Romanchenko, S.N. Khomenko, D.V. Gunderov, V.V. Stolyarov, R.Z. Valiev. Materials Science Forum, 503, 55 (2006).
17. E.D. Tabachnikova, V.Z. Bengus, A.V. Podolskiy, S.N. Smirnov, D.V. Gunderov, R.Z. Valiev. Materials Science Forum, 503, 633 (2006).
18. V.V.Pustovalov. Low Temp. Phys. 26, 375 (2000).
19. Ya. D. Starodubov, P. A. Khaimovich, Problemi Prochnosti, 10, 116 (1975).
20. I.A. Gindin, Ya. D. Starodubov, V.K. Aksenov,UFZ. 19, 1834 (1974).
21. Ya.B. Fridman. Mechanical properties of metals, Oboronizdat, (1952) 246 p.
22. RAC Slater. Engineering plasticity: theory and application to metal forming processes, London. M (1977) ,105 p.
23. U.F. Kocks, C.N. Tome., H-R. Wenk Texture and anisotropy, Cambridge University Press, (2000), 108 p.
24. H. Fu, D.J. Benson, M.A. Meyers, Acta Mater, 49, 2567 (2001).
25. A. Hasnaoui, H. Van Swygenhoven, P.M. Derlet, Acta Mater, 50, 3927 (2002).
26. H. J. Klam, H. Hahn, H. Gleiter, Acta Met., 35, 8, 2101 (1987) .
27. E. Gruneisen. Handbuch der Physik, 10,1 (1926).
28. S. Trapp, C.T. Limbach, U. Gonser, S.J. Campbell, H. Gleiter, Phys. Rev. Lett. 75,3760 (1995) .
29. S.J. Zhao, K. Albe, H. Hahn. Scripta Mater. 55, 473 (2006).

Вісник ХНУ, серія «Фізика», вип. 28, 2018. с. 68-72

PACS: 74. 72. –h
UDC: 538.945

The crystal-chemical structure and "high-temperature" superconductivity (HTSC) of multi-component metal – oxide compounds

Yu.I. Boyko[1], V.V. Bogdanov[1], R.V. Vovk[1]

1 V. Karazin Kharkov National University, 4 Svobody Sq., 61022 Kharkiv, Ukraine,

ORCID: *0000-0003-2634-3549*

DOI: 10.26565/2222-5617-2018-28-07

An analysis of the crystal structure of high-temperature superconductors of the $YBa_2Cu_3O_{7-x}$ type is provided and the reasons for the formation of specific chemical bonds between different ions leading to the formation of negative U-centers clusters in this compound is discussed. Experimental facts are also discussed, which indicate a close relationship between the crystal-chemical structure of metal-oxide compounds and their anomalous electric conductivity.

On the basis of the analysis, the conditions for the selection of elements for the synthesis of compounds characterized by a higher temperature of transition to the superconducting state are formulated.

Keywords: high-temperature superconductors, structure, negative U-centers.

В роботі проведено аналіз кристалічної структури високотемпературних надпровідників типу $YBa_2Cu_3O_{7-x}$ і обговорені причини формування специфічних хімічних зв'язків між різними іонами, що призводять до утворення кластерів з негативних U-центрів в цієї сполуці. Обговорено також експериментальні факти, що свідчать про тісний взаємозв'язок кристалохімічної структури метал–оксидних сполук з їхньою аномальною електричною провідністю.

На підставі проведеного аналізу сформульовані умови вибору елементів для синтезу сполук, що характеризуються більш високою температурою переходу до надпровідного стану.

Ключові слова: високотемпературні надпровідники, структура, негативні U-центри.

We dedicate our work to the memory of the outstanding scientist and teacher Yakov Yevseevich Geguzin in connection with the 100th anniversary of his birth. The authors remember with great warmth the years of close cooperation with Ya. E., note his great enthusiasm, benevolence, and also thank for the many tips that contributed to the emergence of new ideas and publications, including this article.

Introduction

The discovery in 1986 – 1987 of the "high-temperature" superconductivity (HTSC) of multi-component metal-oxide compounds (anomalous electrical conductivity in the range of temperatures exceeding the boiling point of liquid nitrogen 77 K) aroused great interest in the study of the properties of this class of materials [1, 2]. These materials include a number of compounds which can be described by the general chemical formula, $RBa_2Cu_3O_{7-x}$, were R = Y, Nd, Sm, Eu, Gd, Dy, Ho, Tm, Yb, Lu. Among them the $YBa_2Cu_3O_{7-x}$ compound was most thoroughly and comprehensively studied. The temperature of transition to the superconducting state of this compound is $T_c \approx 90$ K, which is an order of magnitude higher than the T_c of metallic superconductors. In addition to the above-mentioned compounds, the group of metal-oxide high-temperature superconductors also includes compounds $Bi_2Sr_2Ca_2Cu_3O_{10-x}$ and $Tl_2Ba_2Ca_2Cu_3O_{10-x}$, characterized by the maximum transition temperature observed up to the present time: T_c = 110 и 125 K respectively.

The most important task of researches which are carried out after discovery of high-temperature superconductors, is searching for new compounds which have a superconductivity at even higher temperatures, up to room ones (≈ 300 K). However, to date, this problem has not been solved, and the main cause of failure of many attempts to obtain such a compound, is the lack of understanding of the mechanism of unique microscopic electric conduction of HTSC oxides. An attempt to explain this phenomenon using the BCS theory ("Phonon" pairing of electrons, which causes low-temperature superconductivity of simple metals and their alloys [3]), was unacceptable. This conclusion was made after publication of the so-called "isotope effect" study results [4]. In this study in the $YBa_2Cu_3O_{7-x}$ compound 75% of ^{16}O oxygen ions were replaced by ^{17}O ions of the "heavy" oxygen isotope. Such a substitution significantly affected the phonon spectrum of the crystal, however, it did not lead to a noticeable change in the transition temperature T_c. In this case, a detailed study of the nature of elementary charge carriers in $YBa_2Cu_3O_{7-x}$ showed that

superconductivity in this compound is realized by paired electrons, as in the case of "low-temperature" superconductivity of metals.

Thus, the physical nature of the mechanism that determines the pairing of electrons, as well as the reason for the stability of these pairs up to a temperature of ≈ 100 K, remain unconfirmed until now. A large number of different models were proposed to answer the above questions. In particular, the possible role of electronic excitations was discussed: plasmons, excitons, spin fluctuations etc. in the process of formation of coupled charge carriers [5, 6]. In addition, the possibility of electron pairing was also associated with formation of specific structures – the so-called "superlattices", characterized by a parameter that is much higher than the lattice parameters of the main substance [7, 8]. However, none of the above models was confirmed by an adequate experiment, which clearly demonstrates in its favor.

In this respect, the most reasonable and consistent with a large number of experimental evidence is a concept proposed by the authors [9, 10]. According to the idea developed in these papers, the pairing of electrons in high-temperature superconductors is due to the formation in them of special elements of the structure – clusters consisting of a set of "negative U-centers". Upon reaching a certain size and number of clusters a special energy spectrum of electrons is formed, allowing two-electron transitions from oxygen ions to neighboring pairs of copper ions, which ultimately determines the superconductivity of metal-oxide compounds.

In the work we propose, using the $YBa_2Cu_3O_{7-x}$ compound as an example, we analyze the crystal structure and discuss the reasons for the formation of specific chemical bonds between different ions, leading to the formation of negative U-centers clusters in this substance. Experimental facts are also discussed, which indicate a close relationship between the crystal-chemical structure of metal-oxide compounds and their anomalous electric conductivity.

The results of this work can be used in further studies to find ways of obtaining new compounds, having electrical superconductivity at temperatures much higher than the boiling point of liquid nitrogen, up to room temperature.

Analysis of crystal-chemical structure of metal-oxide compounds on the example of compound $YBa_2Cu_3O_{7-x}$

From the position of crystal-chemistry multi-component metallic oxide $YBa_2Cu_3O_{7-x}$ belong to complex isodesmic substances with an ion-covalent bond type [11]. In this compound the oxygen ion O (anion) forms chemical bonds with three different metal ions – Y, Ba, Cu (cations). A peculiarity of the structures of this type is the following: while the metal ions are necessarily only bound to oxygen, each oxygen ion is bound to three different cations.

To achieve a stable (thermodynamically equilibrium) structure of this compound, the electric charge of the anion must be locally neutralized. To fulfill this condition, it is necessary that the sum of the electrostatic valencies of the individual anion bonds with all cations should be equal to the value of its negative charge. In turn, the electrostatic valence of each cation is determined by its charge, reduced by a factor of n, where n is the coordination number (the number of ions surrounding the cation). In accordance with this, when forming an isodesmic structure, the number of ions around each cation should always exceed its individual valence. The presence of three different cations and of one anion in $YBa_2Cu_3O_{7-x}$ and the requirement of the stability of this compound cause the formation of a specific "perovksite-like" crystal structure defective in oxygen [11]. In this case, the actual value of the charges of all ions and their exact distribution in the forming crystal lattice is a secondary factor. The requirement of fulfilling the electrical neutrality condition of the compound leads to the situation that some of ions can change their valency, and some of them may be absent, breaking the stoichiometry of the compound, however, while maintaining the necessary correspondence between the electric charges.

The specified features of the $YBa_2Cu_3O_{7-x}$ crystal-chemical structure formation leads to the fact that its crystal lattice in the absence of a deficit in oxygen, i.e. with the value of the parameter $x \approx 0$, is characterized by a specific mutual arrangement of ions, which from the point of view of crystallography is described by an orthorhombic unit cell (Fig. la). A distinctive feature of this cell is that it is layered and contains two configurations of the oxygen surroundings by copper ions: tetrahedral pyramid in planes CuO_2 and a rhombus in the form of chains CuO in the basal plane (ab) [12]. In this case, the Cu ions in the basal plane neighbor with the O ions only along the axis (b), and along the (a) axis in this plane there are no O ions at all, which in turn determines the orthorhombic symmetry of the forming elementary crystal cell. The Cu ions located along the (c) axis in the space between the planes of the Ba and Y ions are surrounded by five O ions, forming the planes CuO_2.

With decrease in the oxygen content, i. e. with increase in the parameter $x > 0$, oxygen vacancies arise mainly in the basal plane, since the CuO chains are characterized by the minimum energy of the chemical

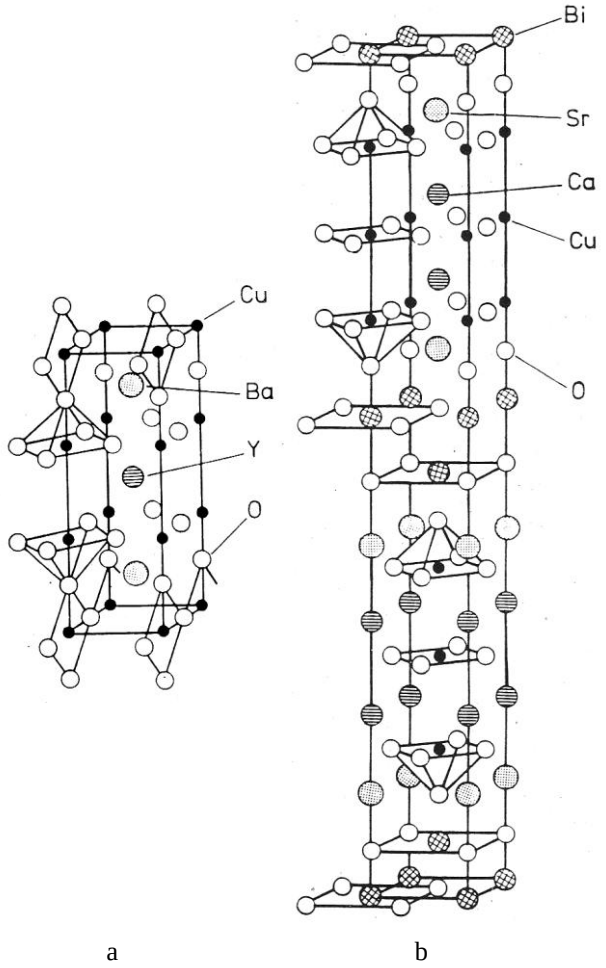

Fig. 1. Crystal structures of elementary cells of HTSC metal-oxide compounds: a) $YBa_2Cu_3O_7$, b) $Bi_2Sr_2Ca_2\ Cu_3O_{10}$.

bond. When the value of $x \approx 0{,}5$ is reached, the O ions and oxygen vacancies approximately in the same proportion are distributed along the axes (a) and (b) in the (ab) plane, and at $x \approx 1$ the basal plane remains without O ions at all, which leads to the transformation of orthorhombic lattice into tetragonal one. The formation of such a specific crystal-chemical structure, the presence of different configurations of Cu and O ions, as well as the phase transformation in the $YBa_2Cu_3O_{7-x}$ compound are experimentally confirmed in many works and, in particular, in the works [13, 14].

It should be noted that the crystal-chemical state and electrical conductivity of this substance are closely interrelated and depend significantly on the concentration of oxygen ions in it, that is, on the value of the parameter x. With a large deficit of oxygen ions ($x > 0{,}5$), when the tetragonal crystal structure is realized, the superconductivity does not occur. As the oxygen concentration increases and when the value of the parameter $x \approx 0{,}4$ the phase transformation is observed: the tetragonal crystal cell turns into orthorhombic one. Simultaneously with the phase transformation in the $YBa_2Cu_3O_{7-x}$ compound the superconductivity is appears at temperature $T_c \approx 50$ K, and when $x \approx 0$ the superconducting state is realized at the maximum value of the transition temperature for this compound $T_c \approx 90$ K (see Fig. 2).

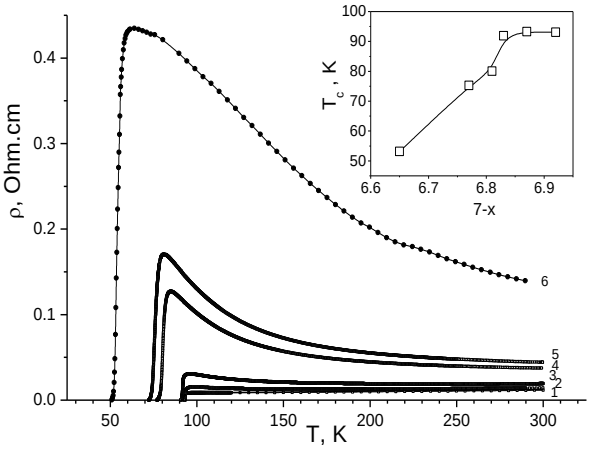

Fig. 2. The dependence of electric resistance of the $YBa_2Cu_3O_{7-x}$ compound on temperature with variation of the parameter x: 1 – 0,08; 2 – 0,13; 3 – 0,17; 4 – 0,2; 5 – 0,23; 6 – 0,35 [16]. The inset shows the dependence of the transition temperature T_c on the parameter x. The same type of dependencies were obtained in [17].

Thus, based on the above analysis, it can be concluded that it is the specific crystal-chemical structure that is the determining factor which causes the anomalous electrical conductivity of the poly-component metal-oxide compounds. More concretely this correlation is discussed in the next section of the paper.

Crystal-chemical structure of the $YBa_2Cu_3O_{7-x}$ compound and the appearance of paired carriers of electric charge

As it already mentioned, according to the concept proposed in the works [8, 9], the main elements of the structure responsible for the generation of electron pairs,

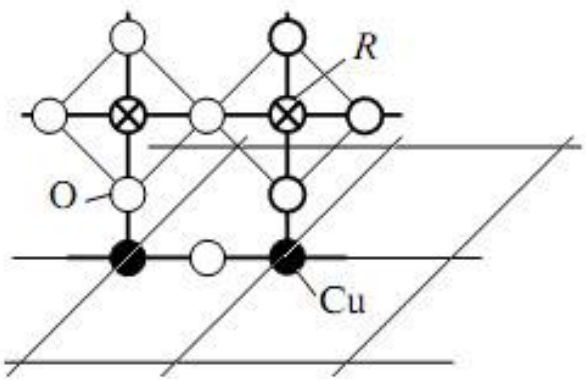

Fig. 3. The scheme of the negative U-center in the $YBa_2Cu_3O_{7-x}$ compound [10].

which cause the anomalous conductivity of metal-oxide compounds, are the clusters formed from negative U-centers. Each separate U-center consists of two neighboring Cu cations embedded in the CuO_2 plane and of their surrounding O ions (Fig. 3).

The existence of such a configuration of Cu and O ions in the $YBa_2Cu_3O_{7-x}$ compound was confirmed in the works [13, 14]. In these studies by the X-ray spectroscopy and by the internal friction methods was found that copper and oxygen ions take part in the formation of specific chemical bonds characterized by different ion valencies. This result provides the additional evidence of the negative U-centers formation in the $YBa_2Cu_3O_{7-x}$ compound.

The U-centers clusters formation causes the appearance in the electrons energy spectrum of a level that allows a local pair transition from an oxygen ion to two neighboring copper ions (Fig. 4) [9]. In this case, separate (not connected to clusters) U-centers cause some "excess" insignificant electric conductivity at temperature $T^* >> T_c$ (this is a so-called fluctuation superconductivity). The deviation from the "normal" conductivity at the temperature T* is a "messenger" of the transition to the superconducting state, and the temperature T* was called the temperature of opening of the "pseudo-gap". In fact, at this temperature the first pair charge carriers appear.

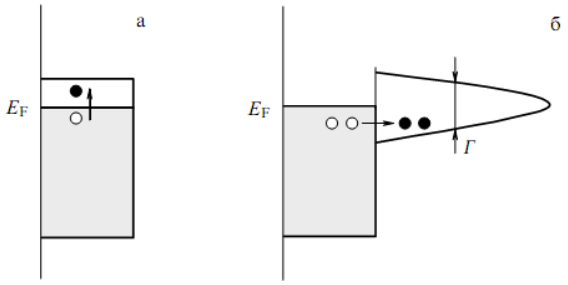

Fig. 4. The scheme of the band structure of the energy spectrum of a) ordinary metal, b) HTSC metal-oxide compound [10]. • – electron; ○ – hole; Γ – the width of the energy level for a pair of electrons

The minimum cluster size that determines the possibility of the pair transition of electrons is determined by the coherence length in the CuO_2 plane and equal ≈ 10 Å. As the concentration of oxygen ions in the metal-oxide increases, that is when $x \to 0$, the average size of the clusters increases, and the temperature T* gradually go up (Fig. 5) [9].

An important experimental fact, which also give evidence to the favor of the above scheme, is the result of the work [15], in which the process of size increasing of U-centers clusters was activated (accelerated) by applying of external hydrostatic pressure $p \approx 7$ GPa. As it was shown in this study, in $YBa_2Cu_3O_{7-x}$ compound samples with not complete stoichiometry ($x \approx 0{,}4$) the pressure intensifies the process of cluster size growth due to their (clusters) diffusion coalescence. The coalescence process is realized as a result of the redistribution of oxygen ions and of decrease in the vacancy concentration in the anion sublattice, which is accompanied by decrease in the parameter $x \to 0$. In accordance with the above described scheme, this process should be accompanied by increase of temperature T_c, approaching it to the maximum value ≈ 90 K, as it was observed in the experiment.

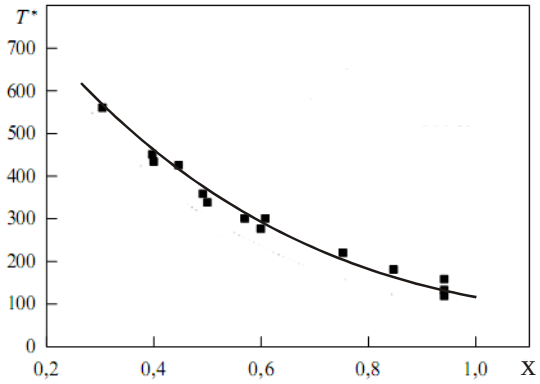

Fig. 5. The dependence of the "pseudogap" opening temperature T* in the $YBa_2Cu_3O_{7-x}$ compound on the parameter x [10].

In addition to the above information, attention should be paid to the following important fact. As mentioned, the $Bi_2Sr_2Ca_2Cu_3O_{10-x}$ and the $Tl_2Ba_2Ca_2Cu_3O_{10-x}$ compounds also refer to metal-oxide superconducting substances. They are characterized by the maximum superconducting transition temperatures recorded to date: $T_c \approx 110$ and ≈ 125 K respectively. As the $YBa_2Cu_3O_{7-x}$ compound these oxides are also characterized by the rhombic crystalline cell and by the presence of several "perovksite-like" structural blocks containing planes CuO_2 (Fig. 1b). Besides, these compounds do not have CuO chains in the basal planes (ab), however, in their structure there are solitary copper-oxygen planes of CuO separated by Ca planes. This fact once again demonstrates the important role of the crystal structure in formation of pairs of charge carriers in the metal-oxide superconductors: the CuO_2 planes provide the formation of the negative U-centers which cause the appearance of the paired charge carriers. The presence of CuO planes provides anomalous conductivity by the paired electrons in all compounds discussed. At the same time it is the "sandwiching" of solitary CuO planes by the planes formed by additionally introducing ions (in this case of "bismuth-thallium" oxides by planes of Ca), increases to a certain limit the value of the superconducting transition temperature. Consequently, an increase in the number of solitary CuO planes with metallic conductivity is the

important factor for multi-component metal-oxide "high-temperature" superconductors, which promote in increasing T_c. The role of the other ions is actually reduced to maintain the required crystal structure.

Conclusions

Summarizing the above considerations, we can make the following conclusion.

There are no fundamental limitations on increase of the transition temperature T_c into the superconducting state when using multi-component metal-oxide "high-temperature" superconductors.

When choosing elements of a substance characterized by a higher temperature of transition to the superconducting state, it is necessary to have in mind the realization of the following conditions:

1) the material should have a crystal-isodesmic complex structure, characterized by the orthorhombic unit cell, containing as component elements perovksite-like blocks separated by planes that do not contain oxygen ions;

2) as the ions forming perovksite-like structural unit, in addition to the oxygen ion, it is necessary to use a metal ion which, on the one hand, should be characterized by a "normal" (metallic) electric conductivity, and on the other hand, it must actively react with oxygen and form chemical bonds of various configurations, that is, capable to change its valence state;

3) the metal ions specified in paragraph 2, together with oxygen ions, besides participation in the formation of blocks with a perovskite-like structure, must form either the basal planes (ab) or the solitary "conducting" planes parallel to the basal planes;

4) increase in the number of planes with metallic conductivity when additional ions (cations) are introduced along the axis (c) of the unit cell, promotes in increase the superconducting transition temperature T_c;

5) the metal-oxide compound having a "high-temperature" superconductivity with the maximum possible transition temperature T_c should be characterized by complete stoichiometry in oxygen.

References

1. J. G. Bednorz, K. A. Mueller, Z. Phys.,B64, p. 189, 1986.
2. M. K.Wu, J. R. Ashburn and all, Phys. Rev. Lett., v. 57,p. 908, 1987.
3. J. Bardeen, L. N. Cooper, J. R. Schrieffer, Phys. Rev.,v. 108, p. 1175, 1957.
4. B. Batlog, R. G. Cava and all, Phys. Rev. Lett., v. 58 p. 2333, 1987.
5. V. L. Ginzburg, E. G. Maksimov, Phys C, v. 235 – 240, p.193, 1994.
6. M. L. Cohen, S. A. Wolf, V. Z. Kresin, Novel Superconductivity, Plenum Press, London, p. 1095, 1987.
7. O. V. Abramov, O. M. Gradov, A. Yu. Kyrie, Physica Scripta, v. 46, p. 76, 1992.
8. O. V. Abramov, O. M. Gradov, A. Yu. Kyrie, Physica Scripta, v. 48, p. 620, 1993/
9. K. V. Mitsen. O. M. Ivanenko. ZhETF. t. 118. s. 666. 2000.
10. K. V. Mitsen. O. M. Ivanenko. UFN. T. 1744. № 5. s. 545. 2004.
11. R. Evans. Vvedeniye v kristallokhimiyu. 1948. s. 367.
12. K. Yvon, M. Francois, Z. Phys., v. 76, p. 413, 1989.
13. M. Weller, H. Jaeger, G. Kaiser, K. Schulze, Phys. C, v. 162, p. 953, 1989.
14. H. Jaeger, S. Hofman, G. Kaiser, G. Petzow, Phys. C, v.153, p. 133, 1988.
15. Yu. I. Boyko, V. V. Bogdanov, R. V. Vovk, G. Ya. Khadzhai, S. V. Savich, Low Temperature Physic, v. 44, № 1, p. 63, 2018.
16. R.V.Vovk. M.O.Obolenskiy. A.A.Zavgorodniy. O.V.Bondarenko. M.G.Revyakina. N.N.Chebotayev. Visnik Kharkivskogo universitetu. seriya fizichna. vip. 3 (31). № 744. 2006. s. 94-96.
17. G. Fuchs, A. Gladun and all, Journ. of the Less – Common Metals, v. 151, p.103, 1989.

Вісник ХНУ, серія «Фізика», вип. 28, 2018. с. 73-78

PACS: 47.20.-k, 64.75.+g, 82.65.-i
UDC: 530.1/539.8

Dissolution of a heavy liquid droplet deposited onto free surface of unlike liquid solvent

O.Yu. Zaitseva[1], K.A. Chishko[2]

1 Physical Department, Karazin National University, 4 Svobody Sq., Kharkiv, 61022, Ukraine
2 Theoretical Department, B. Verkin Institute for Low Temperature Physics and Engineering, 47, Prospect Nauky, 61103 Kharkiv, Ukraine
chishko@ilt.kharkov.ua

DOI: 10.26565/2222-5617-2018-28-08

Dissolution dynamics and kinetics of a heavy liquid droplet deposited onto the free surface (or inserted at a certain depth under the surface) of a massive liquid solvent have been studied experimentally. As the solvent are selected distilled water, as well as concentrated solutions of sugar or common salt. As the soluble media were chosen the colored substances of different types (aniline ink, Indian ink, medical solutions of brilliant greenery or iodine), which allowed us to observe and register on the camera all the evolution stages of the heterogeneous system (a colored drop spreading in a transparent solvent) within the convective mixing regime. If the temperature of the solvent is high enough (T>40^{o}C), the convective mode is not realized, and the droplet is almost immediately dissolved into the homogeneous solution, at a low temperature (in our case it is room temperature of 18-20 ^{o}C), the spreading configuration is very complicated: after deposition on the surface, the droplet spreads over it, then in the central part of the spot appear one or several vertical channels (the number of channels depend on the size and mass of the initial droplet, as well as the dynamics of surface spreading which is controlled by the surface tension), along which the solution penetrates into the interior of the solvent. When penetrating the solvent, the channels begin branching and forming secondary flows, and so on, until the bottom of the cell is reached by initial droplet material. If a liquid stream is introduced to the solvent under pressure (we use injection from a syringe needle), a single well defined vertical channel is formed, but its head at some depth undergoes reflection with the formation of backward flows and complex spreading patterns in the upper volume of the solvent.

Keywords: dissolution hydrodynamics and kinetics, solubility, convective regime.

Динаміка та кінетика розчинення краплі важкої рідини, вміщеної на вільну поверхню (або на певну глибину під цю поверхню). В якості розчинників вибрані дистильована вода а також концентровані розчини цукру або солі. У якості речовини, що розчиняється, обрані забарвлені субстанції різних типів (анілінове чорнило, креслярська туш, медичні розчини зеленки або йоду), і це дозволяє нам спостерігати та реєструвати на камеру усі стадії еволюції гетерогенної системи (забарвлена крапля розповсюджується у прозорому розчиннику) в межах конвективного режиму змішування. Якщо температура розчинника достатньо висока (T>40^{o}C), конвективна мода не реалізується, і крапля практично моментально переходить в однорідний розчин, натомість як при низький температурі (у нашому випадку це є кімнатна температура 18-20^{o}C) конфігурації розповсюдження зовнішньої краплі є досить складними: після нанесення на поверхню розчинника крапля розтікається вздовж поверхні, після чого у центрі поверхневої плями з'являються декілька вертикальних каналів (число каналів залежить від розміру та маси початкової краплі, а також від динаміки поверхневого розтікання, що контролюється поверхневим натягом), вздовж яких концентрований розчин починає стікати у тіло розчинника. Проникаючи у тіло розчинника, канали починають формувати вторинні потоки з новими каналами, і так далі, доки матеріал первинної краплі не досягне дна посудини. Якщо рідка речовина введена у розчинник під тиском (ми вводили речовину через голку медичного шприца), формується єдиний, добре визначений вертикальний канал, але на певній глибині він зазнає відбиття завдяки впливу граничних вимог та формує зворотній потік зі складними фігурами розтікання у верхніх шарах розчинника.

Ключові слова: гідродинаміка та кінетика розчинення, розчинність, конвективний режим.

Ця робота присвячена пам'яті професора Я.Є. Гегузіна.
This paper is written in memory of Professor Ya.E. Geguzin.

Introduction

Experimental studies of sintering mechanisms of dissimilar crystalline solids brought into contact on surfaces with different crystallographic indices and exposed at different temperature conditions have a highly significant place in the scientific heritage of Prof. Ya.E. Geguzin [1-4]. In fact, the case at hand is the mechanism of mutual dissolution of unlike solids, which occurs through a surface spreading of the components and mutual volume diffusion in the contact zone enriched by structure imperfections of the crystal lattice. In this sense, the process can be interpreted as a diffusion-dislocation flow (creep) of the contacting components, which in the promoted stages of the process can be described as mass exchange between two extremely viscous liquids. On a qualitative level, this phenomenon can also be considered as a spreading-dissolution of a foreign substance droplet deposited on the surface of a viscous liquid or a solid. Moreover, the dynamics of droplets was the subject of special interest of Ya.E. Geguzin, the droplet dynamics was a subject of special research described in his famous book [5].

In the present paper we study an analogous problem realized on a simple model of two dissimilar liquids, one of which has the form of an isolated colored droplet introduced onto a free surface of massive optically transparent liquid solvent. This setup allows us the direct real-time observation of the dissolution kinetics[1)]. Of course, the mutual solubility, the effective viscosity and the surface tension at the points of contact of the components in the present case turns out to be much smaller in comparison with similar parameters for solid crystalline systems, but the relaxation times in the liquid solution are acceptable in order to observe and real-time registering the evolution of the system in different regimes of the droplet penetration into the solvent.

Experimental results

Figure 1 shows the configuration of an aniline ink droplet within a few seconds after its dropping on the free surface of the solvent which is distilled water. The experiments were performed at room temperature. Just after deposition of the ink droplet to the water surface it begins spreading over the surface of the solvent under gravity forces and surface tension. As a result, from the spherical droplet a biconvex lens has been formed, with thickness decreases from the center to the edges. The spreading is due to the vertical pressure gradient within liquid droplet, which tends to flatten the droplet to minimize the pressure difference between the upper and the lower part of the lens, but complete flattening is impeded by the curvature of the edge contour of the lens in the cross-section, perpendicular to the water surface. The shape of the lens in its lower part (immersed in water) is maintained through balance of forces at the water-ink boundary. At a certain moment, this boundary loses its stability, and this breakdown occurs mainly in the central part of the lens, as can be seen in Figure 1. In this case, a thin vertical primary channel is formed, and the ink from the upper basin flows into bulk solvent, while it can be seen that a stream of unevenly "diluted" ink flows through the channel.

As the channel penetrates into the interior of the solvent, the pressure in the head of the channel $p = \rho g h$ increases (h is the coordinate of the head channel, measured from the surface of the solvent, and ρ is density of the solvent), and at a certain depth h_0 the channel advance will be blocked, after which begins the secondary spreading of ink coming through the channel from the upper pool. This secondary spreading occurs already near

Fig. 1: Spreading and dissolving a droplet of aniline ink deposited to the surface of distilled water.

the horizontal plane $h = h_0$, which leads to the formation of two (as in Figure 1) or several (as in our other experiments) new vertical channels. As can be seen from Fig. 1, the secondary channels have an irregular structure due to thermal and pressure fluctuation within the ink solution. In addition, it can be seen from Fig. 1 that in heads of secondary channels begin to form droplets, which after a while will become centers a new stage of spreading.

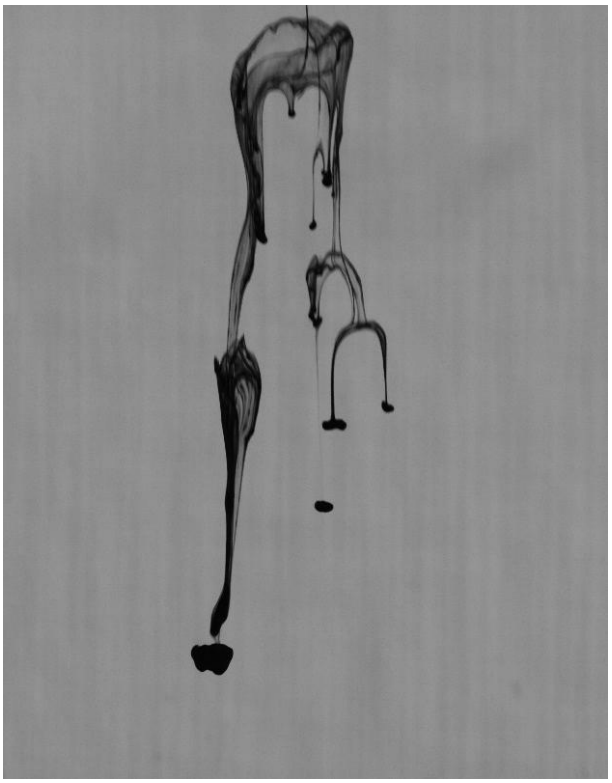

Fig. 2: Multistage spreading-dissolution of an aniline ink droplets penetrating beneath the surface of the solvent.

The multi-stage flow is illustrated in Figure 2, which shows how the run of a channel is stopped at a certain depth, and a new drop begins to form in the head of the stopped jet, which is similar to the formation of the drop at the end of the syringe needle, from which a viscous

[1)] This problem was announced in the Problem List of International Physicists Tournaments 2018 (MFTI, Dolgoprudny, Moscow region). Experimental results were obtained by O. Yu. Zaitseva and discussed in her report presented at the IPT 2018.

liquid is released. Thus, the development of a vertical channel can be regarded as the introduction of a viscous liquid under the surface of the solvent (special experiments of this kind were carried out by means of liquid injection from a syringe, the needle of which sank to a certain depth, but in view of the limited volume of the paper we do not discuss here the corresponding results). The droplet at the end of the stopped channel grows because the flow of liquid from the upper reservoir continues along the channel, and as a result, the secondary drop spreads underwater, with the formation of new secondary channels, The created substance penetrates deeper and deeper into the solvent until it reaches the bottom of the cell, after which the progress of the moving vertical channel stops.

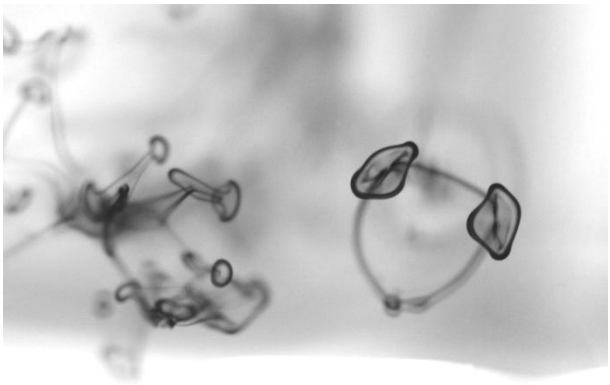

Fig. 3: Formation of ring structures when the drop is spreading under the surface of the solvent (top view to the surface solvent, the camera is focused on rings that are below the level of the primary subsurface spreading).

Extremely interesting is the process of the secondary spreading below the surface after the channel stop. The droplet formed in the head of the stopped channel continues to receive a dissolving substance, and from Figures 1 and 2 it is seen that the concentration of the colored liquid in the secondary droplets is higher than in associated channels, that is, the dissolved substance accumulates in the channel head, which leads to eventually secondary spreading. Figure 3 shows the configuration of the spreading subsurface droplets recorded by the camera on the side of the top of the solvent (the camera is focused so as to clearly record the process at the depth of secondary spreading). It can be seen that the secondary distribution of the flow occurs by forming rings unevenly filled with a solute, and already from these rings are nucleated the secondary channels through which the solution continues to flow down to the bottom of the vessel. The tendency to form ring structures during underwater spreading takes place because the droplet introduced at the determined depth is under a concentrated load from the upper column of solution, which crushes the drop from the center to the edges, and this process is restricted by the surface tension at the boundary between the droplet and the solvent. In the common sense, the droplet is profitable to accept the configuration of its outer surface in contact with the solvent, which would have as large as possible curvature with maintaining the maximal volume of the substance, for which it is difficult to form a homogeneous molecular solution with a concentration exceeding a certain thermodynamically equilibrate value of solubility (thermodynamically determined for the given temperature and pressure). In the thermodynamics of solutions, this effect is known as a limited solubility [7.8], which leads to the decay of both liquid and solid solutions where the concentration of components exceeds the limit of solubility. This process directly is associated with the mechanism of secondary phase nucleation during phase transitions of the first kind or the formation of precipitates upon the decomposition of solid mixtures. In our case, a subsurface droplet takes configuration of the torus (Figure 3), which allows to retain a significant amount of undissolved matter in a region restricted by a surface of large curvature. The curvature of the torus surface,

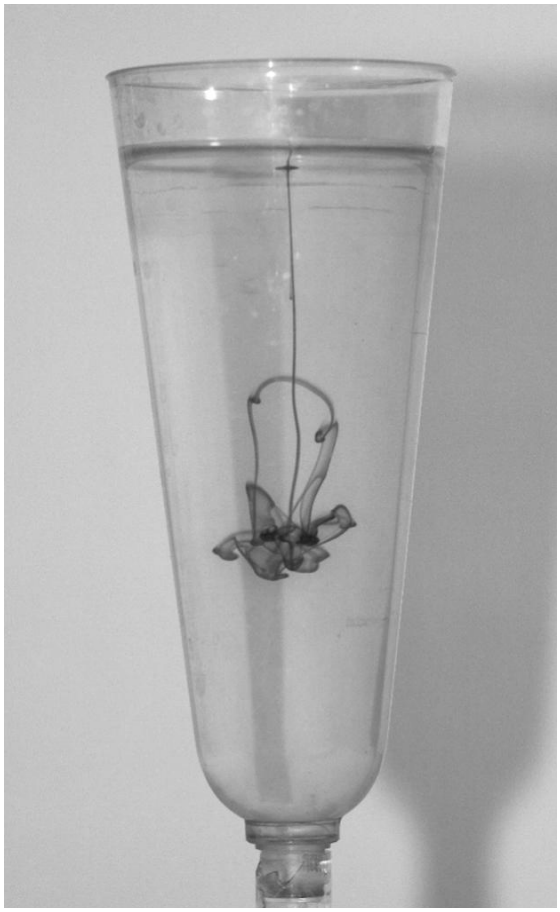

Fig. 4: Spillage outlet resulting from the introduction of a jet of ink at a high initial speed into the solvent.

however, can not be arbitrarily large, since the transition (evaporation) of precipitate molecules to the solvent is more simple from a curved surface, and this process is controlled by the equilibrium conditions with respect to pressures and chemical potentials on the boundary between the contacting phases. The shift of this equilibrium leads to a diffusive redistribution of the solution components between the contacting phases. In our case, the observed dissolution process is essentially nonequilibrate, under the determining control of the hydrodynamic (convective) regime in the gravitation field. Diffusion is activated at all stages of the process, but convective motions are predominant at the initial stage of dissolution at all temperatures of our experiments.

It can be seeing in the upper part of Figure 1, that there is a separation of the "tails" from the edge of the liquid spot on the solvent surface. This is a process of two-dimensional surface dissolution of precipitate which can be interpreted as surface diffusion of an external substance introduced into the solvent. Fluid penetrated into the solvent through channels, partially diffuses through the channel boundary, but it can be seen that the channels have very small diameter, which is the result of the same tendency to limit the distribution of concentric-bath solution with a large curvature surface to support the spatial stratification between liquid phases of different concentrations in a spatially inhomogeneous system.

And, finally, we present the result of another experiment (Figure 4), which refers to the jet of ink, put under the surface of the solvent from the syringe needle with high pressure and, therefore, with a high initial velocity. It is quite obvious that in this case we could expect the propagation of a well-defined flow of the injected liquid, because in this case the motion is purely hydrodynamic (diffusion characteristic times are large in comparison with the time of development of the hydrodynamic pattern). In principle, one would expect that a jet without essential destruction will reach the bottom of the vessel and, reflecting from its bottom will go in the opposite direction. However, as can be seen from Fig. 4, reflection occurs far from the bottom in the solvent, with the formation of secondary localized reflected jets, and with complicated scattering of the most part of the primary stream. It is important to note that the lower level of the reflection is strictly determined, and below this reflection boundary the solvent remains absolutely transparent. The reflection effect is due to the fact that the hydrodynamics of the primary jet stimulates the hydrodynamic motion of the entire system as a whole, and that is, the velocity field in the jet has been associated with the velocity field in the solvent by the boundary conditions on the boundary layer between the primary jet and bulk solvent (and the same reason holds true for the pressure field, as well as to the thermo-dynamic relations in a heterogeneous system). This means that the jet feels the presence of the boundary conditions on the walls and bottom of the vessel (in addition to everything, in our case the vessel has the shape of a cone, which, of course, complicates the problem) at each moment, and the normal components of the stream velocities at the bottom of the vessel are strictly equal to zero. Thus, the streamlines themselves are wrapped into the volume of the vessel. Reflection of the primary jet occurs then, when this jet enters the region of the reverse flow of the whole system, generated by the boundary conditions on the bottom of the vessel.

Discussion

The phenomenon studied in the present paper is a direct analog of the processes of mutual dissolution (mixing) of solids observed during the sintering in crystals brought into contact with their surfaces and placed in the conditions necessary for an active microscopic mass diffusion between these bodies (the diffusion is going both on the surface and in the volume of the crystals). In our case, the experiment is performed on dissimilar liquids, and therefore purely diffusive dissolution is complicated here by obvious hydrodynamic movements in a highly inhomogeneous liquid media. The macroscopic inhomogeneities are well-defined regions of the colored solution with evidently different concentrations of the components. In a sense, this picture resembles the evolution of decay in solid solutions. However, the solid solutions after disintegration are stable heterophase structure (that is, equilibrium at given temperature and pressure), while in our case of mixing liquids this "quasi-heterophase" structure remains metastable and evolves slowly to the state of a homogeneous solution. Of course, as the temperature increases, homogenization occurs faster, and in a solvent with a temperature above 50-60°C, the formation of the structures described above is impossible because the droplet introduced into the hot solvent decays immediately, and after one or two minutes, the state of a homogeneous solution is established. For this reason the experiments described above were performed on cold components (at temperatures of 10-20°C), and only in these conditions a steady reproduction of the pictures shown in Figures 1-4 is possible. Hydrodynamic regime of the initial stage of dissolution in liquid components with formation of channels can be associated qualitatively with the stage of active mass transfer in the developed diffusion zone of solids [4] , where the mutual diffusion

leads to appearance of internal stresses and formation of a large number of crystal lattice defects facilitating the diffusion transfer. Strictly speaking, a strongly distorted crystal is no longer to be interpreted as a proper crystal, but it can be regarded as a viscous continuum deformed within hydrodynamic regime.

The question, however, is of how the surface contact breakdown occurs with the formation of the primary stream that flows into the solvent inside a narrow channel. The reason for this phenomenon is that the substance of a heavy liquid droplet deposited on the surface begins to diffuse in the solvent immediately after its application to the surface, and traces from this diffusion can be seen in Fig. 1. In addition, in Fig. 1 we can see that from the edge of the surface spot some 'tails' are torn off, and the matter spreads along the surface of the solvent. Thus, this is a quite obvious analog of surface diffusion observed at sintering in solids [1-4]. In our case, a droplet of heavy liquid, deposited on the surface of the solvent, forms on this surface a hole, in the center of which the pressing on the surface will be higher than at the edges of the lens [5]. This results that at the center of the spot the drop-solvent boundary will be destroyed, and the ink begins flow into the bulk solvent simply in the form of a localized jet in the usual hydrodynamic regime. The dynamics of a flooded jet is considered, for example, in the book of Landau and Lifshitz [6], but there was investigated only the case when a thin jet of a viscous liquid under pressure is injected into the volume of a complementary liquid with the same density and viscosity.

In our case, the situation seems to be much more complicated, since of mixing the heterogeneous fluids, and therefore it is necessary to describe hydrodynamics of an inhomogeneous medium with regard to the kinetics of mutual dissolution of components with limited mutual solubility. The jet penetrated under the surface flows into the solvent under the gravity forces, and its shape has the form of a cylindrical channel. This shape is supported by surface tension forces on the ink-solvent interface, and also the strength of Archimedes prevents its penetration into the bulk of the solvent. In this case, the movement of the jet head becomes slower, and the leakage of ink from the upper reservoir results in the formation of a bubble at the tip of the stopped jet. The jet stopped at some depth, continuing to grow, but in the form of a secondary lens that grows at a certain depth, eventually forming rings (Figure 3) due to the deformation of the secondary bubbles in a vertical pressure gradient. The ring is a jet curled into a torus, which allows to minimize the influence of the vertical gradient on the unlike liquid bubble introduced into the solvent. The surface of the torus has two principal radii of curvature, essentially different in magnitude: this is, firstly, a large radius of curvature (small curvature) along the generator of the ring and, secondly, a small radius of curvature (large curvature) in the cross-section of the torus.

The curvature of the jet surface has a special significance in our case. On the one hand, under the curved surface on the jet acts the surface tension force, which helps to support its shape. On the other hand, from a curved surface an atom can be easily "evaporated" into the bulk solvent. Thermodynamics of this process is completely analogous to the coalescence of second-phase nuclei in dispersion-hardening alloys or coalescence of pores in crystals [1-4,7]. Thus, the flooding of a vertical jet is a complex process of propagation of a hydrodynamic flow, which at the same time dissolves in the volume of the solvent medium due to both diffusion and branching of the secondary flows. This process is a direct analogy of the formation of 'trees' in separated solid solutions with a small coordination number of the interaction in the mixture [8,9]. As an example can also be given the phase separation of dilute solid solutions of helium isotopes (^{3}He-^{4}He) which, in view of the quantum nature of the interatomic interaction in these systems, undergo decay at any arbitrarily small concentration of the impurity component in solution, so that the coordination number (the number of nearest neighbors) in the second phase does not exceed several units [10-12].

Conclusion

It seems that the problem we are considering here has only purely academic interest, but we can indicate one area where the results can probable find a practical application. The classical problem of heterogeneous mixing is the problem of evolution of oil spots on the water surface, arising from the spillage of oil (or other process fluids) due to accidents in transport or production. Of course, this problem is also interesting from the point of view of direct behavior of model complex heterophase system in the hydrodynamic regime.

References

1. Ya.E. Geguzin. Fizika spekaniya. M. Nauka. 1984.
2. Ya.E. Geguzin. Makroskopicheskiye defekty v metallakh. M. Metallurgiya. 1962.
3. Ya.E. Geguzin. Diffuziya po realnoy kristallicheskoy poverkhnosti. v sb.: "Poverkhnostnaya diffuziya i rastekaniye". M. Nauka. 1969.
4. Ya.E. Geguzin. Diffuzionnaya zona. M. Nauka. 1979.
5. Ya.E. Geguzin. Kaplya. M. Nauka. 1973.
6. L.D. Landau. E.M. Lifshits. Gidrodinamika. M. Nauka. 1986.
7. V. V. Slezov, J. Schmelzer, Phys. Solid State 39, 1971 (1997).

8. I. Prigogine, *The Molecular Theory of Solutions*, North-Holland, Amsterdam (1957).
9. E.A. Guggenheim, *Mixtures*, Clarendon Press, Oxford (1952).
10. T.N. Antsygina, V.A. Slusarev, K.A. Chishko, Low Temp. Phys., 21, 453 (1995).
11. T.N. Antsygina, V.A. Slusarev, K.A. Chishko, Phys. Solid State, 40, 325 (1998).
12. T.N. Antsygina, K.A. Chishko, V.A. Slusarev, J.Low Temp. Phys., 111, 577 (1998).

Вісник ХНУ, серія «Фізика», вип. 28, 2018. с. 79-82

PACS:
UDC: 666.63

Modeling of thermal processes during electroconsolidation

E.S. Gevorkyan[1], V.A. Dutka[2], R.V. Vovk[3], M.V. Kislitsa[1]

1 Ukrainian State University of Railway Transport, 7 Feierbakh Sq., Kharkiv 61050, Ukraine

2 V. Bakul Institute for Superhard Materials, Kiev, 2 Avtozavodskaya str., 04074, Ukraine

3 V.N. Karazin Kharkiv National University, 4 Svobody Sq., Kharkiv 61022, Ukraine

ORCID: *0000-0003-0521-3577, 0000-0002-4143-7650*

DOI: 10.26565/2222-5617-2018-28-09

Practical application of mathematical modeling technologies of heat transfer processes in the main units of the installation for electroconsolidation of powder materials using FAST/SPS technology is considered. A mathematical model of the existing hot pressing unit with direct current transmission is created. The results on the heat distribution in the installation parts and in the compaction zone are obtained. Comparison of simulation results with experimental data is given. The significance of the data obtained by using similar techniques, both from the fundamental point of view and from the practical one, is shown.

Keywords: electroconsolidation, finite element simulation, thermal processes, Al_2O_3-SiC.

Розглянуто практичне застосування технологій математичного моделювання процесів теплопереносу в основних вузлах установки для електроконсолідації порошкових матеріалів за технологією FAST/SPS. Розроблено математичну модель існуючої установки гарячого пресування з прямим пропусканням струму. Отримані результати по розподілу тепла в деталях установки та в зоні компактування. Наведено порівняння результатів моделювання з експериментальними даними. Показана значимість даних, отриманих шляхом застосування подібних методик, як з фундаментальної точки зору, так і з практичної.

Ключові слова: електроконсолідація, скінченно-елементне моделювання, теплові процеси, Al_2O_3–SiC.

Introduction

As is known, the use of oxide ceramic, in particular, nanostructured and composite materials as instrumental is of great demand, because of their high physical and mechanical properties. But along with high hardness and temperature resistance, the use of such materials is limited by their low strength and crack resistance. It is not possible to solve this problem by traditional hot sintering. The reason for this is the rapid growth of grain, competing with the compaction of particles (Fig. 1).

The use of innovative technologies for the consolidation of ceramic materials, such as FAST (Field Activated Sintering Technology), SPS (Spark Plasma Sintering) and their combinations makes it possible to [1-5]. The advantage of these technologies is the obtain new materials with a submicron and nanostructure activation action of the electric field and current, which greatly intensifies the sintering process, in comparison with traditional methods. So, to obtain high-density Al_2O_3-SiC ceramics by hot pressing with direct current transmission (electroconsolidation) (Fig. 2), it was sufficient for about 3 minutes [6].

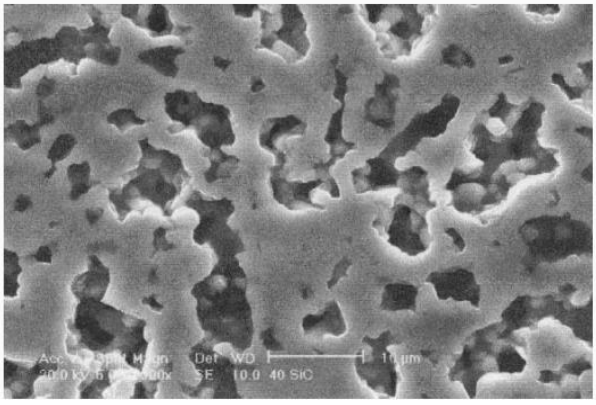

Fig. 1 Microstructure of ceramic sintered in argon atmosphere without activating additives [7]

.

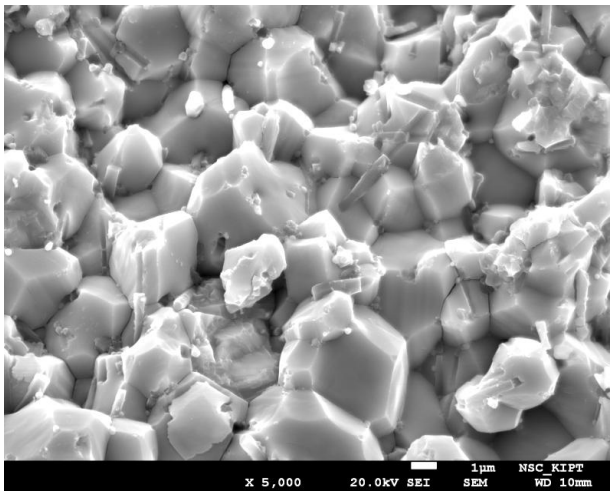

Fig. 2 Microstructure of Al_2O_3-SiC ceramics sintered by electroconsolidation at a temperature T = 1400˚C, pressure P = 30 MPa.

Experiment

The use of such technologies is associated with the need to carefully design equipment that directly participates in the consolidation processes, because the accuracy and predictability of consolidation parameters such as temperature, pressure, etc. is important in order to

achieve the necessary material properties. The priority in this case is obtaining information on the temperature distribution in component parts of the installation, as well as the distribution of electric current in the components involved in its transport. The most accurate source of information necessary for this is computer simulation using specialized software.

For the calculations, a universal software system of finite element analysis ANSYS was used. In Fig. 3 shows the design area in the form of a two-dimensional model of a hot vacuum pressing unit. To solve this problem, the

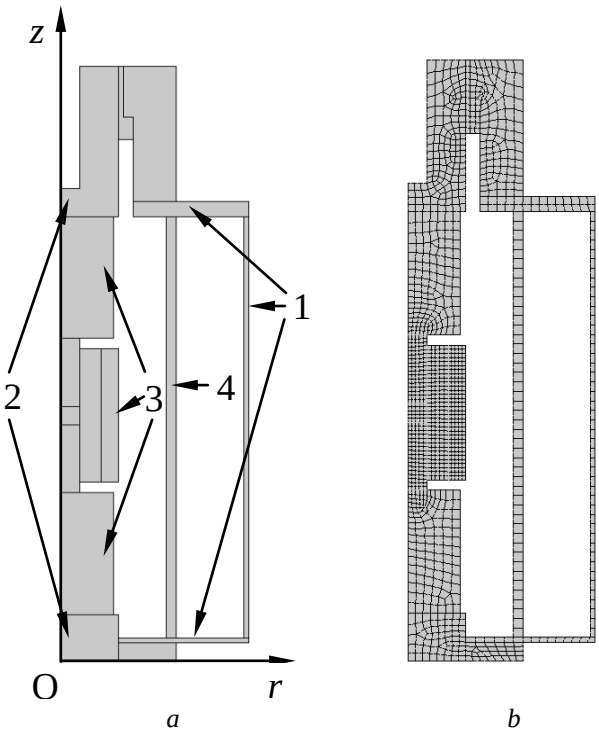

Fig. 3. Calculation area (a) and its decomposition into a finite element grid (b). Oz - axis of pressing; Or is the radial axis of the installation. 1 - body (steel); 2 - water-cooled current leads (brass); 3 - mold and punches (graphite); 4 - lining (thermo-expanded graphite).

finite element method was used together with the radiosity method, and the computational domain was divided into a grid of 923 eight-node elements with quadratic approximation.

The simulation was performed according to the original electrosparking system developed by us [8]. An alternating voltage of the order of 5 V with a frequency of 50 Hz is applied to the surfaces of brass current leads. A distinctive feature of such plants is a short synthesis time, due to the current flow of the order of several kA. The distribution of the heat produced was carried out taking into account convective heat transfer with the heat carrier and the environment, as well as radiant heat exchange inside the installation. The calculations take into account the temperature dependences of the properties of the materials from which the parts of the installation are made. The volume of the material to be compacted (Al_2O_3 powder) is small relative to the whole installation, and its physical properties change during compaction (they depend not only on temperature), they are taken to simplify calculations. The values of the contact electrical and thermal properties and their dependence on the temperature and pressure of pressing are obtained from the literature [9-14].

Results

In Fig. 4 shows the temperature dependence at different points of the sintering zone as a function of time. The time interval from 0 to 400 s corresponds to intensive heating, and from 400 s – approach to the temperature regime and the beginning of sintering. As can be seen from the graph, in pairs of points s1-s4 and s2-s3, the temperature coincides over the entire time interval, which means that there is no axial temperature gradient between the upper and lower punch. The presence of such a balance of heat dissipation speaks about the correctness of calculations of the components of the installation and the cooling system of the upper and lower current leads.

When the sintering temperature is reached, a small temperature divergence is observed at the points s1 and s2 (s3 and s4) due to heat removal through the outer part of the mold by radiation. Despite the presence of a radial gradient, the temperature difference between the center and the periphery of the compact does not exceed 10K, which in this case corresponds to 0.6% of the sintering temperature.

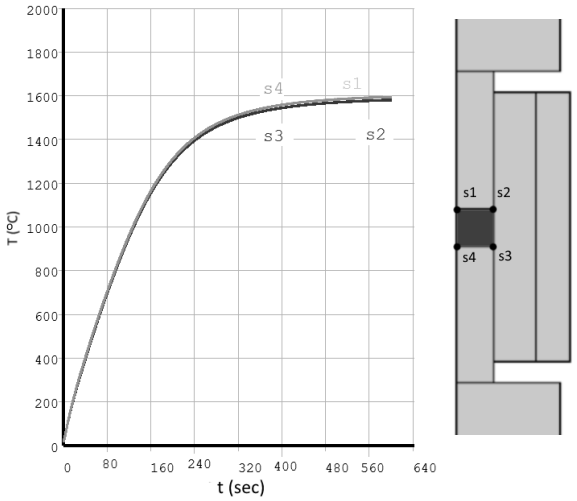

Fig. 4. Change in temperature at points on the surface of the volume being compacted. s1-s2 - upper, s3-s4 - lower plane.

Obtaining predictable and reproducible results in the compacting of powder materials requires precise control of the main parameters of consolidation: temperature, pressure, holding time. The most difficult is the precise

control of the temperature in the pressing zone, since access to it is difficult. A relatively simple solution to this problem is the option of controlling the temperature at the periphery of the mold. In Fig. 5 shows the change in temperature at points on the transverse axis, obtained by mathematical modeling. Thus, it can be seen from the graph that when monitoring the temperature at the periphery of the mold (point c3), the temperature difference $\Delta T \approx 200K$ must be taken into account.

The efficiency of the model can be estimated by comparing the simulation results with the actual measured parameters. In Fig. 6 shows the time dependences of the temperature measured at the periphery of the mold during the electroconsolidation and the simulation results. The differences in the preliminary stage are associated with different initial currents and, correspondingly, the heating rate. The termination of the effect of the electric field for the real process corresponds to the instant of time t = 1100 s, and for the model it was terminated at the time t = 1000 s. If the differences in the magnitude of the current flowing at the initial stage to a minimum are reduced, then the simulation results fully correspond to the real nature of the temperature behavior at the monitored point, which confirms the reliability of the results obtained by modeling.

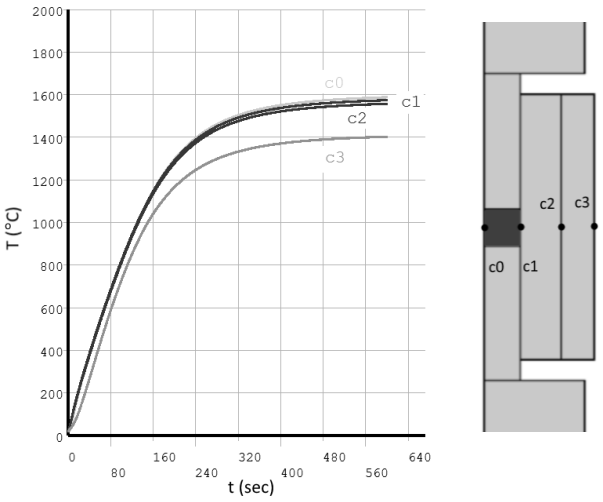

Fig. 5. Change in temperature at points on the transverse axis, *c0* is the center of the volume being compacted, *c1* is the border with the mold, *c2* is the border of the mold and composite shell, *c3* is the outer part of the shell.

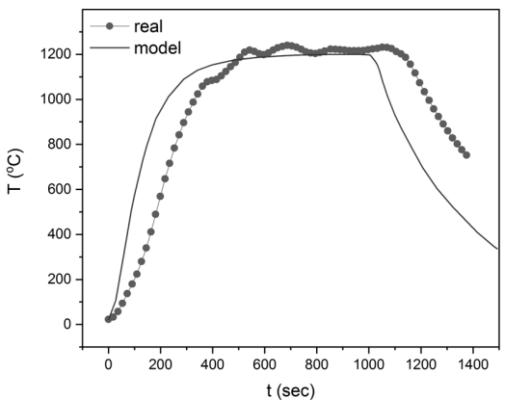

Fig. 6. Dependence of mold shell temperature on time. Points are real measurements, a solid line is the result of modeling.

Conclusions

Accurate understanding of the processes occurring during the consolidation of nanomaterials allows us to create a theoretical foundation for the development of innovative technologies for the production of new materials with increased physical, mechanical and operational properties. With the use of FAST/SPS technologies, all processes take place quite quickly, and the consolidation time is reduced to several minutes, in such conditions the control of current, temperature and mechanical stress distribution is practically unattainable problem, which, however, is easily solved by using mathematical models and mathematical calculations. This approach allows us not only to determine the magnitude of important parameters of consolidation, but also to observe their dynamics in the process of synthesis. In addition, the use of such solutions at the design stage makes it possible to simplify the development of equipment for electroconsolidation, and the results of modeling the temperature distribution in the volume of the mold-simplify temperature control in the sintering zone, which can significantly reduce the cost of manufacturing it.

References

1. Andrievsky R.A., Glezer A.M. (2000) Dimensional effects in nanocrystalline materials.2.Mechanical and physical properties. *Fizika metallov i metallovedenie*, Vol. 89, № 1, pp. 91-112. [in Russian]
2. Gleiter H. Nanostructured materials: state of the art and perspective. *Nanostructured Materials*,1995, № 6, pp. 3-14.
3. Hasanov O.L. Submicrostructure and properties of structural, piezoelectric and ferroelectric ceramics made by the method of dry ultrasonic compacting of nanopowders. *Konstruktsii iz kompozitsionnyih materialov*, 2001, № 4, pp. 3-10. [in Russian]
4. Skorokhod V.V., Uvarova I.V., Ragulya A.V. Physicochemical kinetics in nanostructural systems. *Kiev, Akademperiodika*, 2001, p. 180. [in Ukrainian]
5. Gevorkyan Edwin, Sofronov Dmitry, Lavrynenko Sergiy, Rucki Miroslaw : Synthesis of Nanopowders and Consolidation of Nanoceramics of Various Applications // Journal of Advances in Nanomaterials, 2017. - Vol. 2, - No 3, pp. 153-159.

6. R.V. Vovk, N.M. Prokopiv, V.A. Chishkala, M.V. Kislitsa. Investigation of structure and properties of composite material Al2O3–SiC obtained by electroconsolidation process. Functional Materials, 25 (1), 2018, pp. – 43-47. https://doi.org/10.15407/fm25.01.043
7. Elzbieta Ermer, Ptak Wiesław, Stobierski Ludosław, Influence of sintering activators on structure of silicon carbide.Solid State Ionics 141–142 (2001) 523–528
8. Пат.72841 Україна, МПК (2012.01)B22F 3/00. Пристрій для гарячого пресування порошків шляхом прямого пропускання електричного струму / Азеренков М.О., Геворкян Е.С., Литовченко С.В., Чишкала В.О., Тимофеєва Л.А., Мельник О.М., Гуцаленко Ю.Г.; заявник і патентовласник Геворкян Е.С. - № u 2012 03 031; заявл. 15.03.12; опубл. 27.08.12, Бюл. №16.
9. Maizza G. , Grasso S., Sakka Y. Moving finite-element mesh model for aiding spark plasma sintering in current control mode of pure ultrafine WC powder // J. Mater. Sci. – 2009. – V. 44. – Pp. 1219 – 1236.
10. Rothe S., Kalabukhov S., Frage N., Hartmann S. Field assisted sintering technology. Part I: Experiments, constitutive modeling and parameter identification. – GAMM-Mitt. – 2016. – Vol. 39. – No. 2. Pp. 114 – 148.
11. Rothe S., Hartmann S. Field Assisted Sintering Technology, Part II: Simulation. – GAMM-Mitt. – 2017. – Vol. 40. – No. 1. Pp. 8 – 26.
12. Allen J. B., Walter C. Numerical Simulation of the Temperature and Stress Field Evolution Applied to the Field Assisted Sintering Technique. – ISRN Materials Science. – 2012. – Volume 2012, Article ID 698158, 9 pages.
13. Wei X., Giuntini D., Maximenko A. L., Haines C. D., Olevsky E. A. Experimental Investigation of Electric Contact Resistance in Spark Plasma Sintering Tooling Setup // Journal of the American Ceramic Society. – March 2015. – DOI: 10.1111/jace.13621. – Pp. 1–35.
14. Manière C., Durand L., Brisson E., Desplats H., Carré P., Rogeon P., Estournès C. Contact resistances in spark plasma sintering: From in-situ and ex-situ determinations to an extendedmodel for the scale up of the process. – Journal of the European Ceramic Society. – 2017. – Vol. 37. – Nº 4. – Pp. 1593 – 1605.

Вісник ХНУ, серія «Фізика», вип. 28, 2018. с. 83-89

PACS:
UDC: 548.4: 546.33′15′683

Mechanism of light scattering defects formation in NaI:Tl during crystal growth

A.V. Kolesnikov[1], K.A. Kudin[2], A.M. Kudin[3]

1. Institute for scintillation materials National Academy of Science, 60 Nauki ave., 61001, Kharkiv, Ukraine
2. State Enterprise Ukrainian RTC "Energostal", 9, Nauki ave., Kharkov 61166, Ukraine
3. National University of civil protection of Ukraine, 94 Chernyshevska str., 61023 Kharkiv, Ukraine a.m.kudin@gmail.com

ORCID: 0000-0003-4788-6665

DOI: 10.26565/2222-5617-2018-28-10

Nature of growth light scattering defects in NaI:Tl crystal has been studied by optical and electron microscopy technique. The heterogeneous mechanism of inclusion formation has been proposed. This mechanism consists in three stages. At first stage, sodium oxide diffuses to the internal surfaces of gas bubbles or channels. The oxide then reacts with carbon dioxide and converts into sodium carbonate. At the third stage, a new phase is formed inside the gas-filled channels. Finally carbonates covered internal surface of gas channels due to the shape of inclusion becomes morphologically stable.

Keywords: growth defects, inclusion of new phase, heterogeneous decay of solid solution.

Методами оптичної та електронної мікроскопії вивчено природу ростових дефектів, що призводять до розсіювання світла, у кристалах NaI:Tl. Запропоновано гетерогенний механізм утворення виділень нової фази, що складається з трьох етапів. Спочатку окис натрію дифундує до внутрішніх поверхонь газонаповнених каналів. Далі оксид реагує з вуглекислим газом і перетворюється в карбонат натрію. На третьому етапі фаза, що утворилася, вистилає внутрішню поверхню газового каналу, внаслідок чого його форма набуває морфологічну стабільність.

Ключові слова: ростовые дефекты, выделения новой фазы, гетерогенный распад твердого раствора.

Introduction

First of all, the authors would like to note that their views on the nature of defects in crystals and their evolution were formed under the influence of two monographs by Ya.E. Geguzin: "Macroscopic defects in metals" [1] and "Motion of macroscopic inclusions in solids" [2]. Since all authors are more or less related to the Chair of crystal physics of Kharkiv National University, they fully share conviction of professor Geguzin that a defective structure decisively determines the functional parameters of ready products from single crystals.

In this paper, the nature and mechanism of the regular formation of growth defects in a NaI:Tl crystal is considered. Detectors made from this material are most widely used in science and technology as effective scintillators [3, 4]. For a number of applications needed scintillation detectors of very large size. For example, in nuclear medicine (Anger camera) or in spectrometric portals (control of the spread of radioactive and fission materials), sensitive elements are large-area plates or long cylinders. For these purposes, ingots with a diameter of 500 mm and more are grown by modified Kyropulos technique with feeding by initial salt or melt [5]. The actual problem of the growth of large-sized crystals is the problem of light scattering which is associated with growth light-scattering inclusions (LSD – light-scattering defects). This LSDs are usually concentrated in bands of entrapping.

The photograph presented in Fig. 1 shows the longitudinal cross section of a single crystal in the upper part of a cylindrical ingot. This part of ingot corresponds to the beginning of growth in height. Usually at this transient moment the rate of crystallization is maximal. As it seen on photograph the light-scattering centers surround a front of crystallization and resemble a cloud.

Despite years of efforts to study the LSD in these crystals, the existing views on their nature were contradictory and even mutually exclusive. Nature of LSD was attributed to either gas bubbles, 100-500 nm in size, or inclusion of Na_2CO_3 phase [6]. The second model assumes a homogeneous decay of the impurity solution in the crystal lattice.

Two mutually exclusive viewpoints can be reconciled in the assumption of a heterogeneous decay of a solid solution [7]. As nucleation centers in this case, one should consider gas bubbles. Further studies questioned the last assumption, it turned out that LSDs are formed even at low concentration of CO_3^{2-} ions in the crystal lattice, which is clearly insufficient for effective separation of the second phase.

The present paper is devoted to a consistent presentation of the concepts of the nature of LSD and consideration of the heterogeneous mechanism for the formation of three-dimensional defects, which is not associated with the diffusion of carbonate ions.

Experimental

NaI:Tl crystals have been grown by modified Kyropulos technique with feeding by melt, detailed description of equipment and process has been done in [5, 8]. A typical diameter of ingots was 250 mm while a height was ~350 mm. Ingots were grown in an argon atmosphere [8]. Several experiments have been made in mixed Ar+CO_2 gaseous medium [9] according to recommendations of [10]. The composition of the gaseous medium in the furnace was analyzed using an omegatron-type mass spectrometer, which was connected to a pressure sensor through a leak.

Gas sampling was performed every day throughout the growth process. For example, In Tab. 1 are presented the typical results of gas atmosphere analysis at furnace during the growth of crystal.

Table 1.

Concentration of Ar, CO_2 and H_2O in atmosphere of furnace during the crystal growth

Atmosphere	#	Gas concentration		
		Ar	CO_2	H_2O
Ar	1	92.1	0.3	–
	3	91.2	0.4	–
	5	89.8	0.54	–
Ar+ CO_2	1	81	6.0	4.9
	2	82	6.7	3.4
	3	88	5.3	3.4
	4	82.4	6.6	4.0
	5	86	6.5	4.0
	6	84	6.8	5.0

It can be seen that in the case of Ar medium, water is not detected in furnace volume, contrary to second case when water is recorded throughout the entire growth process. This result is in good agriment with our data obtained earlier in [9]. In cited paper the pulsed injection of CO_2 into the furnace containing only Ar leads to the appearance of water vapours above the melt.

For a deliberate obtaining of LSD in growing crystal, a short pumping of furnace volume was carried out. In this case a large muddy zone was observed. Sometimes the ingot contained a large amount of LSD and even a gas bubbles visible to the naked eye. The advantage of this experiment is that it allows to model the cloudy zone quite simply. Below we will show that in zones of different nature (spontaneous or created intentionally) defects of predominantly one sort are detected.

The form of gas bubble was studied using an optical microscope in a dry room. Electron-microscopic studies were carried out on a transmission microscope EM-250 using the technique of coal replicas. Samples measuring 5×5×15 mm^3 were cleavage along the growth axis from different parts of ingot. The transverse cleavage of the samples was carried out in vacuum. Replicas have been deposited on fresh surface of sample using VUP-5 installation. Shading of replicas has been made by gold.

Model of the band of entrapping

Let's consider the situation, when the gas pressure over the melt is abruptly reduced. Well known that gas solubility in the melt sharply depends on pressure in furnace. Decrease of gas pressure results in appearance of gas bubbles in melt. Some of these bubbles enter to the crystallization front. So, gas bubbles can be incorporated into crystal lattice and form here a gas filled cavities. The zone of ingot containing entrapment of such gas inclusions is schematically depicted in Fig. 2 and is designated as a cloudy or muddy area.

In [6], we showed that the gas filled inclusions obtained in this manner are characterized by the presence of cavities in the form of prolonged channels. A gas bubble, often faceted, has a continuation in the form of a gradually disappearing "tail", elongated along the growth axis. The boundary between the upper transparent part of the crystal and the cloudy zone is quite sharp. As the equilibrium between the gas pressure over the melt and its concentration in the liquid phase is reached, the release of large bubbles ceases. Below the bubble area there is a zone where the LSDs are gradually disappearing. This is due to the fact that gas bubbles have a small size and are not visible in optical microscope [6]. They are detected by the increased scattering of light (in the laser beam), by the deterioration of transmission and by the significant dispersion of the extinction coefficient.

Despite the fact that gas bubbles are not distinguishable here the electron microscopic studies have revealed a huge number of "hollow rods", the skeleton of which is formed by carbonates of sodium and/or thallium [6, 7]. As an example, Fig. 3 shows a photograph of replica, which correspond to the turbid zone of ingot. It can be seen (Fig. 3a) that a large number of rods that stick out from the replica. Presence of the rods on photo means that their solubility in water is small. A separate rod in enlarged form is shown in Fig. 3 b. It is clearly seen that the rod is hollow inside. This fact, like the approximately cylindrical symmetry of the defect, clearly indicates that hollow rod is directly related to gas channel inherently. The electron diffraction pattern obtained from an individual inclusion (like a rod presented in Fig. 3b) shows that the rod has an amorphous structure (the insert in Fig. 3). It should be noted that defects in the form of hollow rods are characteristic for all studied NaI crystals containing such entrapment of inclusions. Gradually, without a sharp boundary between zones, the entrapment area turns again into a clear ingot. Gas bubbles of "classical form" (spherical or ellipsoidal)

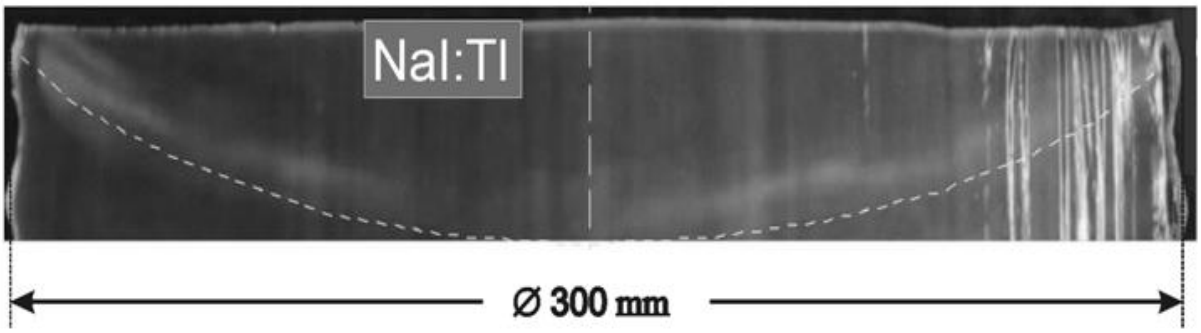

Fig. 1. Photograph of longitudinal section of ingot. The dashed line shows the crystallization front The position of front corresponds to the beginning of growth with constant diameter. The cloud of LSD is located just above the dashed line

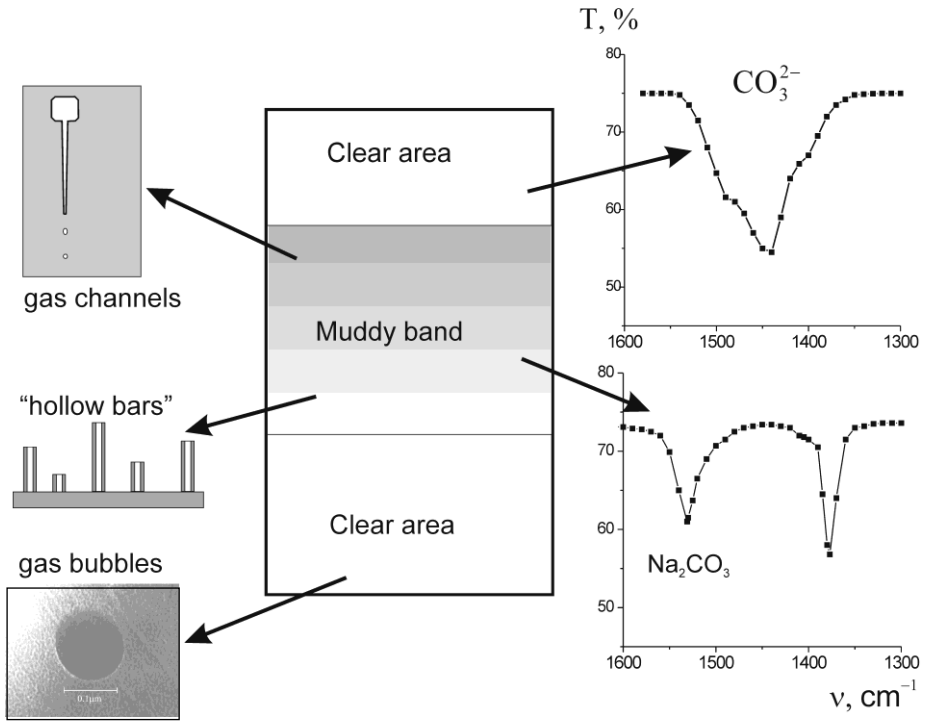

Fig. 2. Schematic imaging of band of entrapping. Explanations are given in the text

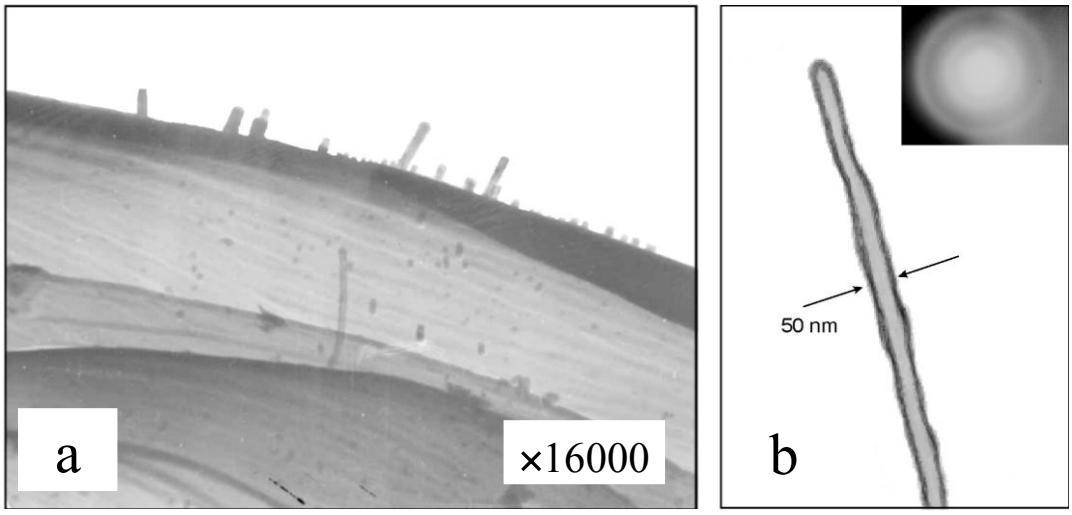

Fig. 3. Replica with hollow rods protruding from it (a). Electron-microscopic imaging of separated rod (b), in insert electron diffraction pattern is shown.

are also found here, but their concentration in clear zone is too small for appreciable scattering of light.

Impurity composition of large crystals

Well known that contamination of large NaI:Tl ingot connected mainly with the presence in crystal lattice the anion impurities like OH^-; CO_3^{2-} and O^{2-}. Activator is the desired impurity in crystal, its concentration (C_{Tl}) in grown ingot is determined by chemical analysis on thallium [11]. The value of C_{Tl} well corresponds to optimum: (4-6)·10^{-2} mole % [12]. Data on the C_{Tl} are presented in Table 2 as concentration in *ppm*, number of Tl^+ in cubic centimeter (cm^{-3}), and as an average distance between activator centers.

The information on the oxide compounds and its concentration is obtained from the analysis of thermally stimulated luminescence (TSL) curves [13, 14]. The setup for TSL measurements is described in [15]. Data on oxide concentration are also given in Table 2 as a number of O^{2-} V_A^+ dipoles.

The concentration of carbonate ions (C_K) is determined from the spectra of IR absorption using a UR-20 spectrophotometer. We shall discuss the IR spectra itself and the changes in them a little later. Here, we note that according to the known Smakula formula, the absorption coefficient (k_{880}) at the maximum of the band 880 cm^{-1} (a deformation vibration ν_1 in CO_3^{2-} ion) is proportional to the number of the absorbing centers: $C_K = b \cdot k_{880}$, where b is the transition coefficient. For NaI crystals, its value is known: $b = 8 \cdot 10^{-2} cm^2$. A vibration ν_1 band is chosen for the reason that its intensity depends little on the local environment of impurity anion. Contrary an intensity of the 1440 cm^{-1} band (valence ν_3-vibration) depends on the environment, therefore, by k_{1440}, the number of non-associated $CO_3^{2-} - V_A^+$ dipoles can be judged. The data on the value of C_K in the transparent part of ingot are given in Tab. 2.

An unexpected result was the fact that the value of C_K turned out to be practically the same in different parts of the crystal, and intensity of 1440 cm^{-1} band does not decrease in the turbid zone, i.e. the formed LSD are not associated with the decay of carbonate solid solution. Moreover, the formation of LSD is observed in crystals with a rather small C_K, when the average distance between identical ions is hundreds of lattice parameters (see column 4 in Table 2). In this situation the diffusion mechanism is not effective to precipitate formation from $CO_3^{2-} - V_A^+$ dipoles.

From the data of Table 2, it is possible to draw a completely definite conclusion that $O^{2-} - V_A^+$ dipoles at annealing should diffuse to the center of nucleation first of all. An internal (like a babble or channel) or external free surfaces will be enriched by sodium oxide.

Table 2.

Concentration of impurities and the average distance between similar centers

Cation / anion	Content, ppm	Content, cm^{-3}	Distance, lattice constant
Tl^+	500	$5 \cdot 10^{18}$	9
CO_3^{2-}	1	$1 \cdot 10^{16}$	464
O^{2-}	900	$9 \cdot 10^{18}$	7

Mechanism of LSD formation

The proposed mechanism for the LSD formation is based on the processes of gas evolution at the crystallization front. The solubility of gases in the melt depends on many factors and varies from the nature of the gas. It is known [16] that the solubility of carbon dioxide exceeds that of argon by two or three orders of magnitude. Therefore, the formation of bubbles at the front is more likely when the growth process is carried out not in Ar, but in CO_2 atmosphere.

Gas evolution at the crystallization front leads to the formation of babbles and gas channels. Such cavity as is known [2] are unstable during annealing and are transformed into a chain of pores of round shape. This slow process is impeded by another, faster process, which takes place simultaneously with the first during the growing process. It is, as shown above, the diffusion of sodium oxide. The $O^{2-} - V_A^+$ dipoles at annealing 450° effectively reach the outer or inner surface of the crystal, as will be shown below, at foreseeable intervals. The formation of an oxide coating on the inner surface just prevents the transformation of gas channels into a chain of bubbles.

Since the babbles have been filled by CO_2 and H_2O, following chemical reactions occur on their internal surface:

$$Na_2O + H_2O \rightleftarrows 2NaOH \quad (1)$$

$$2NaOH + 2CO_2 \rightleftarrows 2NaHCO_3 \quad (2)$$

$$2NaHCO_3 \rightleftarrows Na_2CO_3 + H_2O + CO_2. \quad (3)$$

Analysis of reactions (1-3) shows that carbon dioxide is spent while the amount of water does not decrease during annealing. Water can be transform to $NaHCO_3$ when crystal is cooled.

Diffusion processes lead to the formation of a peculiar framework within the channel. The solubility of Na_2CO_3; $NaHCO_3$ and Tl_2CO_3 compounds in water is much less [7] than the solubility of NaI. For this reason, after dissolution of NaI, almost insoluble inclusions remain on the replica, which are observed in the electron microscope as protruding elongated rods. So, the proposed mechanism explains the origin of the hollow rods, but the way of attaching the protruding rods to the replica is still incomprehensible. An answer is given in scheme on

Fig.4. During the replica making carbon atoms can penetrate into gas channel (if the rod is hollow) and create a spike to attach the rod to replica.

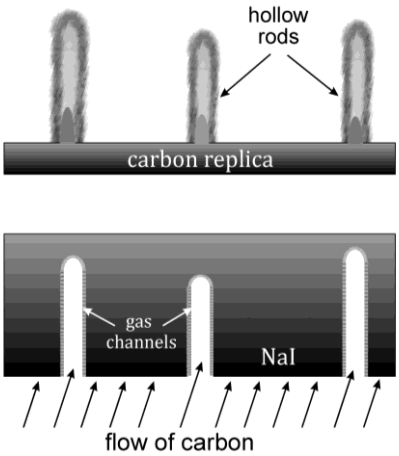

Fig. 4. Process of replica deposition and structure of created carbon replica with attached hollow rods

The mechanism of LSD formation is heterogeneous. This circumstance allows us to reconcile two seemingly opposite viewpoints on the origin of inclusions. As it turned out, their nature is closely related to both gas bubbles and Na_2CO_3 phase. A feature of proposed mechanism is the fact that the second phase formation occurs at crystal-gas interface. Inclusions of new phase are not directly related to decay of the solid solution of sodium carbonate in the NaI lattice. Initially the decay of sodium oxide solid solution occurs, and the final product is formed as a result of chemical reactions with water and CO_2 at the interface. This feature makes it possible to explain the incomprehensible fact that concentration of carbonate in form of $CO_3^{2-} - V_A^+$ dipoles is the same in clear area of ingot and in the muddy zone. The striation theory [17] predicts a sharp decrease in the amount of impurity in the region below the entrapping zone. It is clear that in our case, the muddy zone is associated with gas bubbles and channels not with carbonate.

Moreover, proposed mechanism can explain other, at first sight, unrelated experimental fact. The point is that repeated annealing often reveals the entrapping zone in initially transparent part of ingot. Consider the lower part of the growing crystal, which was least annealed in the growth furnace. If gas bubbles are present in this region but their inner surface has not yet be covered with the new phase, then repeated prolonged annealing will lead to the LSD formation according to mechanism described above. Reflectivity of the "rods" is much higher than just gas bubbles, and for this reason the hidden capture region becomes observable visually.

The nature of the LSD formed by the trapping mechanism of gas bubbles on the crystallization front is well known and described in many works, for example, in the already mentioned monograph [2], also for CsI crystals in [18]. Professor Geguzin touched upon this problem in [19]. The mechanisms of LSD formation associated with the homogeneous decay of the activator subsystem also well known in CsI:Tl crystal [20] and in CsI:Na [21]. The rather complicated mechanism for the formation of the LSD, which includes the trapping of bubbles, the heterogeneous decay of a solid solution and chemical reactions at the interface, as we know, was first discovered in this section.

Experimental confirmations of mechanism

Gas babble composition. The proposed mechanism is based on the assumption that H_2O and CO_2 enter to a bubble, in contrast to the results of [22], where water was not detected. Generally spiking it is clear that the composition of the gas above the melt is qualitatively identical to that in the bubble. Quantitative differences are associated with solubility of individual gas in the melt. It turned out (see an experimental) that H_2O vapors above the melt is always recorded when growth takes place in CO_2 atmosphere. If crystal grows in Ar atmosphere, water is not detected above the melt. However it is known that CO_2 injection causes immediate release of water from the melt [9] in accordance with reaction (3). H_2O molecules are formed in the melt and evaporates through the free surface into the furnace volume. On the front of crystallization water evaporates into the gas bubbles.

So, the gas babbles have to contain water vapors. To check this conclusion, mechanical destruction of the samples carried out in a manner similar to experiments [22]. In accordance with [22] mass-spectra do not show water evaporation from babbles even for samples made from muddy zone. It is known that at room temperature water interacts with Na_2CO_3 and CO_2. As a result of interaction baker soda $NaHCO_3$ is formed. For this reason mass-spectra were measured during heating and melting of sample. Melting of this crystal leads to release of water and carbon dioxide, 30-50 times more intense than when melting transparent samples.

IR spectra. According to Panova and Mustafina [23], the local environment of CO_3^{2-} ions should differ in the transparent part of the crystal in comparison with the muddy zone. In Fig.5 the corresponding IR absorption spectra are presented. For the transparent part of the crystal (regardless of its position relative to the turbid part), a standard set of absorption bands is observed with maxima at 1440 cm^{-1} and 880 cm^{-1}. These bands are most intense and are well manifested even at small CO_3^{2-} concentration, their position is in good agreement with recent our [14, 24] and literature data [23].

Another picture is observed in the muddy zone. The local environment only slightly distorts the deformation vibrations, so the maximum of the ν_1-band is still located at 880 cm^{-1}, while the stretching vibration split into two

bands: 1380 and 1530 cm^{-1}. Well known that the first band is also characteristic for CO_3^{2-} ions, but it is observed in CsI crystals with volume centered lattice [24, 25]. As for the additional band at 1530 cm^{-1}, the authors of [23] observed it in crystals with the LSD at a high concentration of carbonate ions and attributed to the precipitates of Na_2CO_3 phase.

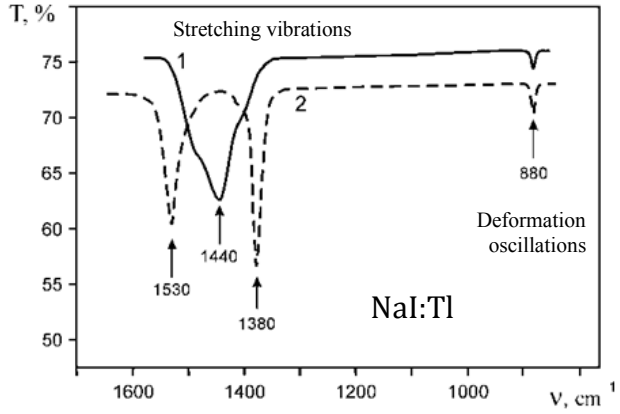

Fig. 5. Spectra of IR absorption in different areas of ingot. 1 – the clear zone, 2 – muddy band.

Usually, the IR absorption spectrum corresponding to the muddy zone consists of overlapping bands at 1380; 1410; 1440 and 1530 cm^{-1}. If the carbonate-ion concentration is low, a band of 1480 cm^{-1}, which is characteristic for an interacted pairs of $Me^{2+}CO_3^{2-}$ [23]. In any case, we can conclude that the local environment of a big part of CO_3^{2-} ions in muddy zone does not correspond to that in regular lattice. Therefore we believe that the 1530 cm^{-1} band is characteristic for the skeleton of hollow bar. A feature of turbid samples is the fact that prolonged annealing at 450°C leads to an increase of absorption bands intensity at 1380 and 1530 cm^{-1}, but practically does not affect the intensity of the 1440 cm^{-1} band.

Second phase manifestation on the free surface of sample after annealing. The next point concerns the experimental verification of the diffusion mechanism of the LSD formation. If internal surface of the gas-filled channels are covered over time by new phase, then almost the same can be observed on the outer surface of the sample. To this end, NaI:Tl crystals with a chipped surface were annealed in inert (Ar) and reactive (CO_2) atmosphere. The annealing time (60 hours) approximately is matched the duration of growth process.

A rather intensive course of diffusion processes could be judged visually by the formation of a yellow coating of TlI on the cold parts of ampoule. It could be expected that less volatile compounds, such as Na_2O; Na_2CO_3 and NaOH at temperature of 550°C will remain on the surface.

The study of annealed samples using a scanning electron microscope revealed the following. On the surface of samples oval precipitates were observed in large numbers, which, judging from the contrast of the image, had a smaller effective atomic number than the matrix, see photograph on Fig. 6. At the same time, crystals grown in vacuum and not containing oxygen impurities were characterized by the absence of such precipitates on the surface. To establish the composition of precipitates, an analysis of characteristic X-ray emission was carried out. Emission has been excited separately in the matrix or in islands with a smaller atomic number. The size of the precipitates (~ 5-7 μm) did not prevent such microanalysis, since the electron beam can be focused on a site with diameter of ~ 1 μm. Spectra of characteristic X-ray emission are shown in parts A and B of Fig. 6.

From obtained results it can be concluded that the main elements of the new phase are sodium, oxygen and carbon. The emission spectrum in the main features corresponds to the spectrum of caustic soda Na_2CO_3 or sodium bicarbonate $NaHCO_3$, which was checked separately. It can be concluded that the mechanism for precipitate formation on the free surface of NaI:Tl crystal is analogous to that in the gas channels.

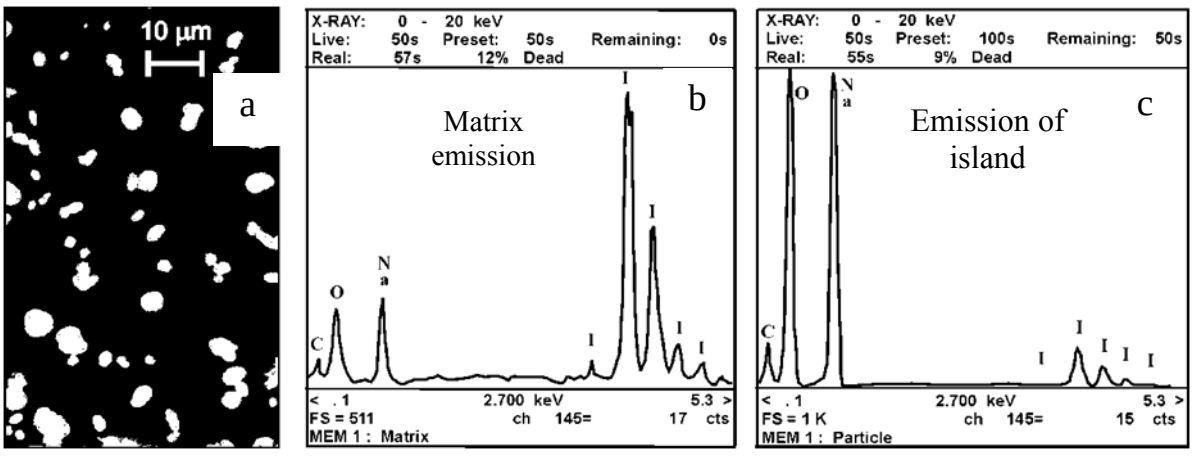

Fig. 6. Photograph of second phase inclusions on free surface of NaI:Tl crystal after annealing (a). Scanning electron microscopy. Characteristic X-ray spectra excited in matrix (b) and new phase inclusion (c)

Conclusion

The existing viewpoints on the nature of the light scattering centers in NaI:Tl crystals are analyzed. It has been shown that contradictory representations can be combined under the assumption of heterogeneous decomposition of the solid solution. The nature of light scattering defects was studied by optical and electron microscopy. It is shown that the primary type of three-dimensional defects in the capture regions is the release of a new phase in the form of hollow rods, which are oriented along the growth axis.

On the basis of the fact that the solubility of the second phase in water is much less than that of the basic substance, it is concluded that the release is associated with sodium and thallium carbonates. This conclusion agrees with the data of IR spectrometry that the local environment of carbonate ions in the capture regions does not correspond to their environment in the regular NaI lattice. The conclusion is made about the heterogeneous mechanism of LSD formation, according to which the focus of decomposition are gas-filled cavities elongated along the growth axis. Mass spectrometric analysis showed that the gas bubbles are filled with carbon dioxide, argon and water.

The conditions for the appearance of centers of light scattering in NaI:Tl crystals are studied. It was found that the formation of carbonate precipitates inside gas bubbles occurs independently of the concentration of carbonate ions in these crystals. By chemical analysis, IR spectroscopy, and thermally stimulated luminescence, it was shown that all light scattering samples contain sodium oxide in comparable amounts ($5\text{-}10^{-2}$ mol%) with an activator concentration. It was found that the decomposition of the solid solution with the formation of second phase precipitates inside gas bubbles occurs in crystals containing carbonate ions in small amounts ($\leq 1\cdot10^{-4}$ mol%). A mechanism is proposed for the formation of precipitates, which includes three stages. At the first stage, sodium oxide diffuses to the outer and inner surfaces of the crystal. On the second, a chemical reaction occurs between the conversion of oxide to carbonate. On the third - the formed phase lays the internal surface of the gas-filled channel. The resulting skeleton gives morphological stability to the gas channels.

References

1. Ya.E. Geguzin. Macroscopic defects in metals, Metallurgizdat, Moscow (1962), 252 p.
2. Ya.E. Geguzin, M.A. Krivoglaz. Motion of macroscopic inclusions in solids, Metallurgiya, Moscow (1971), 344 p.
3. P. Lecoq, A. Gektin, M. Korzhik. Inorganic Scintillators for Detector Systems, Springer (2017), 408 p.
4. Grupen C., Shwartz B.A. Particle Detectors, Cambridge University Press (2008), 651 p.
5. A.V. Gektin, B.G. Zaslavsky. Crystal Growth Technology, John Wiley & Sons, Ltd, Chichester, 511 (2003).
6. K.A. Kudin, V.I. Glushko, V.V. Shlyakhturov, A.Yu. Voloshko A.M. Kudin, Physical Surface Engineering, 9, 395 (2011).
7. A.V. Kolesnikov, K.A. Kudin, V.P. Seminozhenko, P.V. Mateychenko. In: Functional materials for scintillation technique and biomedicine, Kharkov, ISMA, 72 (2012).
8. B.G. Zaslavsky, S.I. Vasetsky, A.M. Kudin, A.I. Mitichkin, J. Crystal Growth, 198/199, 856 (1999).
9. B.G.Zaslavsky, S.I.Vasetsky, A.V. Kolesnikov, B.V. Grinyov, A.I.Mitichkin, K.A. Kudin, Functional Materials, 12, 147 (2005).
10. A.N. Panova, V.I. Goriletsky, T.B. Grinyova, K.V. Shakhova, J. Crystal Growth, 198/199, 865 (1999).
11. E.P.Kisil, L.I Philippovich, V.V. Varchenko, K.N Belikov. Methods and objects of chemical analysis, 9, 125 (2014).
12. L.N. Trefilova, A.M. Kudin, L.V. Kovaleva, B.G. Zaslavsky, D.I. Zosim. NIMA, A486, 474 (2002).
13. A.N. Panova, A.M. Kudin, A.V. Dolgopolova. Optics and Spectroscopy, 63, 444 (1987).
14. K.A. Kudin, A.V. Kolesnikov, B.G. Zaslavsky, A.I. Mitichkin. S.I. Vasetsky, A.Yu. Voloshko, D.S. Sofronov, Functional Materials, 18, 254 (2011).
15. A.V. Dolgopolova, E.N. Kovaleva. A.M. Kudin, A.N. Panova. Single crystal materials, Kharkov, VNII monokristallov, 11, 125 (1983).
16. L.E. Ivanovsky, V.N. Nekrasov. Gases and ions melts, Nauka, Moscow (1979), 371p.
17. Handbook of crystal growth. Bulk crystal growth: Basic Techniques, and Growth Mechanisms and Dynamics, 2-nd ed. Ed. P. Rudolph, Elsevier (2015), 1381 p.
18. L.M. Shamovsky. Crystal-phosphors and scintillators in geology, Nedra, Moscow (1985), 239 p.
19. Ya.E. Geguzin. Bubbles, Nauka, Moscow (1985), 174 p.
20. G.Kh. Rosenberg, G.V. Ptitsyn, L.V. Kovaleva, Solid State Physics, 21, 2970 (1979).
21. G.Kh. Rosenberg, G.V. Ptitsyn, E.F. Tchaikovsky, Yu.T. Vyday. Solid State Physics, 16, 3336 (1974).
22. E.F. Tchaikovsky, N.I. Davydenko, Yu.F. Derkach, E.V. Kovtun. Methods of obtaining and investigation of single crystals, Kharkov, VNII monokristallov, 5, 44 (1980).
23. A.N. Panova, R.Kh. Mustafina. Single crystals and scintillators, Kharkov: VNII monokristallov, 5, 1, 239 (1969).
24. B.V. Grinev, L.N. Shpilinskaya, L.V. Kovaleva, A.M. Kudin, A.I. Mitichkin, T.A. Charkina, Optics & Spectroscopy, 89, 50 (2000).
25. L.N. Shpilinskaya, S.I. Vasetsky, L.V. Kovaleva, A.M. Kudin, A.I. Mitichkin, T.A. Charkina, Functional materials, 6, 364 (1999)

Книги Я.О.Гегузіна, видані за його життя

Нова книжкова серія «Шедеври природознавчої літератури», яка була створена у 2014 році, розпочата виданням науково-популярної книги Я.О.Гегузіна «Крапля»

Книги професора Я.О. Гегузіна є кращими зразками науково-педагогічної літератури. Річка часу виносить у сьогоднішній день найбільш дорогоцінне каміння. Визнання книги, особливо навчальної, шедевром вимагає десятиліть осмислення дуже багатьма людьми.

«Крапля» − перша книжка із серії прекрасних науково-популярних книг видатного фізика, професора Харківського національного університету імені В. Н. Каразіна Я. О. Гегузіна. Академік В. Л. Гінзбург, нобелівський лауреат з фізики, назвав її поемою! Ця книга є уроком радісного знання, «соковитої» фізики і сходить до класичних зразків науково-популярного жанру, таких як знаменита «Історія свічки» Майкла Фарадея.

В цій серії також видано:

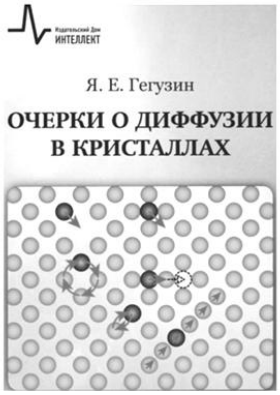

ІНФОРМАЦІЯ ДЛЯ АВТОРІВ СТАТЕЙ

журналу «Вісник ХНУ». Серія «Фізика»

У журналі «Вісник ХНУ». Серія «Фізика» друкуються статті та стислі за змістом повідомлення, в яких наведені оригінальні результати теоретичних та експериментальних досліджень, а також аналітичні огляди літературних джерел з різноманітних актуальних проблем фізики за тематикою видання.

Мова статей – українська, англійська та російська.

ТЕМАТИКА ЖУРНАЛУ

1. Теоретична фізика.
2. Фізика твердого тіла.
3. Фізика низьких температур.
4. Фізика магнітних явищ.
5. Оптика та спектроскопія.
6. Загальні питання фізики і серед них: методологія та історія фізики, математичні методи фізичних досліджень, методика викладання фізики у вищій школі, техніка та методика фізичного експерименту тощо.

ВИМОГИ ДО ОФОРМЛЕННЯ РУКОПИСІВ СТАТТЕЙ

Загальний обсяг тексту рукопису статті повинен займати не більше, ніж 15 сторінок.

Рукопис статті складається з титульної сторінки, на якій вказанно: назва статті; ініціали, прізвища та ORCID авторів, ; поштова адреса установи, в якій була виконана робота; класифікаційний індекс за системами PACS та УДК; анотації із ключовими словами на окремому аркуші з прізвищем та ініціалами авторів і назвою статті, викладені українською, російською та англійською мовами; основний текст статті; список літератури; підписи під рисунками; таблиці; рисунки: графіки, фотознімки.

Анотація українською мовою повинна бути за об'ємом не меньш ніж 1800 сімволів. Стаття повинна бути структорована. Висновки потрібно пронумеровати та в них потрібні бути висновки а не переписана анотація.

Електронний варіант рукопису статті повинен відповідати таким вимогам: текст рукопису статті повинен бути набраний у форматі MicrosoftWord версії 2013, вирівнювання тексту повинне бути здійснене за лівим краєм, гарнітураTimesNewRoman, без прописних букв у назвах, букви звичайні рядкові, з полями ліворуч, праворуч, зверху і знизу по 2,5 см, формули повинні бути набрані в MathType (не нижче версії 6,5), у формулах кирилиця не допускається, символи з нижніми і верхніми індексами слід набирати в MicrosoftWord, ширина формули не більше 70 мм, графіки та фотографії необхідно подавати в графічному форматі, розрізнення не менше 300 dpi, поширення файлів повинно бути *.jpg, шириною в одну чи дві колонки, для однієї колонки розміри: завширшки 8 см, для двох колонок – 16 см. Масштаб на мікрофотографіях необхідно представляти у вигляді масштабної лінійки.

ВИМОГИ ДО ОФОРМЛЕННЯ ГРАФІКІВ

Товщина ліній не більше 0,5 мм, але не менше 0,18 мм. Величина літер на підписах до рисунків не більш 14 pt , але не менше 10 pt, гарнітура Arial.

ПРИКЛАД ОФОРМЛЕННЯ СПИСКУ ЛІТЕРАТУРИ

1. Л.Д. Ландау, Е.М. Лифшиц. Теория упругости, Наука, М. (1978), 730 с.
2. И.И. Іванов. ФТТ, 25, 7, 762 (1998).
3. A.D. Ashby. Phys.Rev., A19, 213 (1985).
4. D.V. Vert. In Progress in Metals, ed. by R. Speer, USA, New York (1976), v.4, p.17.

ДО РЕДАКЦІЇ НАДАЄТЬСЯ

1. Два роздруковані примірники рукопису статті, які підписані її авторами.
2. Електронна версія рукопису та дані щодо контактів для спілкування з її авторами. Для цього потрібно надіслати електронною поштою, тільки на адресу physics.journal@karazin.ua.
3. Направлення від установи, де була виконана робота, і акти експертизи у двох примірниках; адресу, прізвище, повне ім’я та батькові авторів; номери телефонів, E-mail, а також зазначити автора рукопису, відповідального за спілкування з редакцією журналу.

Матеріали рукопису статті потрібно направляти за адресою: Редакція журналу «Вісник Харківського національного університету імені В.Н. Каразіна. Серія: фізика», Лебедєву С.В., фізичний факультет, майдан Свободи, 4, Харківський національний університет імені В.Н. Каразіна. тел. (057)-707-53-83.

Наукове видання

Вісник Харківського національного університету імені В.Н. Каразіна

Серія “Фізика”

випуск 28

Збірник наукових праць

Англійською, українською та російською мовами.

Комп’ютерне верстання К.О.Мозуль

Підписано до друку 3.09.2018. Формат 60x84 1/8.Папір офсетний.
Друк ризограф.
Ум. друк. арк. 11,3. Обл.-вид. арк 13,1
Наклад 100 пр. Зам. №

61022, Харків, майдан Свободи, 4
Харківський національний університет імені В.Н.Каразіна
Видавництво

Надруковано: ХНУ імені В.Н. Каразіна
61022, Харків, майдан Свободи, 4. Тел.+38-057-705-24-32
Свідоцтво суб'єкта видавничої справи ДК №3367 від 13.01.09